Fall 2010

Synthesis and characterization of conducting polymer nanostructures and their application in sensors

Zhe-Fei Li

Department: Materials Science and Engineering

SYNTHESIS AND CHARACTERIZATION OF CONDUCTING POLYMER NANOSTRUCTURES AND THEIR APPLICATION IN SENSORS

by

ZHEFEI LI

A DISSERTATION

Presented to the Faculty of the Graduate School of the

MISSOURI UNIVERSITY OF SCIENCE AND TECHNOLOGY

In Partial Fulfillment of the Requirements for the Degree

DOCTOR OF PHILOSOPHY

in

MATERIALS SCIENCE AND ENGINEERING

2010

Approved by

Frank D. Blum, Advisor
Chang-Soo Kim
Robert W. Schwartz
Michael R. Van De Mark
F. Scott Miller

PUBLICATION DISSERTATION OPTION

This dissertation has been prepared in the styles utilized by the journals to which parts of it have been submitted. In the paper section, Paper 1 (pages 16-31) has been published in *Sensors and Actuators B: Chemical*. Paper 2 (pages 32-48) has been submitted to *Analytical Chemistry*. Papers 3 and 4 will be submitted. NOTE: Paper 1 is based on an earlier version included in my master thesis.

ABSTRACT

A one-step synthesis technique has been used to fabricate sensors by growing polyaniline nanofibers and polyaniline/metal nanocomposites in the active area of an interdigitated electrode array. Polyaniline nanofiber sensors can be fabricated by irradiating an aqueous precursor solution containing aniline, HCl, a metal salt, and ammonium persulfate (APS) with a high pressure Hg lamp. The sensors are ready for operation after polymerization is complete, and no additional processing steps are necessary. These sensors showed faster and more intensity response to various organic vapors than conventional bulk polyaniline sensors due to their larger surface area. A chemisorption model and a diffusion model were used to fit the sensor response of nanostructured polyaniline sensors. Both models can mathematically fit the sensor response as a function of time. Fitting errors from the two models were in a reasonable range, both allowing reasonable mathematical forms for the time-dependent and concentration behavior.

An oligomer-assisted polymerization method was carried out to synthesize polythiophene nanofibers. In this approach, a solution of thiophene, $FeCl_3$, and terthiophene was dissolved in acetonitrile. Compared to conventional chemical polymerization, a polythiophene oligomer, terthiophene or bithiophene, was added to assist the formation of nanofibers. The polythiophene collected after the 12 h reaction time was found to have nanofibrilar morphology with an average diameter of about 40-50 nm. Unlike other hard-template or soft-template techniques, this method does not require the introduction of a heterogeneous phase.

ACKNOWLEDGMENTS

This dissertation and my entire research process was made possible though the guidance, assistance, and support of many people. First of all, I would like to thank my advisor, Dr. Frank D. Blum, for his constant support and mentorship throughout my graduate studies at the Missouri University of Science and Technology. I am also very grateful for Dr. Massimo F. Bertino and Dr. Chang-Soo Kim's advice and guidance. I thank my advisory committee members, Dr. Robert W. Schwartz, Dr. Michael R. Van De Mark, and Dr. F. Scott Miller for their assistance and discussions.

I am grateful to members of Dr. Frank D. Blum's research group, Manikantan Nair, Piyawan Krisanangkura, Boonta Hetayothin, and Krunal Waghela for their help in experiments and discussions. Thank you all for wonderful parties and fun during the past four years! Barbara Harris's assistance in proofreading the research work is greatly appreciated. I am also grateful to Missouri University of Science and Technology's Department of Materials Science and Engineering, Department of Chemistry and the National Science Foundation for financial assistance.

Most of all, I must give the greatest thanks to my parents and my wife, Xiaohui Gu, for their abundant love, support, and encouragement throughout my life. I am also grateful to my friends in Rolla, Fei Ren, Xuan Gong, Tun Li, Lei Wen, and Jian Zhang for their help during my graduate study here.

TABLE OF CONTENTS

Page

LIST OF ILLUSTRATIONS

Figure Page

Section 2

Paper 1

Paper 2

Paper 4

LIST OF TABLES

NOMENCLATURE

Symbol	Description
σ	Conductivity
T	Temperature
r_0	Localization length
γ_0	phonon vibration frequency
k	Boltzmann constant
e	electron charge
β	electron-tunneling coefficient
δ	hopping distance
N	Avogadro number
M	molecular mass
R	gas constant
E_a	adsorption activation energy
E_d	desorption activation energy
θ	surface coverage
P	pressure
b	Langmuir adsorption constant
k_1	adsorption rate constant
k_{-1}	desorption rate constant
D	diffusion coefficient
t	time
C'_H	maximum sorption uptake

k_D	Henry's law dissolution constant
ΔG_v	volume Gibbs energy
γ	specific surface energy
I^*	nucleation rate
τ_a	adsorption time constant
τ_d	desorption time constant

SECTION

1. INTRODUCTION

A polymer is a molecule composed of a large number of covalently-bonded repeating structural units. Applications of polymers range from daily uses (e.g., plastics, rubbers, fibers, paints, adhesives, etc.) to cutting-edge uses (aircraft, bullet-proof vests, artificial joints, etc.). All polymers were thought to be excellent insulating materials until the 1970's, when Hideshi Shirakawa, Alan G. MacDiarmid, Alan J. Heeger and their coworkers reported the high conductivity of polyacetylene doped with AsF_5.[1,2] Since then, extensive research has been carried out on conducting polymers because of their excellent electrical and optical properties. These materials have broad application in areas ranging from anticorrosion coatings, to chemical sensors and biosensors, light-emitting devices, and solar cells, as well as many others.[3]

Polyaniline is one of the most common conducting polymers, which can be synthesized either by chemical oxidation polymerization[4-6] or electropolymerization[7]. Conventional chemical polymerization is conducted by polymerizing aniline monomers in the presence of a free radical activator. Polyaniline, prepared via chemical polymerization with a protonic acid, is typically called doped polyaniline or emeraldine salt. Generally, conventional bulk chemical synthesis produces only bulk-like polyaniline. One-dimensional (1D) nanostructures of conducting polymers such as nanowires, nanofibers, and nanotubes, have been intensively investigated because they possess superior properties due to their high surface area-to-volume ratio. In the past two decades, a variety of methods have been used to synthesize polyaniline nanofibers, including electrospinning[8], interfacial polymerization,[9] rapid-mixing,[10] nanofiber

seeding,[11] templates,[12] and surfactants,[13] or oligomer-assisted polymerization.[14] However, nanofiber devices suffer from a major problem, namely, the up-scalability of the fabrication processes. For instance, electrospinning and template polymerization can only produce a laboratory amount of polymer nanofibers. The interfacial polymerization requires toxic organic solvents. More importantly, nanofiber devices based on all these above methods have to be conducted in multi-steps. Therefore, it is still of interest to develop a facile, inexpensive, and environmental friendly one-step method to produce high-performance polyaniline nanofiber devices, such as sensors, biosensors, etc.

Polythiophene is another class of conducting polymer with a low band gap and high stability, both in the doped state and undoped state.[15] Similar to polyaniline, polythiophene can also be synthesized by chemical or electrochemical polymerization. Chemical polymerization can be simply carried out in an organic solution containing thiophene and $FeCl_3$, which can serve as both the oxidant and dopant. By substituting long flexible chains in the 3-position, high solubility (i.e. better processibility) can be achieved. Several organic solvent soluble[16-17] and even water-soluble[18] 3-substituted polythiophenes with high conductivities have been prepared. It was discovered that regioselectively synthesized Head-Tail (HT) poly(3-alkylthiophenes) possesses higher conductivity because of its homogeneous structure.[19] Regioregular poly (3-alkylthiophenes) nanofibers or nanowhiskers can be obtained by recrystallization from a saturated poly (3-alkylthiophenes) solution.[20-21] However, HT poly(3-alkylthiophenes) are generally produced by a Ni-catalyzed Grignard reaction of 2-iodo-3-alkylthiophenes. It has been reported that the addition of a 2,2'-bithiophene or 2,2':5',2''-terthiophene to the electropolymerization of 3-alkylthiophenes seems to reduce the number of head-to-head

linkages in polymer chains.[22] Polyaniline and polypyrrole nanofibers can be prepared by oligomer-assisted polymerization.[14,23] Thus, this oligomer-assisted polymerization may allow us to synthesize polythiophene and its derivative nanofibers for future applications in OLED, and solar cells.

A technique has been developed in our laboratory that allows the preparation and photopatterning of thin films of polyaniline nanofibers by UV-irradiation of an aqueous precursor solution.[24] These materials have been prepared in a one-pot, single-step synthesis. This dissertation demonstrates that our technique can be applied to fabricate sensors by growing nanofibers in the active area of an interdigitated electrode array. Typically, a polyaniline nanofiber sensor can be fabricated by irradiating an aqueous precursor solution of aniline, HCl, and ammonium persulfate (APS) with a high pressure Hg lamp. The sensors are ready for operation after polymerization is complete, and no additional processing steps are necessary. The responses to gases of sensors fabricated with bulk polyaniline and polyaniline nanofibers were compared. Due to their higher surface area, the response of polyaniline nanofibers was considerably faster and more intense than that of bulk polyaniline.

In addition to polyaniline nanofiber sensors, this technique can also be employed to fabricate nanofiber/Ag and nanofiber/Pt composite sensors. It have been observed that nanofiber sensors, with and without Ag or Pt particles, had a comparable response when exposed to toluene, an analyte that only induces swelling of the composites but does not alter doping or react strongly with nanoparticles of noble metals. When exposed to triethylamine, a weak base that can change the doping degree of polyaniline, the response time of Ag-containing composites was about 3 times faster than that of the nanofibers

alone and about 1.5 times faster than that of Pt-nanofiber composites. The change in resistivity was about 6 times larger for Ag nanocomposites and more than 4 times larger than for the Pt nanocomposites. The Raman spectra indicated that charge was transferred to Ag and to a lesser extent to Pt by the nanofibers. Exposure to triethylamine reduces the charge transfer and therefore the doping, thereby amplifying the response to the analyte. This shows a possibility that the response can be made more specific by adding to the composite nanoparticles of metals that interact strongly with the target analyte, and open the way tailoring response via multiplexing.

Although a large amount of research has been carried out in the field of conducting polymer sensors,[25-26] there are still some basic problems left unanswered, especially with respect to modeling of nanostructured conducting polymer sensors. The modeling of time-dependent sensor response is particularly relevant. In this work, a chemisorption model and a diffusion model were proposed to fit the sensor response against the exponential decay function. The equilibrium absorption amount, obtained by the chemisorption model, was found to obey a Langmuir isotherm, while the diffusion model predicted that the sorption undergoes a dual sorption process, i.e., Langmuir isotherm and gas dissolution. In addition, the diffusion coefficient obtained in the diffusion fit was found to increase with the vapor concentration, probably due to the swelling effect by organic vapors. Fitting errors from the two models were in a reasonable range, both allowing reasonable mathematical forms for the time-dependent and concentration behavior. The results also show the potential for studying the adsorption or diffusion process of conducting polymers based on conductivity measurements.

An oligomer-assisted polymerization method was carried out to synthesize polythiophene nanofibers. In this approach, a solution of thiophene, $FeCl_3$, and terthiophene was dissolved in acetonitrile. Compared to conventional chemical polymerization,[27] a polythiophene oligomer, terthiophene or bithiophene, was added to assist the formation of nanofibers. The polythiophene collected after the 12 h reaction was found to have nanofibrilar morphology with an average diameter of about 40-50 nm. The UV-vis and FT-IR spectra of polythiophene nanofibers are similar to those of conventional bulk polythiophene. Unlike other hard-template or soft-template techniques, this method does not require the introduction of a heterogeneous phase, which mostly can influence material properties. It has been demonstrated that this method can be utilized to prepare polythiophene nanofibers and this may lead to a broad application in the fabrication of polythiophene-based devices.

2. BACKGROUND INFORMATION

2.1. CONDUCTING POLYMERS

2.1.1. Basics of Conducting Polymers. When one thinks of polymers, one perhaps envisions common plastics or rubbers, which are very good insulators. Even many conducting polymers were well known in their nonconducting forms before their electrical properties were discovered. For instance, chemical oxidative polymerization of aniline was reported by Letheby as early as 1862.[28] However, it was not until a hundred years later, in the 1970s, that Hideshi Shirakawa, Alan G. MacDiarmid, Alan J. Heeger, and coworkers reported the high conductivity of polyacetylene. They discovered that after doping with AsF_5, the conductivity of cis-polyacetylene became about 220 S/cm at room temperature.[1,29] Since then many intrinsically conducting polymers with unique electrical and optical properties, such as polyaniline (PANI), polythiophene (PT), polypyrrole (PPy), and other related materials, have been synthesized. These polymers are often called "organic semiconductors" or "synthetic metals".

The electrical conductivity of conducting polymers results from mobile charge carriers introduced into the π-conjugated system that is formed by the continuous overlap of extended and delocalized p-orbitals along the polymer chain's backbone. However, conducting polymers without doping generally exhibit very low conductivity at room temperature. Their conductivity can be varied by adding a dopant to change the charge carrier density on the polymer backbone. It has been documented that the conductivity of those polymers ranges from 10^{-10} S/cm (an insulator) to about 10^{-5} S/cm (a semiconductor) to greater than 10^{4} S/cm (a metal), depending on the doping level.[3,30]

Therefore, it is important to understand why conductive polymers can alternatively behave as a metal, semiconductor, or insulator.

2.1.1.1. Band model. Materials in the real world can generally be classified into three categories according to their electrical conductivity: insulators, semiconductors, and conductors.

A band model explains why some materials conduct electrical charge, while some do not, as shown in Figure 2.1. According to the band model,[31-33] the overlapping of individual molecular electronic states can produce electronic bands. The valence electrons overlap to form a valence band, while electrons in the conduction band have higher energies, which are sufficient to allow electrons to move freely within the materials. The energy difference between these two bands is called band gap, generally denoted as E_g. In metal conductors, the valence band and the conduction band overlap; thus, electrons can move freely in a background of positive charge formed by the ion cores. The band gap of insulators is generally very high, resulting in a low conductivity at room temperature. If the band gap is small (e.g., 2 eV), the valence electrons can be excited into the conduction band by thermal or phonon excitation. The electrons then become mobile, and the material is termed a semiconductor. Thus, a conducting polymer, when in an appropriate oxidized or reduced state, is usually a semiconductor resulting from the extended π-conjugation. The overlapping of the π-bands is the valence band, and the π*-band is the conduction band in the conducting polymers. If the band gap is removed by further extending the π-conjugation, a conducting polymer can be as conductive as a metal.[34]

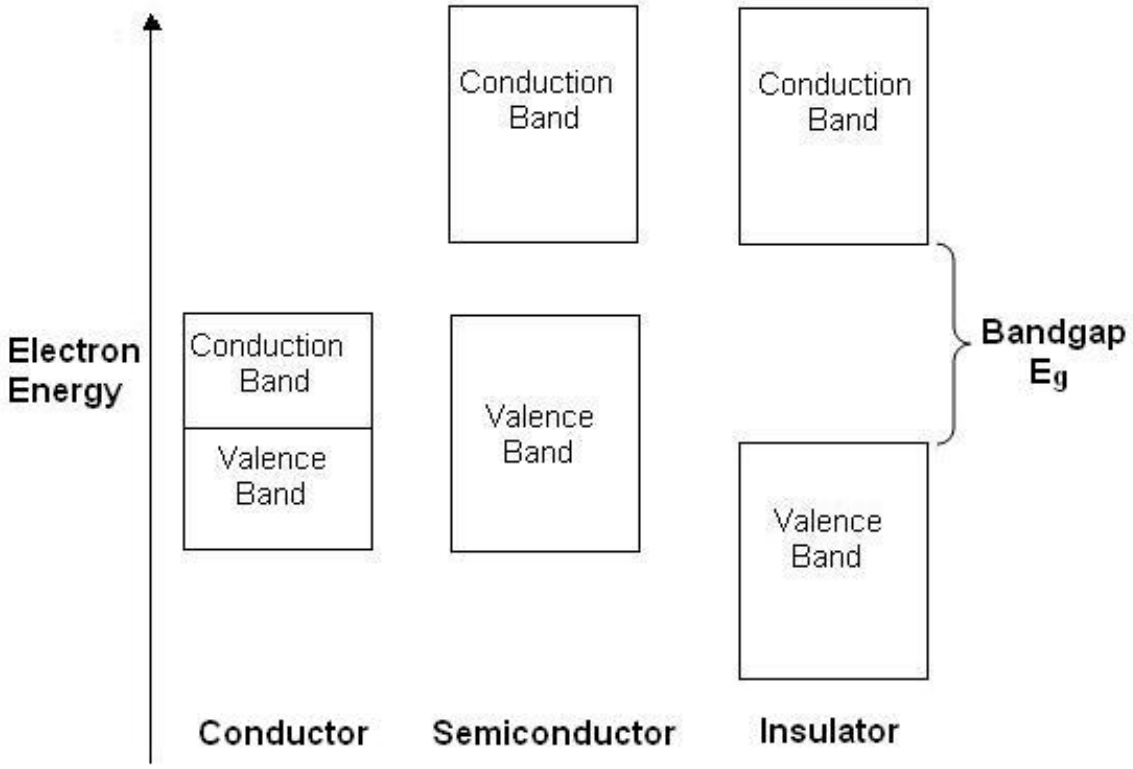

Figure 2.1. Schematic figure of band model.

2.1.1.2. Doping. Doping is the process of introducing impurities (dopants) as a means of increasing the conductivity of a material. The doping of conducting polymers implies (1) charge transfer (by oxidation, p-type doping or by reduction, n-type doping), (2) the associated insertion of a counter ion for the overall neutrality, and (3) the simultaneous control of chemical potential.[35-36] Primary doping can be accomplished chemically or electrochemically. The doping level depends on the type of dopant and on its distribution in the polymer.[37-39] P-type doping, achieved by chemical or electrochemical oxidation, is essentially the removal of electrons from the valence band, leading to the presence of positive charges on conducting polymers. Electrons can also be added to the conduction band, causing an n-type doping. P-type doping is generally more

common than n-type because most n-type doped conducting polymers are not as stable in the air due to oxidation by O_2.[40]

Charge carriers can be formed during doping by a redox reaction or protonation. The formation of a polaron results from local distortion of the conducting polymer structure, followed by removal of an electron. If another electron is further withdrawn from the valence band, a bipolaron can be generated. For trans-polyacetylene, two equivalents exist, (i.e., degenerate, ground-state structures), that differ only in the alternation of double and single bonds. Consequently, when a bipolaron structure is generated, they can readily separate (known as a soliton). Figure 2.2 shows an example of polaron and bipolaron structure for PANI.

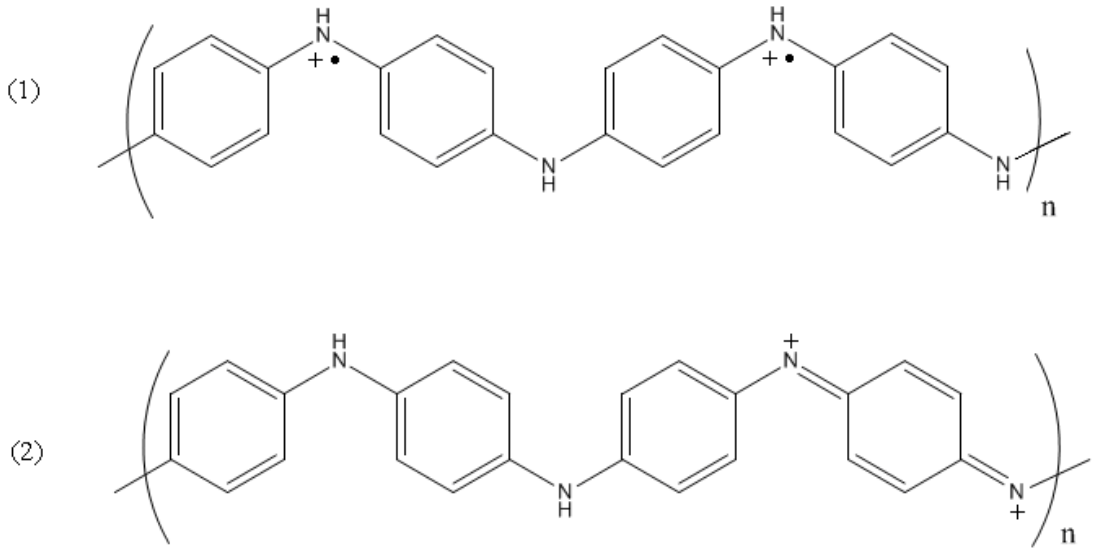

Figure 2.2. Schematic illustration of PANI repeating units for (1) polaron form and (2) bipolaron form.

2.1.1.3. Conduction model. Ideally, the conduction in conducting polymers can be described as the hopping of charge carriers, such as polaron, bipolaron, and soliton. Assuming that the electron hopping was dependent on the initial and final energy states between which hopping occurred, a VRH (Variable Range Hopping) model was proposed by Mott and coworkers.[41-42] This model successfully predicted the dependence of conductivity as a function of time for disordered semiconductors, such as α-Ge. This VRH model predicts that the conductivity can be expressed by:

$$\sigma = \sigma_0 \exp\left(-\left(\frac{T_0}{T}\right)^{\frac{1}{n+1}}\right) \qquad (2.1)$$

with:

$$T_0 = \frac{24}{(\pi r_0^3 k N(E_f)}$$

$$\sigma_0 = \frac{9}{4}\sqrt{\frac{3}{2}\pi e^2 \gamma_0 \sqrt{\frac{r_0 N(E_f)}{kT}}}$$

where n is the dimensionality of the material, r_0 is the localization length, k is the Boltzmann constant, γ_0 is the phonon vibration frequency (about 10^{12}-10^{13} Hz), e is the electron charge, $N(E_f)$ is the density of states at the Fermi level, and T is the temperature. This model has been widely used to study conductivity/temperature correlations in conducting polymers. For instance, the conductivity data of polyacetylene as a function of temperature were fit to a 3-D hopping model,[43] while for PANI, a quasi 1-D hopping model was found to fit with the experimental data.[44]

The conductivity of a conducting polymer is also dependent on the hopping distance, i.e., the interchain distance. It can be expressed as an exponential: [45-49]

$$\sigma = \sigma_0' \exp(-\beta\delta) \qquad (2.2)$$

where σ_0' is the preexponential constant, β is the electron-tunneling coefficient, δ is the hopping distance.

2.1.1.4. Synthesis of conducting polymers. Synthesis of conducting polymers generally consists of two classes:

- *Chemical*

In a typical chemical polymerization, a monomer, a dopant, and an oxidant are dissolved in a solution kept at a certain temperature. The polymerization mechanism is still uncertain. Many research groups have adopted the cation-radical mechanism even though there is disagreement about the steps involved in chain growth.[50-52] The monomer is first oxidized into a radical cation, which has several resonance forms of cations. The coupling of two radical cations results in a dimer. The dimer can then be oxidized into a dimer radical cation and continuation (propagation) of these reactions produces oligomers followed by polymers until termination of the chain. The polymerization time ranges from minutes up to a few days, depending on reaction conditions. The mixture is then filtered, washed, and dried to yield pure conducting polymers.

- *Electrochemical*

Similar to chemical polymerization, the radical cation is generated at the initial step via an applied potential. In a typical electrochemical route, a potential is applied across an electrolyte solution containing a monomer and a dopant. A three-electrode (working, reference, counter electrodes) or a two-electrode (working, reference electrodes) mode may be used. Electrochemical polymerization is convenient, since the polymer does not need to be isolated and purified.

As discussed above, in both polymerization cases, the initial step is the formation of the radical cation, followed by coupling reaction of radical cations.[53] A scheme of the polymerization is illustrated in Figure 2.3.

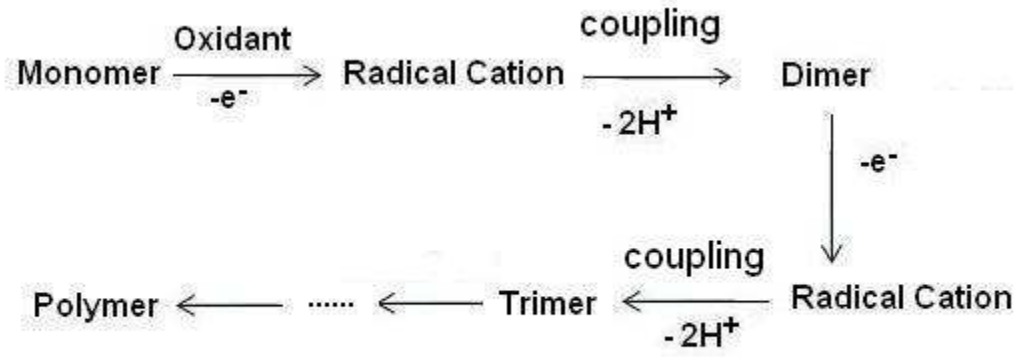

Figure 2.3. Polymerization scheme of a conducting polymer.

2.1.2. Classes of Conducting Polymers. Most common conducting polymers include polyacetylene, polypyrrole, poly(p-phenylene), polythiophene, PANI, etc. Emphasis in this thesis is placed on PANI and polythiophene because they are the target materials of our work.

2.1.2.1. Polyaniline. Polyaniline (PANI) is one of the most widely studied conducting polymers because of its inexpensive cost, facile synthesis, and easy doping/dedoping. PANI, also known as aniline black, was first discovered as a dye and has been studied over 100 years. It was not until the middle 1980's that its chemical and electrical properties were reported.[4,7,44,54] PANI can exist in several different oxidation states, fully reduced leucoemeraldine, protoemeraldine, emeraldine, nigraniline, and fully oxidized pernigraniline.[5] However, the fully oxidized and reduced state of PANI is not conducting. Only when the moderately oxidized states (especially the emeraldine form) are doped, does PANI become conductive. The structure of PANI in different forms is shown in Figure 2.4.

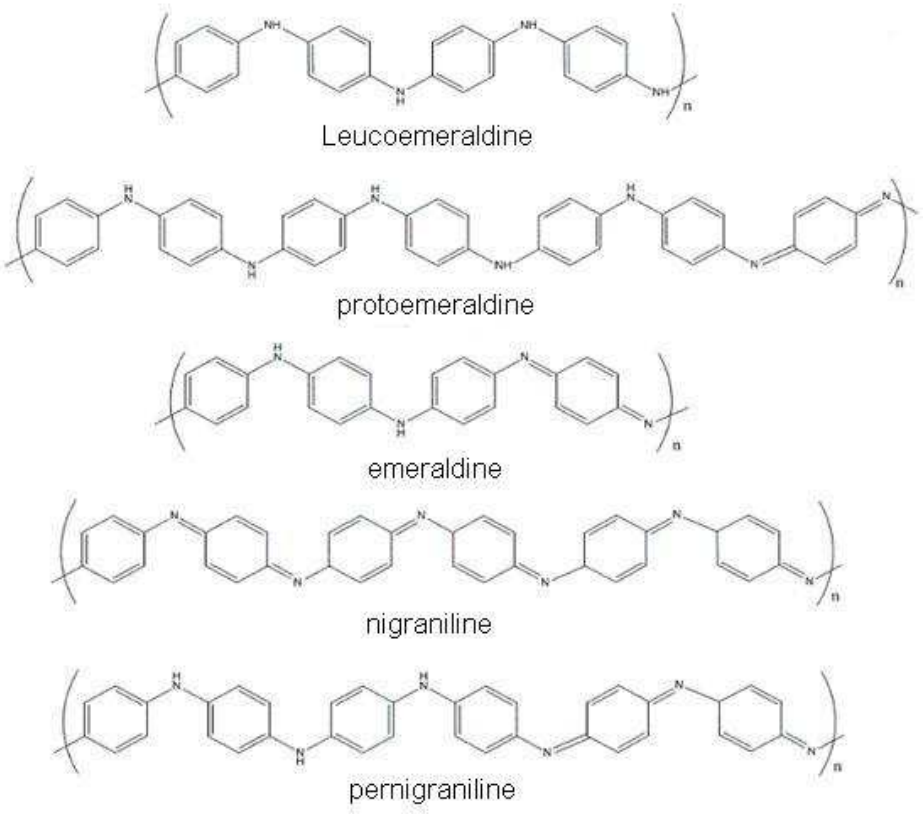

Figure 2.4. Different oxidized states of PANI.

PANI can be synthesized chemically[4] or electrochemically[55]. Conventional chemical polymerization is conducted by polymerizing an aniline monomer in the presence of an oxidizer. PANI prepared via conventional chemical polymerization with protic acid is doped PANI or emeraldine salt. An emeraldine base can be obtained by dedoping an emeraldine salt with a basic compound. Reverse switching between emeraldine salt and emeraldine base can be achieved via the protonation and deprotonation process, as illustrated in Figure 2.5. The conductivity of PANI varies with the doping level, which is the protonation degree of imine groups (-N=) adjacent to quinoid groups ().

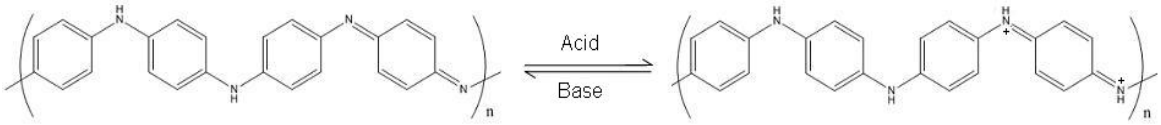

Figure 2.5. Schematic illustration of the doping and dedoping process by an acid or a base.

2.1.2.2. Polythiophene. Polythiophene (PT) is one of the earliest studied conducting polymers with a low band gap (i.e., 2eV for unsubstituted PT). From a theoretical viewpoint, PT has been often considered as a model for the study of charge transport in conducting polymers. It has a nondegenerate ground state and good environmental stability for both doped and undoped states which has led to various applications in electronic devices.[56] Similar to PANI, PT can be prepared via a chemical or electrochemical route. Although electrochemical polymerization was found to be the quickest way to obtain highly conductive PT, chemical polymerization methods are still

preferred due to simple synthetic routes and the absence of electrochemical instruments. Grignard coupling of 2,5-dihalothiophenes in the presence of transition metal complexes has been extensively employed for the synthesis of PTs. Later, chemical oxidative polymerization of bithiophene[57] and thiophene[27,58] was carried out using copper(II) perchlorate and ferric chloride, respectively. The structure of PT consists of repeating thiophene units linked at the 2- and 5- positions, as shown in Figure 2.6.

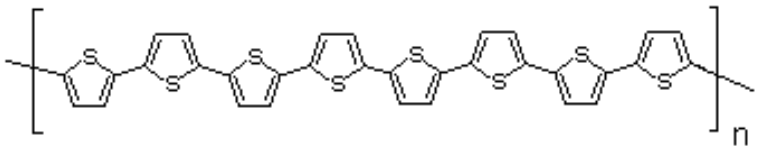

Figure 2.6. Chemical structure of PT.

The solubility of PT, however, is very poor in most common solvents. 3-alkyl substituted polythiophene had been synthesized to increase the solubility with the sacrifice of some conductivity.[16-17,59] The substitution of thiophene by electron-donating groups can produce a decrease in the oxidation potential and hence a stabilization of the corresponding radicals. Molecular design of novel 3-position substituted PT can result in polymers with a smaller band gap.[60] There is an interesting relationship between the optical properties of conducting polymers and the band gap E_g. If E_g is greater than 3 eV, the undoped insulating polymer is almost transparent while, after doping, the conducting polymer is typically absorbing in the visible region. If, however, E_g is small (i.e., 1.0-1.5 eV), the undoped polymer will absorb visible light whereas, after doping, visible absorption will be very weak.[56] This renders the possibility of developing conducting polymers that are transparent in the visible region by 3-position substitution of PT.

2.1.3. Nanostructured Conducting Polymers. Low dimensional nanoscale materials, especially "pseudo" 1-dimensional nanostructures, have attracted considerable attention in recent years.[61] Nanostructured conducting polymers, such as nanorods, nanowires, nanofibers or nanotubes, have shown significant advantages in field-effect transistors, sensing, and catalytic applications over conventional bulk PANI due to their large surface areas.[62-66] A variety of methods have been carried out to synthesize conducting polymer nanofibers. Physical methods, such as electrospinning, have been developed.[67-68] Template-synthesis procedures have also been employed using different templates, such as porous alumina and polycarbonate membranes, to control the morphology of the polymer. [12,69] In order to simplify template removal, hard templates were replaced by soft templates, such as surfactants and micelles.[13,70] Recently, research has been focused on template-less synthesis methods, such as interfacial polymerization,[9] rapid-mixing,[71] dilute polymerization,[72] oligomer-assisted polymerization,[14,23] and nanofiber seeding.[11,73-74] In our group, we have developed a one-step synthesis of PANI nanofibers by irradiating precursor solutions with gamma-rays or UV-irradiation.[24,75]

Some properties of conducting polymer matrix nanocomposites have been studied in detail. Novel properties of PANI nanocomposites can be derived from the successful combination of the nanostructured PANI with other nanomaterials. Generally, the inorganic nanoparticles used to meet specific requirements include silica,[76] conducting metals (Au, Ag, Pd, Pt),[77] magnetic particles,[78] metal oxide,[79] and carbon nanotubes.[80] These materials have shown very promising applications in batteries, field-effect transistors, electrochromic devices, non-volatile memories, nonlinear optics, sensors, etc.[81]

2.2. SENSORS

A sensor is a device that can detect a physical, chemical, or biochemical quantity and transduce it into a signal, which can be analyzed by an observer or an instrument.[82] Sensors have been widely used in many areas, such as environmental monitoring, imaging, manufacturing, medical and biological applications.[83] At present, sensors chiefly consist of the following: 1) electrochemical, 2) optical, 3) electromechanical, and 4) thermal etc. The working sequence and classification of sensors are shown in Figure 2.7. Sensors have been fabricated using a variety of candidate materials, such as metal oxide,[84] carbon nanotube,[85] and polymers,[86] etc. Recently conducting polymers, especially PANI, have been investigated for sensor application because of their fast response and sensitivity to many chemical species.[25,87]

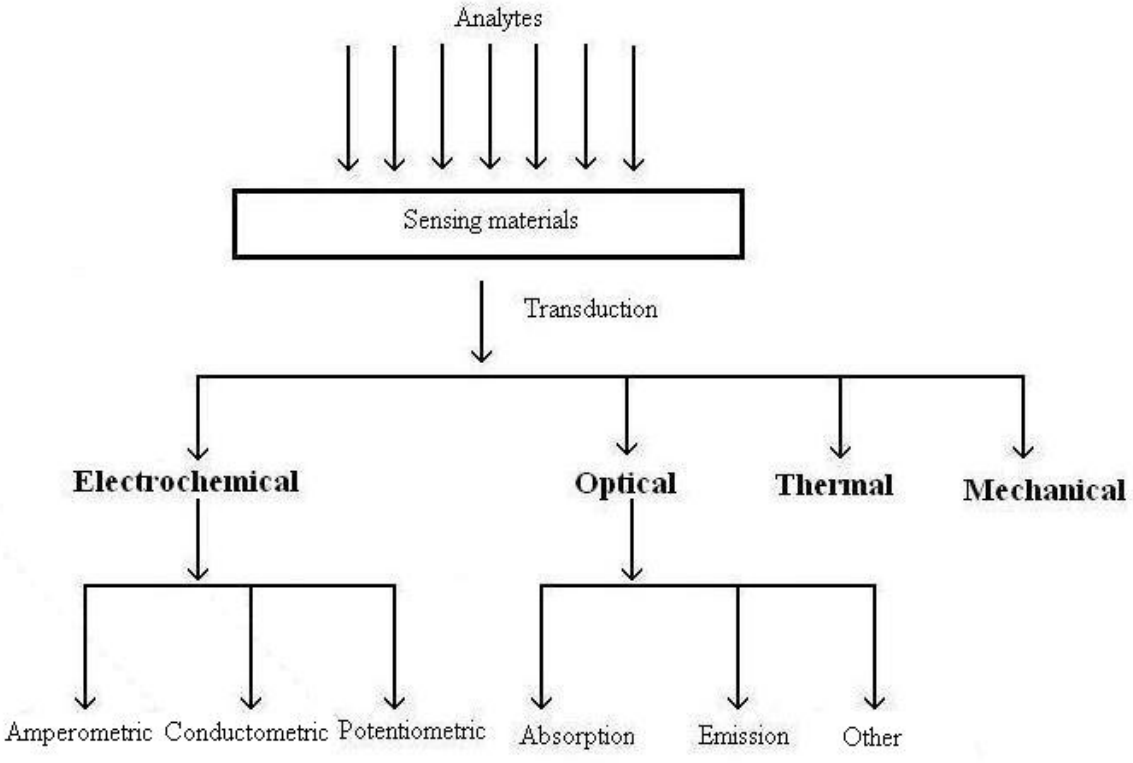

Figure 2.7. Working sequence and classification of sensors.

2.2.1. Conductometric Gas Sensors. Conductometric mode is the most widely employed for gas sensors based on PANI. A typical conductometric gas sensor consists of a substrate, electrodes, and the polymer selective layer, as shown in Figure 2.8. A constant voltage is applied between these electrodes and the change in current is monitored by an electrometer.

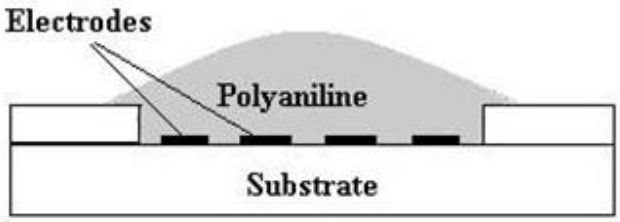

Figure 2.8. The schematic configuration of a PANI gas sensor.

As discussed in the previous section, the conductivity originates from the delocalization of the π-conjugation structure. The conductivity of PANI depends on both the ability to transport charge carriers along the polymer backbone and the capability of the carriers to hop between polymer chains. Consequently, any interaction with PANI that alters either of these processes will influence the conductivity. PANI is a special conducting polymer because its doped state can be easily controlled by acid/base reactions, which makes PANI a promising sensing material for detecting acidic and basic gases. PANI-based ammonia sensors have been fabricated and characterized by many groups.[88-90] Oxidative gases, such as NO_2 and I_2, can be detected by PANI because they can remove electrons from the polymer backbones of PANI, resulting in increased conductivity.[91] PANI is also sensitive to organic solvents, such as benzene, chloroform, and toluene, which can swell the polymer chains, thereby decreasing the conductivity.[92-93]

The use of nanostructured PANI is beneficial in gas sensing applications, because the higher surface area and porosity makes gas molecules diffuse more easily into the PANI structure. Several techniques have been developed to prepare a nanostructured PANI thin film. Typical PANI sensors are fabricated by depositing a thin film of PANI on the electrodes. Electrochemical deposition is one method of doing this and the thickness of the film can be easily controlled by the total charge during the fabrication.[94] Other methods, such as self-assembly,[95] ink-jetting,[96] and dip-pen nanolithography,[97] can also be used to fabricate PANI nanofiber-based devices. Unfortunately, most of these techniques are very complex and time-consuming, thus a simple inexpensive technique for fabricating and incorporating nanostructured PANI into electronic devices is in great demand.

2.2.2. Optical Sensors. Much attention has been paid to optical sensors recently because of their fast responses and promising applications in remote sensing.[98] Optical sensors are generally based either on measuring an absorption intensity change in one or more light beams (UV, visible or IR) or on observing emission intensity changes (Luminescence, Raman Scattering). Techniques used in the case of intensity sensors include light scattering (both Rayleigh and Raman), spectral transmission changes (i.e., simple attenuation of emitted light due to absorption), and spectral emission changes. For example, PANI-based optical sensors using visible and Near IR absorption have been fabricated and analyzed.[99-100]

2.3. ADSORPTION

Adsorption is a process of binding one or more components in an interfacial layer. Adsorption can be classified into two classes depending on the activation energy: physisorption and chemisorption. They can be distinguished as follows:[101-103]

1) Physisorption is generally a phenomenon with a relatively low specificity, while chemisorption is dependent on the reactivity of the adsorbent and adsorbate.
2) Chemisorbed molecules are bonded to reactive sites on the surface, and the adsorption is confined to a monolayer. Physisorption can occur as a multilayer.
3) Activation energy is often involved in chemisorption and, at a low temperature, the system may not have sufficient energy to achieve thermodynamic equilibrium. Physisorption systems generally attain equilibrium fairly rapidly, but the equilibration may be slow if the transport process is rate-limiting.

2.3.1. Chemisorption. Chemisorption basically follows the following processes. The first process is that the adsorbate particle makes contact with the surface. The particle needs to be trapped onto the surface and the probability of an impinging molecule losing enough kinetic energy to trap in a molecularly adsorbed state is called the condensation coefficient. Then the adsorbate reacts with the surface site or simply desorbs. The adsorption rate constant is given in Eq. 2.3.

$$k = \frac{Nc\sigma}{\sqrt{2\pi MRT}} \exp\left(-\frac{E_a}{RT}\right) \qquad (2.3)$$

where N is Avogadro's number, c is the condensation coefficient, σ is the surface area occupied by an adsorbed molecule, M is the molecular mass of the adsorbate, T is the temperature, R is the gas constant, and E_a is the adsorption activation energy.

The rate of adsorption is then

$$R_a = \frac{d\theta}{dt} = kf(\theta)P \quad (2.4)$$

where θ is the surface coverage, P is the vapor pressure of the gas, and f(θ) is the fraction of available surface taken to be (1-θ) in the simple Langmuir derivation.

The desorption activation energy can be much larger than these for adsorption. The desorption rate can be written in the form of

$$R_d = -\frac{d\theta}{dt} = \frac{1}{\tau_0} f'(\theta)\exp\left(-\frac{E_d}{RT}\right) \quad (2.5$$

where τ_0 is the residence time of the adsorbate molecules, f'(θ) is equal to θ in this case, and E_d is the desorption activation energy.

2.3.2. Langmuir Adsorption Isotherm. Langmuir Isotherm is the most commonly used isotherm in chemisorption.[104] The derivation was essentially given by Langmuir in 1918. The surface of an absorbent is assumed to consist of a certain number of sites S of which S_1 is occupied and S_0 is free. The rate of evaporation is taken to be proportional to S_1 and the rate of condensation is taken to be proportional to S_0 and the gas pressure. Thus, at equilibrium,

$$k_1 S_1 = k_2 P S_0 = k_2 P(S - S_1) \quad (2.6)$$

where k_1 is the rate constant of evaporation and k_2 is the rate constant for condensation. Since $S_1/S = \theta$, the Eq. 2.6 can be written in the form

$$\theta = \frac{bP}{1+bP} \quad (2.7)$$

where

$$b = \frac{k_2}{k_1} \quad (2.8)$$

In most cases, the complete adsorption (100%) can not be achieved. Then Eq. 2.7 can be written as

$$\theta = \frac{M_0 bP}{1+bP} \tag{2.9}$$

where M_0 is the maximum adsorption amount.

2.4. DIFFUSION IN POLYMERS

2.4.1. Fick's Law. Diffusion is a process of a random transport of something from one part of a system to another, such as molecular diffusion and heat diffusion.[105] The fundamental equations of diffusion were derived in 1855 by Adolf Eugen Fick based on the mathematical equation of heat conduction.[106] The theory proposed that the rate of diffusion in isotropic substances through the unit area of a section is proportional to the concentration gradient normal to that section, or:

$$J = -D\left(\frac{\boldsymbol{dc}}{\boldsymbol{dx}} + \frac{\boldsymbol{dc}}{\boldsymbol{dy}} + \frac{\boldsymbol{dc}}{\boldsymbol{dz}}\right) \tag{2.10}$$

where D is the diffusion coefficient, c is the concentration of diffusant, t is the time, and x is the space coordinate measured as normal to the section. This equation is called Fick's first law.

Considering that there is an equilibrium between the rate of diffusion substance in a three dimensional space and the amount of diffusion substance increase, Fick's second law can be obtained in the form of

$$\frac{dC}{dt} = \frac{d}{dx}\left(D\frac{dC}{dx}\right) + \frac{d}{dy}\left(D\frac{dC}{dy}\right) + \frac{d}{dz}\left(D\frac{dC}{dz}\right) \tag{2.11}$$

When the diffusion occurs in a cylinder, the equation may be transformed by setting:

$$x = r\cos\theta,$$

$$y = r\sin\theta,$$

one can attain the equation for diffusion in a cylinder, in spherical-polar coordinates:

$$\frac{dC}{dt} = \frac{1}{r}\frac{d}{dr}\left(rD\frac{dC}{dr}\right) \quad (2.12)$$

Diffusion Coefficient may be dependent on the penetrant concentration depending on the interaction between the penetrant and, for example, a polymer. For instance, if the penetrant diffusion rate is much less than that of the relaxation of the polymer chain, solution equilibrium can be rapidly established, leading to no dependence on swelling kinetics. On the other hand, if the diffusion and the relaxation rates are comparable, the penetrant sorption may then be complicated by a strong dependence on swelling kinetics.

2.4.2. Sorption Isotherm. Barrer et al. in 1958 suggested a dual sorption model to describe the sorption isotherms of small gas molecules in polymers.[107] In glassy polymers, there exists a distribution of "holes" frozen in the structure. These "holes" can immobilize a portion of penetrant molecules by entrapment or by binding at high energy sites at their molecular peripheries (similar to adsorption). Therefore, this model consists of two concurrent mechanisms of sorption: ordinary dissolution and "hole-filling". The equilibrium sorption uptake can be expressed by the following equation:[108-109]

$$C = C_D + C_H = k_D P + \frac{C_H' bP}{1+bP} \quad (2.13)$$

where k_D is the Henry's law dissolution constant, P is the vapor pressure of the penetrant, C_H' is the maximum uptake in holes, b is the hole affinity constant. The first term C_D represents sorption of normally diffusible species, while the second term C_H represents the sorption in "holes".

2.5. NUCLEATION

2.5.1. Homogeneous Nucleation. Homogeneous nucleation occurs when no foreign nuclei or surfaces are present. The growth process of nuclei is shown in Figure 2.9. The Gibbs energy ΔG of a nucleus initially increases with size and then decreases. The maximum in ΔG corresponds to the critical size nucleus.[110-111]

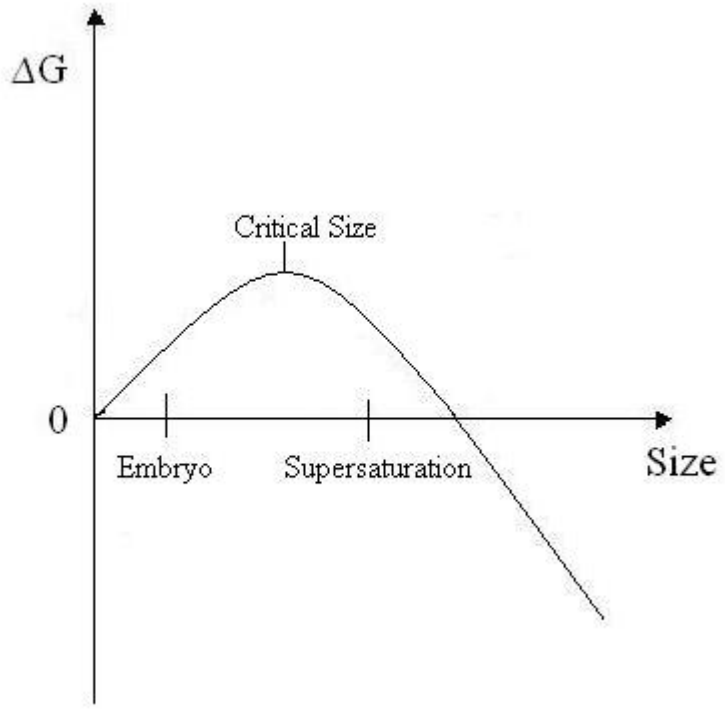

Figure 2.9. The Gibbs Energy of a nucleus as a function of size during the nucleation.

The Gibbs free energy of a nucleus can be given by

$$\Delta G = V\Delta G_v + A\gamma \qquad (2.14)$$

where ΔG_v represents the volume Gibbs Energy, V is the volume of a nucleus, A is the surface area of a nucleus, and γ stand for the specific surface energy. Thus, the Gibbs

Energy of a nucleus of critical size, ΔG^*, can be computed by differentiation of Eq. 2.14 with respect to the size of nucleus r.

$$\frac{d\Delta G}{dr} = 0 \text{ at } \Delta G = \Delta G^* \quad (2.15)$$

The rate of nucleation I^* has been derived by Turnbull and Fisher using the absolute reaction rate theory to be[112]

$$I^* = \frac{NkT}{h} \exp\left(-\frac{\Delta G^* + \Delta G_\eta}{kT}\right) \quad (2.16)$$

with N standing for the number of uncrystallized elements and ΔG_η representing Gibbs Energy that governs the short distance diffusion of the crystallizing element across the phase boundary. ΔG_η, similar to viscosity, is expected to be dependent on temperature, expressed by:

$$\frac{\Delta G_\eta}{kT} = a + \left[\frac{b}{T - T_0}\right] \quad (2.17)$$

2.5.2. Nucleation of Polymers. Different from the nucleation of small molecules, homogeneous nucleation can involve only one part of one macromolecule or even several portions of several macromolecules. Oligomers of appropriate length have to be polymerized first before nucleation can proceed. Macromolecules basically can follow four nucleation paths: 1) intermolecular fringed micelle nucleus, 2) intramolecular folded chain nucleus, 3) intermolecular oligomer nucleus, and 4) intramolecular folded chain nucleus of a polymerizing molecule.[113] For nucleation of molecules grown from the monomer during the polymerization, paths 3 and 4 are of importance in this study. The monomer size is much smaller than the dimensions of the critical nucleus. Thus, a certain concentration of at least oligomers must be formed before intermolecular oligomer nucleation can occur. Two examples of nucleation during polymerization of phosphate and formaldehyde have been studied by Wunderlich.[114] Intermolecular oligomer

nucleation has been proposed to explain the nucleation process during polymerization of polyphosphates. The oligomer nucleus, especially if it were rigid, would be expected to have a cylinder-like shape and active growth sites at the chain ends. One-dimensional growth is favored when further nucleation of additional molecules on the nucleated crystal is inhibited. It has been also pointed out that the greater the value of end surface energy of a nucleus, $\gamma_{e,}$ is relative to the side surface energy, γ, the more fibrous will be the shape of the nucleus.

PAPER

1. ONE-STEP FABRICATION OF A POLYANILINE NANOFIBER GAS SENSOR

Zhe-fei Li[a], Frank D. Blum[a,b,*], Massimo F. Bertino[c], Chang-Soo Kim[d,e], and Sunil K. Pillalamarri[b,f]

[a] Department of Materials Science and Engineering, Missouri University of Science and Technology[‡], Rolla, MO 65409

[b] Department of Chemistry, Missouri University of Science and Technology[‡], Rolla, MO 65409

[c] Department of Physics, Virginia Commonwealth University, Richmond, VA 23824

[d] Department of Electrical and Computer Engineering, Missouri University of Science and Technology[‡], Rolla, MO 65409

[e]Department of Biological Sciences, Missouri University of Science and Technology[‡], Rolla, MO 65409

[f]current address: Freescale Semiconductor, Austin, TX

[‡] formerly University of Missouri-Rolla

1. ABSTRACT

A single-step, bottom-up technique has been used to fabricate sensors, based on conducting polymer nanofibers. A small amount of an aqueous solution of aniline, a

dopant, and an oxidant was placed on an interdigitated electrode array. Ultraviolet (UV)-irradiation of the solutions affected polymerization, yielding a highly porous film of polyaniline nanofibers with a mean diameter of around 100 nm and a length on the order of 1 μm. Solutions that were not irradiated formed bulk-like polyaniline (PANI) films. Nanofibers and bulk polyaniline sensors were exposed to chloroform, a weak proton donor; toluene, a vapor that causes polymer swelling; and to triethylamine, which alters the doping level. Because of their higher surface areas, the response times of the fiber sensors were about a factor of 2 faster, with the current variations up to 4 times larger than those of the bulk polyaniline sensors. These results suggest methods for the advancement of simple and environmentally-friendly production of organic nanofiber-based sensors and electronic devices.

Keywords: polyaniline, nanofibers, sensors, nanomaterials

2. INTRODUCTION

A large amount of basic and applied research is currently being conducted on nanofibers of electrically conducting polymers. From the basic science viewpoint, fibers represent an ideal candidate for the study of low-dimensional electric conductors. On the applied side, fibers are being used to fabricate electronic devices such as sensors [64,87,115-116], diodes [117], transistors [118-120], logic gates [121], non-volatile memories [122-123], and photoelectrochromic cells [124-125]. Reviews have appeared recently that focused on the basic [126] and the applied side [127] of this field, respectively.

While extremely promising, nanofiber devices suffer from a major problem, namely, the up-scalability of the fabrication processes. For example, field effect transistors have been fabricated by electrospinning, a technique that can hardly be used on large scale [128]. Non-volatile memories have been fabricated with a series of top-down fabrication steps that include synthesis of polyaniline (PANI) fibers with an interfacial method, followed by decoration of the fibers with Au nanoparticles and spin coating of the composites to obtain films [122]. The limited solubility of polyaniline and the use of toxic solvents, makes this approach difficult to scale-up. Large-scale applications of nanofiber technology would clearly benefit from a technique that was bottom-up in character and compatible with microfabrication techniques.

A technique was recently developed in our laboratories that allows the preparation and photopatterning of thin films of polyaniline nanofibers by UV irradiation of an aqueous precursor solution [24]. In this work, we demonstrate that the technique can be applied to fabricate sensors by growing nanofibers in the active area of an interdigitated electrode array. The sensors are ready for operation after polymerization is complete, and

no additional processing steps are necessary. The responses to gases of sensors fabricated with bulk polyaniline and polyaniline nanofibers were compared. Due to their higher surface area, the response of polyaniline nanofibers is considerably faster and more intense than bulk polyaniline. Our results show that nanofiber-based devices can be produced by our bottom-up lithographic technique, and that the resulting material has superior features.

3. EXPERIMENTAL

1. Materials. Aniline and chloroform were purchased from Alfa Aesar. Ammonium persulfate (APS), nitric acid, hydrochloric acid, and toluene were obtained from Fisher Scientific. Triethylamine was from Lancaster Synthesis. All chemicals were used as received, except for aniline which was distilled before use.

2. Synthesis of bulk polyaniline and polyaniline nanofibers. Polyaniline was synthesized by in-situ chemical oxidation polymerization of aniline with ammonium persulfate as the oxidant. The reactions were performed based on 10 mL precursor solutions containing distilled water with aniline (0.1 M), hydrochloric acid (0.1M), and ammonium persulfate (APS, 0.05 M). Nitric acid or benzoyl peroxide could also be used as the dopant or oxidizer, respectively. Polyaniline nanofibers were prepared by exposing the precursor solution to UV light for 30 min. Bulk polyaniline was obtained by the same procedures except without UV-irradiation.

3. Fabrication. Interdigitated gold microelectrode sensors were fabricated as follows. Flexible Kapton® substrates (duPont), were cleaned in successive rinses of acetone, methanol, and deionized water, and then dehydrated in an oven. A thin film of

chromium as an adhesion layer, followed by a 0.2 µm film of gold was deposited on the substrate by DC magnetron sputtering. Positive photoresist (Shipley) was spin-coated, selectively exposed through the photomasks with broad-band UV light, and developed to pattern the electrode features. The gold/chromium layers were etched chemically by immersion in etching solutions. After removal of the photoresist with the stripper, the substrate was cleaned with organic solvents and dehydrated in preparation for the application of the polyimide passivation layer to define active areas of microelectrodes. Photosensitive polyimide (HD Microsystems) was spin-coated to a thickness of about 2.0 µm and exposed to UV in the same manner as the photoresist. Subsequent development and thermal curing of the polyimide defined the gold microelectrodes. An image of the fabricated array is shown in Figure 1.

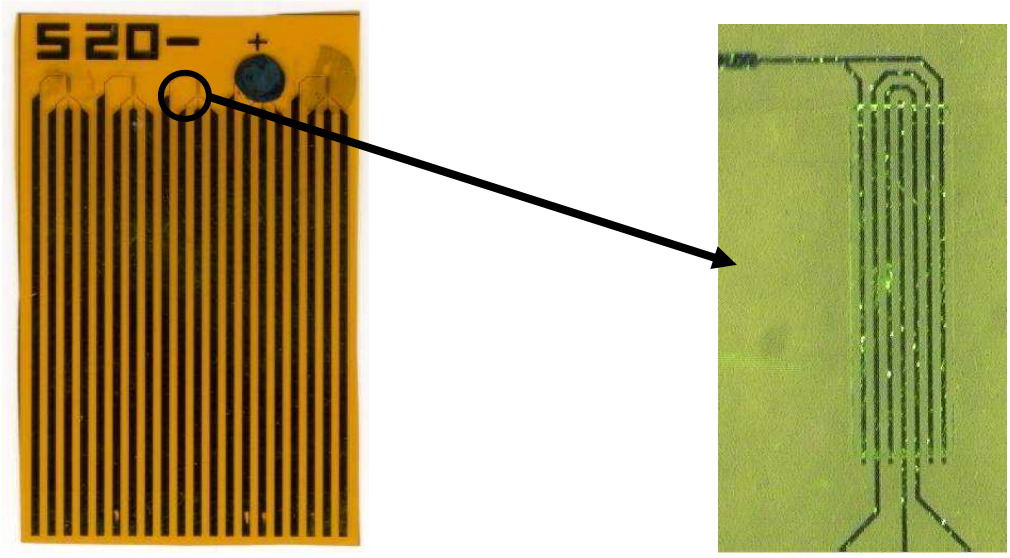

Figure 1. Image of five gold microelectrodes sensors (left) taken with an optical scanner and magnified view (right) of interdigitated microelectrodes taken with an optical microscope. The active array area had a length of 1,000 µm, the width of each electrode was 20 µm, and the spacing between the electrodes was 20 µm.

Sensors were fabricated by placing a 10 μL drop of precursor solution on the active area of an interdigitated microelectrode array. Immediately after preparation, the precursor solution was deposited on the substrate and illuminated with ultraviolet (UV) light from a high pressure, 100 W Hg lamp (Midwestern Instruments). The total reaction and exposure time was about 30 min. After the reaction (approximately 30 min), the film was washed with water and then dried at room temperature before measurement.

4. Characterization. For the solvents reported here, argon gas was passed through a bubbler containing neat liquid samples and then over the sensor. The concentration of gases was determined by:

$$C = (M/\rho)/[(M/\rho) + L)] \quad (1)$$

where M is the weight loss rate of the liquid sample (in g/min), ρ is the density of vapor sample (in g/L), and L is the argon gas flow rate (in L/min).

The changes in current for bulk polyaniline and polyaniline nanofiber thin film sensors were measured at room temperature. The real-time current changes were monitored by a Keithley 617 programmable electrometer to bias the anode to 0.1 V versus the cathode. The morphology was characterized by a Hitachi S-4700 scanning electron microscope (SEM) operated at accelerating voltages of 2 kV and 5 kV.

4. RESULTS AND DISCUSSION

Polyaniline films were produced on the interdigitated electrodes with and without UV irradiation. Figure 2a shows the typical morphology of polyaniline films that were made without irradiation (these will be referred to us unirradiated samples). These films

had a granular bulk-like structure. A fiber-like morphology started developing in samples illuminated for 5 to 10 min as shown in Figure 2b, and was completed after illumination for ca. 30 min, as shown in Figure 2c. The mean thickness of the films was about 4 μm for unirradiated polyaniline and about 8 μm for samples irradiated for about 30 min. The larger thickness of the irradiated samples was consistent with their porosity. The bulk-like and fibrous polyaniline structures were similar to those previously reported by our group [24]. It has been previously shown that γ-irradiation can also produce similar, but not identical structures [129].

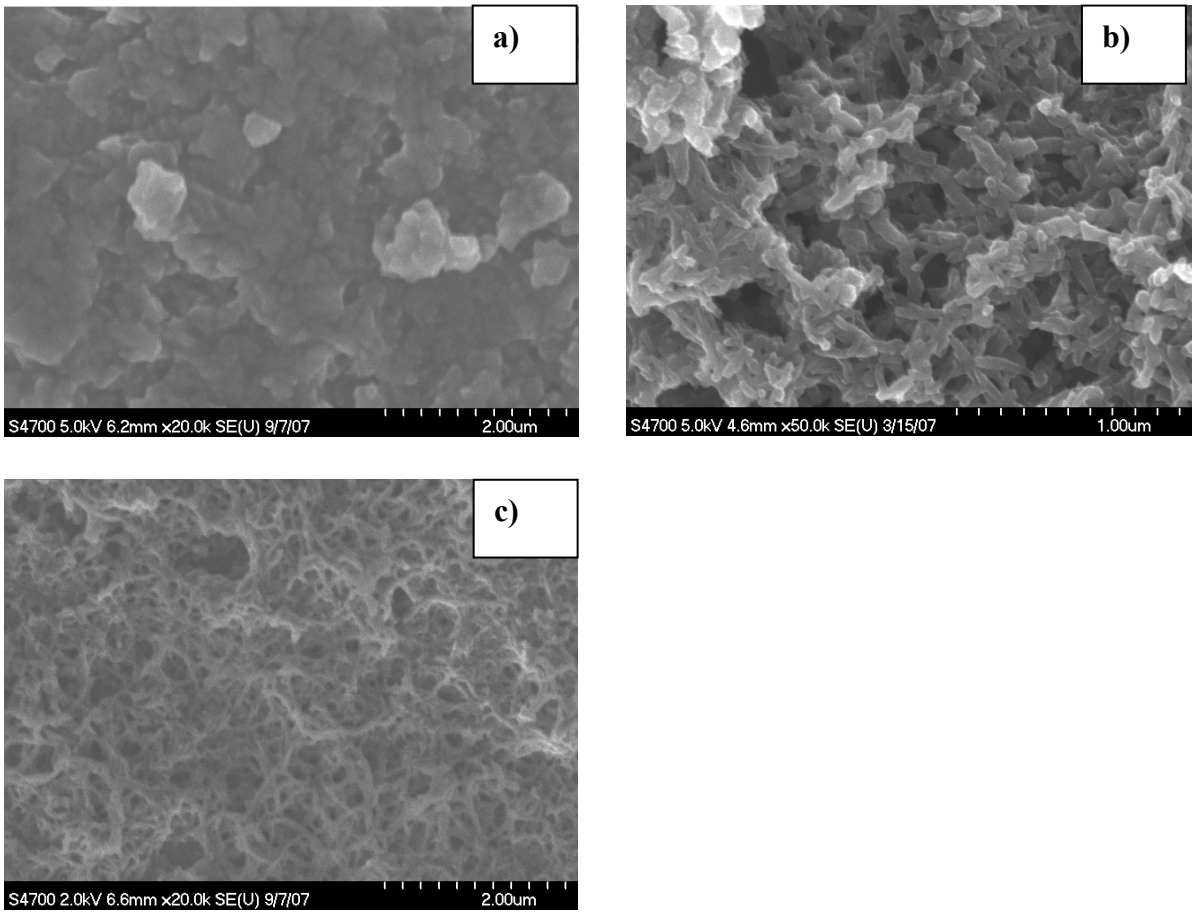

Figure 2. Scanning electron microscope images of films deposited on interdigitated electrodes: a) unirradiated film; b) after 5 min of UV exposure; and c) 30 min of UV exposure.

Sensors made with bulk polyaniline and polyaniline nanofibers were exposed to various gases using Ar as the carrier gas. The response depended on the type of vapor and sensor used. Shown in Figure 3 are the responses of the sensors to chloroform vapor, plotted in terms of the normalized current (I_{norm}(t), current/current at the beginning of the experiment). While the absolute current magnitude depended on the details of the sensor production, etc., the values of the normalized currents were very reproducible. The currents typically ranged from 1 to 200 μA with the currents for the nanofiber sensors being higher. Both sensors had relatively rapid responses, with the response to the chloroform being stronger and faster in the nanofiber sensor. The response of the sensors to chloroform was modeled with a single exponential decay in the form of:

$$I_{norm}(t) = (1 - I_{\infty}) \exp(-t/\tau) + I_{\infty} \quad (2)$$

where I_{∞} is the normalized current after the sensor has stabilized under the vapor of interest (i.e., $I_{\infty} = I_{norm}(t)$ when $t=\infty$). The results of the fitting to the model are also shown in the curves. In the case of chloroform, the I_{∞} is rather high. The results of the fitted parameters are also shown in Table 1. Alternately, we define the response time, $\tau_{response}$ as the time to reach 90% of the total change of $(1 - I_{\infty})$ to chloroform; the response times for bulk polyaniline and polyaniline nanofibers were around 100 seconds and 50 seconds, respectively.

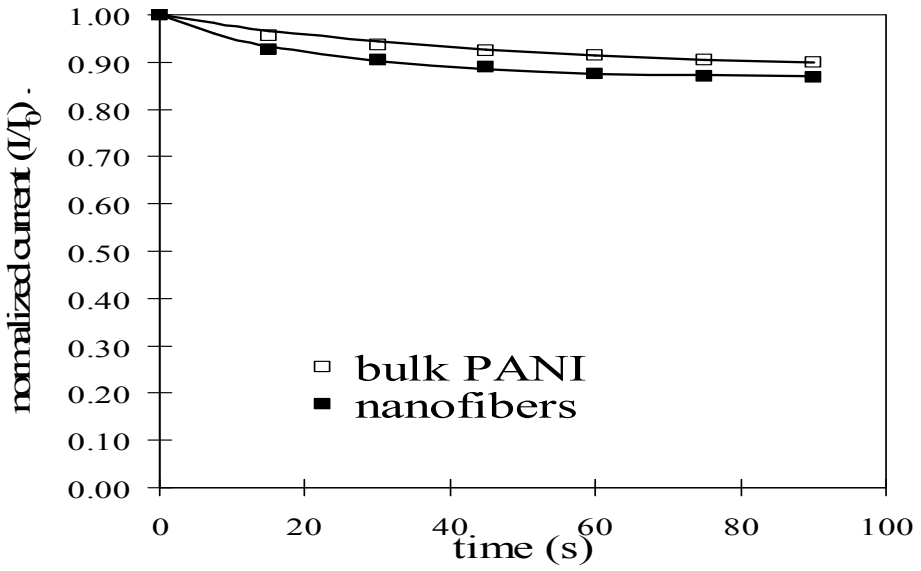

Figure 3. Sensor responses of bulk and nanofiber based sensors to chloroform. The curves shown are best fits to exponential decays with the variables given in Table 1. The concentration of chloroform in the carrier gas was about 2.2%. The y-scale was set to provide a direct comparison with the other gases.

The responses of bulk polyaniline and polyaniline nanofibers to toluene exposure are shown in Figure 4. It was observed that the responses to toluene were both faster and of larger magnitude than those for chloroform. Again, the nanofibers showed faster and larger responses than those of the bulk PANI. A simple exponential seems to fit the sets of data quite well. The values of $\tau_{response}$ for toluene were around 56 seconds and 34 seconds, for the bulk and nanofiber PANI, respectively.

Lastly, the responses of the sensors to triethylamine are shown in Figure 5. The results are much more striking than those for the other two solvents. Again, the nanofibers showed a faster and more intense response than did the bulk PANI. The values of $\tau_{response}$ for triethylamine were around 20 and 14 s, for the bulk and nanofiber PANI, respectively.

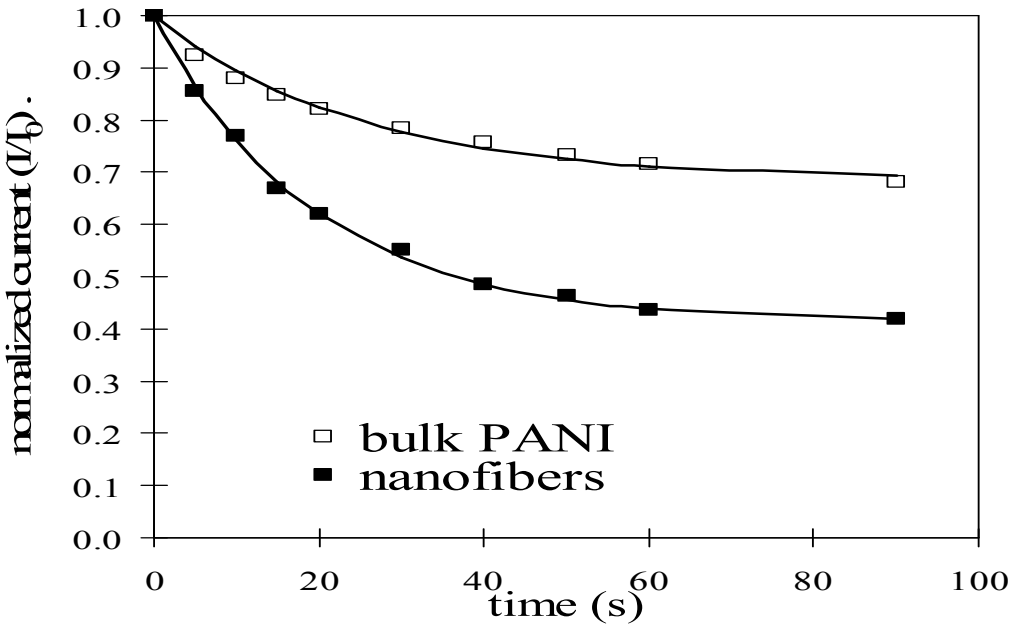

Figure 4. Sensor response of bulk and nanofiber based sensors to toluene. The curves shown are best fits to exponential decays with the variables given in Table 1. The concentration of toluene in the carrier gas was about 1.7%.

The advantages of sensors from nanofibrous PANI have already been demonstrated [64,125]; however, it is interesting to compare the different responses of the sensors to the different gases. Interaction of gases with the polymer may cause both physical and chemical changes and each can affect the current. The smallest response was to chloroform, which has a hydrogen that tends to be weakly acidic. The conductivity, which in this case depends on the acid concentration (HCl dopant), was not particularly sensitive to the presence of chloroform. The response of PANI to chloroform was similar to that previously reported for bulk PANI [92].

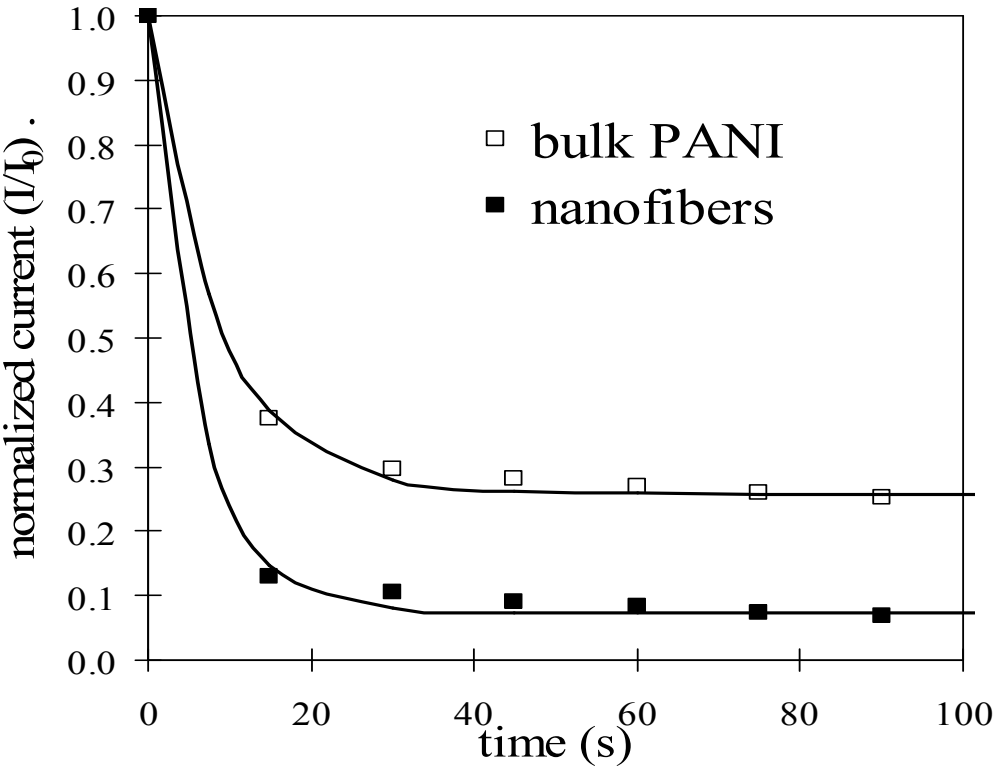

Figure 5. Sensor responses of bulk and nanofiber based sensors to triethylamine. The curves shown are best fits to exponential decays with the variables given in Table 1. The concentration of triethylamine in the carrier gas was about 1.8%.

The response to toluene was greater than that for chloroform. Toluene, like several other organic molecules, does not react with polyaniline and does not affect the doping level. Rather, toluene was absorbed in the polymer and caused swelling, which in turn decreased the conductivity [130-131]. A decrease in conductivity was therefore observed for both types of PANI, independent of the polymer morphology. However, the responses of the nanofiber samples were about twice those of the bulk polymers. Since the adsorption at short times occurred near the interface of the polymer, the larger surface area of the nanofibers made them more accessible to external molecules.

Table 1. Characterization of bulk and nanofiber PANI to different solvents

System	Solvent	τ (sec)[a]	I_∞ [a]	$\tau_{response}$ (s)[b]
chloroform	Bulk PANI	44.5	0.882	102.4
	Nanofibers	21.9	0.867	50.2
toluene	Bulk PANI	24.4	0.684	56.2
	Nanofibers	19.2	0.413	41.5
triethylamine	Bulk PANI	8.59	0.258	19.8
	Nanofibers	5.94	0.074	13.7

[a] From equation 1
[b] time required for the signal to reach 90% of its final value, the total change of $(1 - I_\infty)$.

The changes due to triethylamine were much larger, as much as a factor of 10 in the reduction of current for the nanofibers. The magnitude of the responses of bulk polyaniline and polyaniline nanofibers was comparable to and consistent with previous experimental results from the Kaner group [64]. Triethylamine is also a liquid at room temperature with a relatively high vapor pressure (121 kPa at 20 °C). It is also important because the detection of amines is critical in the detection of numerous and highly volatile by-products of methamphetamine production. Amines change the conductivity because they remove the dopant through the formation of hydrochloride salts, as shown in the scheme below (Figure 6).

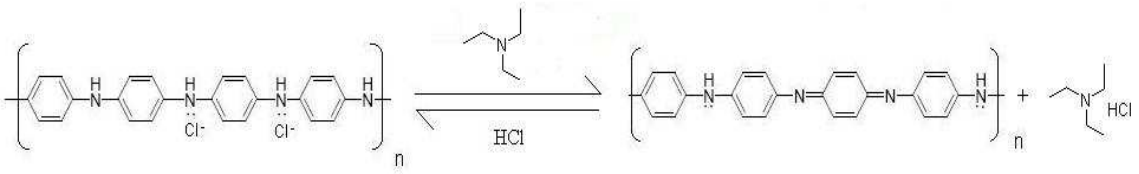

Figure 6. The mechanism of PANI conductance changed due to the dedoping process by triethylamine.

5. CONCLUSIONS

Sensors based on polyaniline nanofiber thin films can be fabricated by UV-irradiation of a precursor solution in a single-step process. The sensors are ready for use immediately after polymerization, and major processing is required only to fabricate the interdigitated array. Sensors fabricated with our technique have characteristics comparable to other polyaniline bulk and nanofiber sensors, thus proving that our technique can be employed for device fabrication.

6. ACKNOWLEDGEMENTS

The authors acknowledge the financial support of the National Science Foundation under grant DMR-0706197 (FDB) and the Missouri University of Science and Technology.

7. BIOGRAPHIES

Z. Li has been a graduate student in Materials Science and Engineering at the Missouri University of Science and Technology since 2006. Currently, his research interests are nanomaterials and conducting polymer-based sensors.

F. D. Blum is a Curators' Professor of Chemistry, Adjunct Professor of Materials Science and Engineering, and Senior Investigator in the Graduate Center for Materials Research at the Missouri University of Science and Technology. His research activities include conducting polymer nanocomposites and dynamics in interfacial materials.

M. F. Bertino is Associate professor of Physics at Virginia Commonwealth University. His research activities include photolithographic synthesis of metal, oxide and polymer nanoparticles.

C.-S. Kim has been an Assistant Professor of Electrical Engineering at the Missouri University of Science and Technology since 2002. His current research efforts are focused on microsystem technologies for special applications to environmental, agricultural and plant research, etc.

S. K. Pillalamarri is senior packaging engineer at Freescale semiconductor. His research interests include nanostructured conducting polymers, adhesives and coatings for applications in microelectronics. He received his Ph. D. degree in chemistry from the University of Missouri-Rolla (now Missouri S&T) in 2005.

8. REFERENCES

[1] J.X. Huang, S. Virji, B.H. Weiller, R.B. Kaner, Polyaniline nanofibers: Facile synthesis and chemical sensors, J. Am. Chem. Soc. 125 (2003) 314-315.

[2] S. Virji, J.X. Huang, R.B. Kaner, B.H. Weiller, Polyaniline nanofiber gas sensors: Examination of response mechanisms, Nano Lett. 4 (2004) 491-496.

[3] D. Nicolas-Debarnot, F. Poncin-Epaillard, Polyaniline as a new sensitive layer for gas sensors, Analytica Chimica Acta 475 (2003) 1-15.

[4] D.S. Sutar, N. Padma, D.K. Aswal, S.K. Deshpande, S.K. Gupta, J.V. Yakhmi, Preparation of nanofibrous polyaniline films and their application as ammonia gas sensor, Sensors Actuators B 128 (2007) 286-292.

[5] N.J. Pinto, R. Gonzalez, J. Alan T. Johnson, A.G. MacDiarmid, Electrospun hybrid organic/inorganic semiconductor Schottky nanodiode, Appl. Phys. Lett. 89 (2006) 033505.

[6] H.Q. Liu, C.H. Reccius, H.G. Craighead, Single electrospun regioregular poly(3-hexylthiophene) nanofiber field-effect transistor, Appl. Phys. Lett. 87 (2005) 253106.

[7] M.M. Alam, J. Wang, Y.Y. Guo, S.P. Lee, H.R. Tseng, Electrolyte-gated transistors based on conducting polymer nanowire junction arrays, J. Phys. Chem. B 109 (2005) 12777-12784.

[8] A.K. Wanekaya, M.A. Bangar, M. Yun, W. Chen, N.V. Myung, A. Mulchandani, Field-effect transistors based on single nanowires of conducting polymers, J. Phys. Chem. C 111 (2007) 5218-5221.

[9] N.J. Pinto, R. Perez, C.H. Mueller, N. Theofylaktos, F.A. Miranda, Dual input AND gate fabricated from a single channel poly(3-hexylthiophene) thin film field effect transistor, J. Appl. Phys. 99 (2006) 84504.

[10] R.J. Tseng, J.X. Huang, J. Ouyang, R.B. Kaner, Y. Yang, Polyaniline nanofiber/gold nanoparticle nonvolatile memory, Nano Lett. 5 (2005) 1077-1080.

[11] R.J. Tseng, C.O. Baker, B. Shedd, J.X. Huang, R.B. Kaner, J.Y. Ouyang, Y. Yang, Charge transfer effect in the polyaniline-gold nanoparticle memory system, Appl. Phys. Lett. 90 (2007) 053101.

[12] N.T. Kemp, D. McGrouther, J.W. Cochrane, R. Newbury, Bridging the gap: Polymer nanowire devices, Adv. Mater. 19 (2007) 2634-2638.

[13] X.F. Yu, Y.X. Li, N.F. Zhu, Q.B. Yang, K. Kalantar-zadeh, A polyaniline nanofibre electrode and its application in a self-powered photoelectrochromic cell, Nanotech. 18 (2007) 015201.

[14] A.N. Aleshin, Quasi-one-dimensional transport in conducting polymer nanowires, Phys. Solid State 49 (2007) 2015-2033.

[15] D. Zhang, Y. Wang, Synthesis and applications of one-dimensional nano-structured polyaniline: An overview, Mater. Sci. Eng. B 134 (2006) 9-19.

[16] N.J. Pinto, A.T. Johnson, A.G. MacDiarmid, C.H. Mueller, N. Theofylaktos, D.C. Robinson, F.A. Miranda, Electrospun polyaniline/polyethylene oxide nanofiber field-effect transistor, Appl. Phys. Lett. 83 (2003) 4244-4246.

[17] L.K. Werake, J.G. Story, M.F. Bertino, S.K. Pillalamarri, F.D. Blum, Photolithographic synthesis of polyaniline nanofibres, Nanotech. 16 (2005) 2833-2837.

[18] S.K. Pillalamarri, F.D. Blum, A.T. Tokuhiro, J.G. Story, M.F. Bertino, Radiolytic Synthesis of Polyaniline Nanofibers: A New Templateless Pathway, Chem. Mater. 17 (2005) 227-229.

[19] J.G. Roh, H.R. Hwang, J.B. Yu, J.O. Lim, J.S. Huh, Oxidant effects on polypyrrole and polyaniline sensor for several volatile organic gases, J. Macromol. Sci., A 39 (2002) 1095 - 1105.

[20] E.S. Tillman, M.E. Koscho, R.H. Grubbs, N.S. Lewis, Enhanced Sensitivity to and Classification of Volatile Carboxylic Acids Using Arrays of Linear Poly(ethylenimine)-Carbon Black Composite Vapor Detectors, Anal. Chem. 75 (2003) 1748-1753.

[21] B. Li, S. Santhanam, L. Schultz, M. Jeffries-El, M.C. Iovu, G. Sauve, J. Cooper, R. Zhang, J.C. Revelli, A.G. Kusne, J.L. Snyder, T. Kowalewski, L.E. Weiss, R.D. McCullough, G.K. Fedder, D.N. Lambeth, Inkjet printed chemical sensor array based on polythiophene conductive polymers, Sensors Actuators B 123 (2007) 651-660.

2. AMPLIFIED RESPONSE AND ENHANCED SELECTIVITY OF METAL-PANI FIBER COMPOSITE SENSORS

Zhe-Fei Li[a], Frank D. Blum[a,b,c,], Massimo F. Bertino[d], Chang-Soo Kim[e,f],

[a] Department of Materials Science and Engineering, Missouri University of Science and Technology, Rolla, MO 65409

[b] Department of Chemistry, Missouri University of Science and Technology, Rolla, MO 65409

[c] Department of Chemistry, Oklahoma State University, Stillwater OK, 74078

[d] Department of Physics, Virginia Commonwealth University, Richmond, VA 23824

[e] Department of Electrical and Computer Engineering, Missouri University of Science and Technology, Rolla, MO 65409

[f] Department of Biological Sciences, Missouri University of Science and Technology, Rolla, MO 65409

1. ABSTRACT

Nanocomposites of polyaniline (PANI) nanofibers and metal nanoparticles were fabricated using a single-step photo-assisted technique and tested as sensors. Nanofiber composites containing Ag- and Pt-nanoparticles were exposed to toluene and triethylamine and their response was compared to that of bare nanofibers and bulk PANI produced with the same technique. The larger surface area of the nanofiber-based sensors resulted in shorter response times and in larger changes in conductivity than for bulk PANI sensors for all analytes. Nanofiber sensors with and without Ag or Pt particles had a comparable response when exposed to toluene, an analyte that induces swelling of the

composites but does not alter doping or react strongly with nanoparticles of noble metals. The composites reacted quite differently to triethylamine. The response time of Ag-containing composites was about 3 times faster than that of the nanofibers alone and about 1.5 times faster than that of Pt-nanofiber composites. The change in resistivity was about 6 times larger for Ag nanocomposites and more than 4 times larger than for the Pt nanocomposites. To better understand the stronger response of Ag nanocomposites, Raman spectra were taken which indicated that charge was transferred to Ag and to a lesser extent to Pt by the nanofibers. That is, Ag acts as a dopant. Exposure to triethylamine reduces the charge transfer and therefore the doping, thereby amplifying the response to the analyte.

Key words: PANI, PANI/metal nanocomposites, gas sensor, toluene, triethylamine.

2. INTRODUCTION

Polyaniline (PANI) nanofibers are versatile materials that are being considered for applications as wide ranging as permanent memories, chemical sensors, catalysts and electrochromic devices.[132-133] For several of these applications (electrochromic, catalysis, sensing) PANI nanofibers are superior to bulk PANI because of their higher surface area.[134-136] For permanent memories, composites of PANI nanofibers and metal nanoparticles have been employed[122] where the application of a bias voltage threshold induces a charge transfer from the polymer to the nanoparticles.[123] The trapped charge acts as a dopant, thereby allowing switching of the conductivity of the nanocomposites.

While extremely promising, PANI nanofiber composites present processing difficulties, since PANI can be re-dispersed only in aggressive solvents such as m-cresol. Our group has addressed the processibility issues resulting in the development of a photo-assited technique producing, in a single step, PANI nanofibers on planar substrates. In our technique, the precursors: aniline, water, an acid dopant, and an oxidant such as ammonium persulfate, and metal ion are deposited on a substrate and exposed to ultraviolet (UV) light. UV exposure alters the morphology of the polymer and induces formation of nanofibers instead of bulk PANI.[24] We recently applied our technique to device production and showed that nanofiber chemical sensors can be fabricated in a single step on an interdigitated electrode array.[136] Here, we report the effect of metal nanoparticles on PANI nanofiber sensors. We found that analytes can induce charge transfer between the metal and the polymer thereby changing the doping level of the polymer and its conductivity. The observed charge transfer effects can be exploited to amplify the response of sensors and to enhance their specificity. The specificity

improvement is particularly relevant. PANI nanofiber sensors are quite sensitive and versatile, having been used to detect analytes ranging from hydrazine to toluene. However, sensitivity to several analytes can give rise to false positives in field applications, where sensors are exposed to a mixture of different molecules. Our experiments show a possibility that the response can be made more specific by adding to the composites nanoparticles of metals that interact strongly with the target analyte, and open the way to tailor response via multiplexing.

3. RESULTS AND DISCUSSION

The synthesis of nanostructured PANI was achieved using a UV lamp to induce the formation of PANI nanofibers. Sensors were fabricated on interdigitated electrodes following a previously reported procedure.[136] Figure 1 shows the scanning electron microscopy (SEM) and transmission electron microscopy (TEM) of different PANI thin films grown on the interdigitated electrodes. These images show a nanofiber structure with fiber diameters smaller than 100 nm. These fiber structures are quite similar to those that have previously been reported with PANI nanofibers produced with UV[24] and the metal nanoparticles were well dispersed in the nanofibers as previously produced with γ-radiation.[77] The morphology of the PANI was not substantially changed in the presence of the metal nanoparticles. Approximately 18 and 20 wt% residual mass due to the metals was observed by TGA for PANI/Ag and PANI/Pt, respectively. The thermogravimetric curves are shown in Figure S1 in the Supporting Documentation.

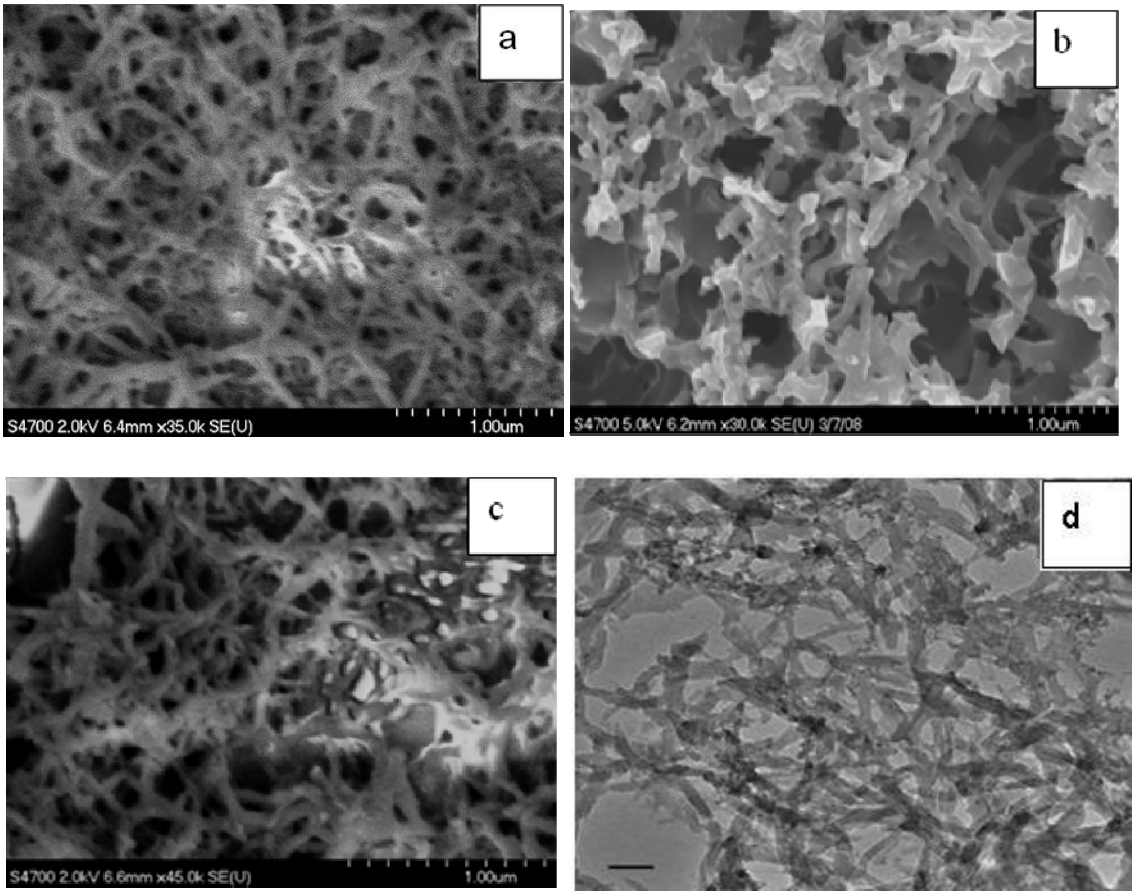

Figure 1. SEM images of films deposited on interdigitated electrodes: a) PANI nanofiber thin film irradiated for 30 min, b) PANI/Pt nanocomposites, c) PANI/Ag nanocomposites, and d) TEM image of PANI/Ag nanocomposites with the metal particles showing as dark regions.

Sensors made with PANI nanofibers and PANI/metal nanocomposites were exposed to various vapors using nitrogen as the carrier gas. The responses of the sensors based on PANI Bulk, PANI nanofibers, PANI nanofibers with Pt, and PANI nanofibers with Ag to toluene and triethylamine are shown in Figures 2 and 3, respectively.

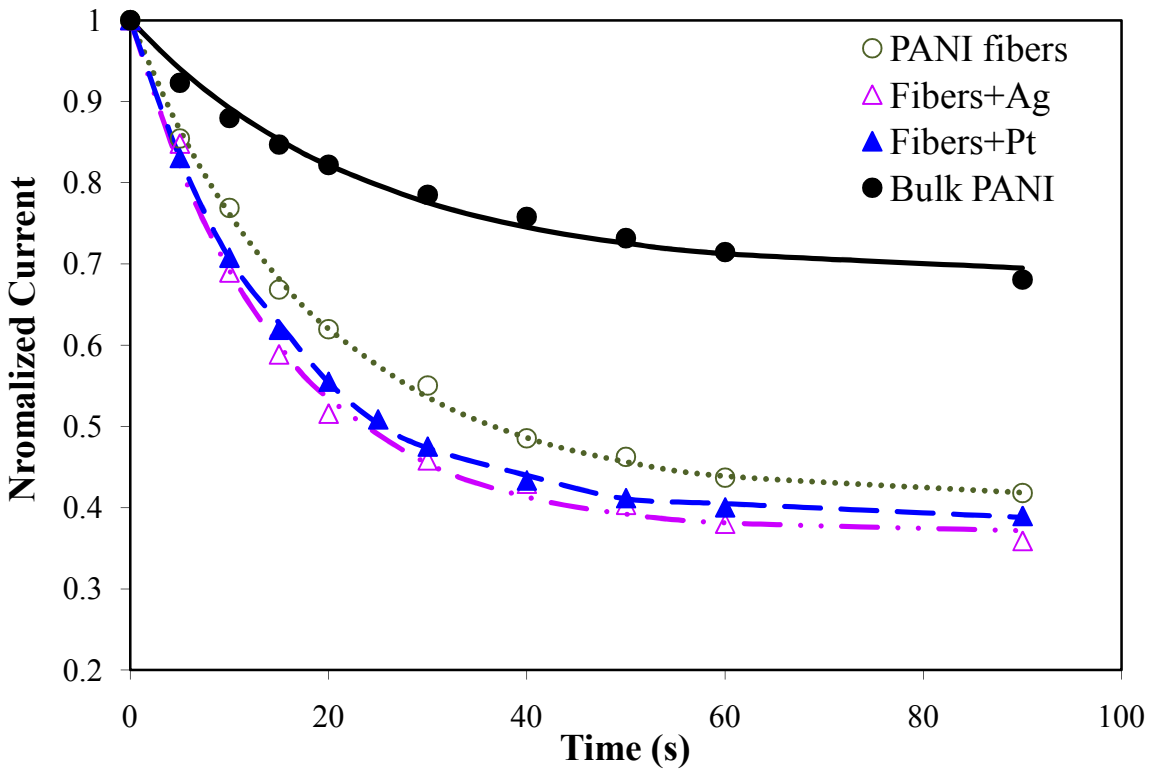

Figure 2. Sensor response of PANI sensors to a toluene vapor. The curves shown are best fits to exponential decays with the variables given in Table 1. The concentration of toluene in the carrier gas is estimated to be about 1.7%.

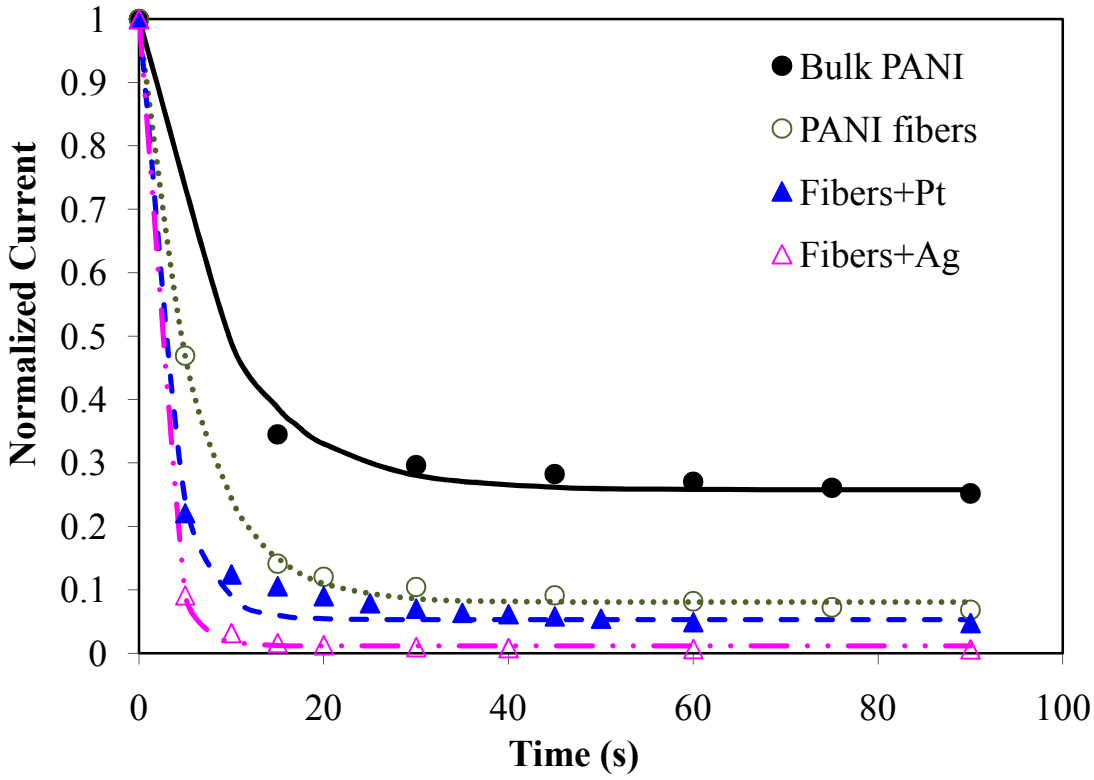

Figure 3. Sensor response of PANI sensors to gaseous triethylamine. The curves shown are best fits to exponential decays with the variables given in Table 1. The concentration of triethylamine in the carrier gas is estimated to be about 1.8%.

The response of the sensors was plotted in terms of the normalized current ($I_{norm}(t)$= current/initial current = $I(t)/I_0$). The currents typically ranged from 1 to 200 mA with the currents for the PANI/metal nanocomposite sensors being 5-10 times higher than PANI sensors. The response of the sensors was modeled as a single exponential decay using the following equation:

$$I_{norm}(t) = (1 - I_\infty) \exp(-t/\tau) + I_\infty \qquad (1)$$

where I_∞ is the normalized current after the sensor has stabilized under the vapor of interest (i.e., $I_\infty = I_{norm}(t)$ when $t = \infty$). The curves fit the experiment data fairly well. The results of the fitted parameters are listed in Table 1. In addition, as an alternative method

of defining the response, a response time ($\tau_{response}$) was calculated as the time to reach 90% of the total current change of (1 - I_∞). These values are also shown in Table 1.[5]

Table 1. Fitting constants of PANI nanofibers and PANI/metal nanocomposites to different analytes

	System	τ (sec)[a]	I_∞ [a]	$\tau_{response}$ (sec)[b]
Toluene	Bulk PANI	24.4	0.684	56.2
	PANI Nanofibers	19.2	0.413	41.5
	Nanofibers/Ag	14.8	0.370	34.2
	Nanofibers/Pt	15.4	0.388	35.5
Triethylamine	Bulk PANI	8.59	0.258	19.8
	PANI nanofibers	5.94	0.074	13.7
	Nanofibers/Ag	2.01	0.012	5.1
	Nanofibers/Pt	3.14	0.053	9.8

[a] From equation 1
[b] Time required for the signal to reach 90% of its final value with a total change of (1 – I_∞).

The responses of PANI nanofibers and PANI/metal nanocomposites to toluene (Figure 2) showed that the nanofiber composites exhibited faster response times and larger changes in conductivity than bulk PANI, as expected from surface area considerations.[64] The response times of metal-containing nanofibers were 15 to 20% faster, while the changes in conductivity were within 10% of those of nanofibers alone. Changes in response times and conductivities did not depend strongly on the type of metal and were within 10% for Pt and Ag composites. These observations can be

explained based on the interaction of toluene with PANI and with metal particles. Toluene is not expected to interact significantly with either the dopant or metal particles. However, toluene can be absorbed by the polymer and cause it to swell.[92,130] The conductivity of PANI not only depends on the charge carrier transport along the polymer chain, but also the charge carrier hopping between neighboring polymer chains.[137-139] The swelling of PANI probably results in an increase in the interchain distance, consequently decreasing the conductivity. Toluene is usually only weakly chemisorbed on metal surfaces, which explains the comparable response of Ag and Pt composites.

The sensor response to compounds that alter the doping level of the conducting polymer was much greater than the response in the case of swelling agents like toluene. In general, for the responses to triethylamine (Figure 3), PANI/metal nanocomposites showed a faster and more intense response than PANI nanofibers. However, as reported in Table 1, Ag composites responded more than twice as fast as the Pt composites, and almost three times faster than metal-free PANI. The conductivity at long times, I_∞, of Ag composites was also about 4 times smaller than the conductivity of Pt composites and about 6 times lower than that of metal-free nanofibers.

To explain the faster, greater response of Ag composites, we examined the Raman spectra of the sensors before and after exposure to triethylamine. The results are reported in Figure 4 and show that exposure to triethylamine did not significantly change the vibrational spectrum of the metal-free polymer nanofibers. However, Ag composites exhibited a strong peak around 1370 cm^{-1} accompanied by a weaker peak around 1330 cm^{-1}. These bands are characteristic of $C\text{-}N^+$ bands.. The fact that the 1370 cm^{-1} band is prominent in Ag composites indicates that charge is being transferred from the polymer

to the metal nanoparticles. This result is in agreement with previous observations of PANI thin films deposited on noble metals and of PANI/metal nanocomposites, which all detected a charge transfer to the metal, and, correspondingly, an increase in the protonated bands and a large (~ 10 times) increase in conductivity that could not be explained on the basis of percolation theory.[122,140-144] In Ag composites, exposure to triethylamine weakens the band at 1370 cm^{-1} and the 1330 cm^{-1} band becomes predominant. The weakening of the 1370 cm^{-1} band indicates that triethylamine reduces the charge transfer to the nanoparticle. Therefore, we believe that triethylamine affects the conductivity of the polymer fibers by reacting with the acid dopant and also by reducing the charge transferred by the polymer to the Ag nanoparticles, which is tantamount to an additional reduction of the doping level. Our conjecture is verified by the Raman spectra of Pt nanocomposites, which are reported in the Supporting Information. In Pt composites, the intensities of the 1370 and 1330 cm^{-1} peak were comparable, pointing to a smaller amount of charge transfer (shown in Figure S2 in the Supporting Documentation). More importantly, the 1370 cm^{-1} band decreased by only about 20% upon exposure to triethylamine, pointing to a smaller charge transfer induced by the analyte.

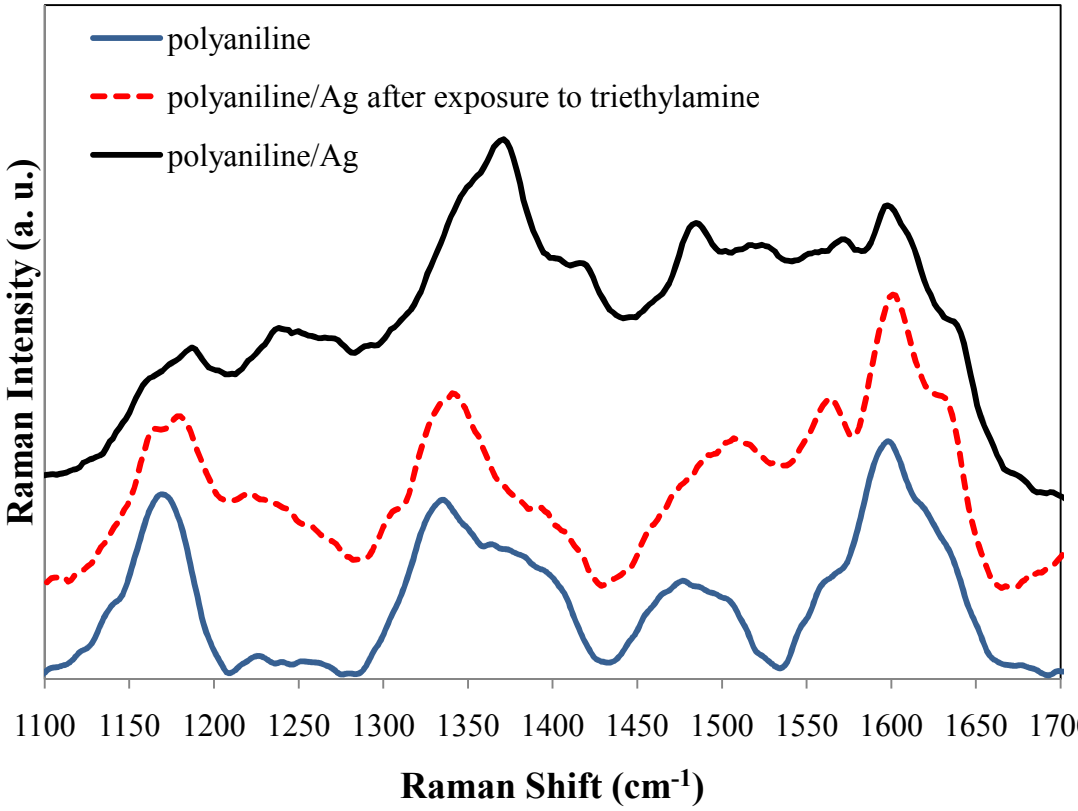

Figure 4. Raman spectra of PANI, PANI/Ag nanocomposite, and PANI/Ag nanocomposite after exposure to triethylamine.

Our results suggest that adsorption of gas molecules on the metal nanoparticles can weaken the interaction between metal nanoparticles and the PANI. It is not surprising that Ag composites show the strongest effect, since amines have a stronger affinity for Ag than for Pt and most other metals.[145-147] A further confirmation of our hypothesis comes from the Raman spectra of nanocomposites exposed to toluene shown in Figure S3, which did not exhibit any change before and after exposure to the analyte.

4. CONCLUSIONS

In summary, this work has demonstrated that nanostructured PANI-based thin film sensors can be fabricated by irradiating an aqueous precursor solution with UV light

in an environmentally friendly, one-step process. These sensors are ready for use immediately after polymerization and drying; they require no additional processing steps. Our sensors showed good response to organic vapors, such as toluene and triethylamine. The most relevant result of our experiment is the demonstration that the response to analytes can be both enhanced by introducing metal nanoparticles that interact strongly with the analyte. This strong interaction can affect the charge transfer between polymer and nanoparticles and also alter the doping level of the polymer. Our finding could be used to prepare multiplexed sensors with a high degree of sensitivity and specificity.

5. EXPERIMENTAL

1. Materials. Aniline, chloroform, $AgNO_3$ and $KPtCl_4$ were purchased from Alfa Aesar. Ammonium persulfate (APS), nitric acid, hydrochloric acid, and toluene were obtained from Fisher Scientific. Triethylamine was from Lancaster Synthesis. All chemicals were used as received, except for aniline which was distilled before use.

2. Synthesis of PANI nanofibers and PANI/metal nanocomposites. Aniline, 0.1 M and 0.1 M nitric acid were dissolved in 10 mL distilled water after which 0.05 M ammonium persulfate was added. PANI nanofibers were obtained by irradiating the precursor solution immediately after mixing with a high pressure Hg lamp (Midwestern Instruments). For PANI-metal nanocomposites, water soluble metal salts ($AgNO_3$ and $KPtCl_4$) were used as the source for metal nanoparticles. Aniline of 0.1 M, nitric acid of 0.1 M and 0.01 M metal salts were dissolved in 10 mL distilled water. Immediately after the addition of 0.05 M ammonium persulfate, the solution was irradiated with the UV lamp.

3. Fabrication of PANI nanofiber and PANI/metal nanocomposite sensors. Sensors were fabricated by placing a 10 μL drop of precursor solution on the active area of an interdigitated microelectrode array of sputtered-deposited gold thin film.[136] The precursor solution had the same composition as described above. A drop of the precursor solution was placed on the electrode and then illuminated with UV light. After the 30 min reaction, the PANI thin films were washed with water and dried at room temperature before being used for measurement.

4. Characterization. The morphology of the PANI was characterized using a Hitachi S-4700 scanning electron microscope (SEM) operated at accelerating voltages of 2 and 5KV. The transmission electron microscope used was a JEOL JEM-2100. Thermogravimetric analysis (TGA) was carried out to determine the amount of metals incorporated in PANI on a TA Instrument 2950 Thermogravimetric Analyzer, at a heating rate of 20°C/min, under an air atmosphere. The changes in current for bulk PANI and PANI nanofiber-based sensors were measured at room temperature using a Keithley 617 programmable electrometer operated at 0.1V applied between anodes and cathodes of the electrode array. To test the sensors, nitrogen was used as the carrier gas and diluting gas. The nitrogen gas was passed through a bubbler in liquid samples, diluted by another nitrogen flow and then directed to the sensor, kept at room temperature. The total flow rate was about 1.5 L/min.

6. ACKNOWLEDGEMENTS

The authors acknowledge Terry Colberg and Balika Khatiwada for assistance in obtaining the TEM pictures. FDB acknowledges the financial support of the national Science Foundation under grant DMR-1005606 and of Materials Research Center, Missouri S and T.

7. REFERENCES

(1) Sangodkar, H.; Sukeerthi, S.; Srinivasa, R. S.; Lal, R.; Contractor, A. Q. *Anal. Chem.* **1996**, *68*, 779-783.

(2) Virji, S.; Kaner, R. B.; Weiller, B. H. *Chem. Mater.* **2005**, *17*, 1256-1260.

(3) Yan, X. B.; Han, Z. J.; Yang, Y.; Tay, B. K. *Sens. Actuators, B* **2007**, *123*, 107-113.

(4) Virji, S.; Kaner, R. B.; Weiller, B. H. *J. Phys. Chem. B* **2006**, *110*, 22266-22270.

(5) Li, Z. F.; Blum, F. D.; Bertino, M. F.; Kim, C. S.; Pillalamarri, S. K. *Sens. Actuators, B* **2008**, *134*, 31-35.

(6) Tseng, R. J.; Huang, J. X.; Ouyang, J.; Kaner, R. B.; Yang, Y. *Nano Lett.* **2005**, *5*, 1077-1080.

(7) Tseng, R. J.; Baker, C. O.; Shedd, B.; Huang, J. X.; Kaner, R. B.; Ouyang, J. Y.; Yang, Y. *Appl. Phys. Lett.* **2007**, *90*, 053101

(8) Werake, L. K.; Story, J. G.; Bertino, M. F.; Pillalamarri, S. K.; Blum, F. D. *Nanotechnology* **2005**, *16*, 2833-2837.

(9) Pillalamarri, S. K.; Blum, F. D.; Tokuhiro, A. T.; Bertino, M. F. *Chem. Mater.* **2005**, *17*, 5941-5944.

(10) Virji, S.; Huang, J. X.; Kaner, R. B.; Weiller, B. H. *Nano Lett.* **2004**, *4*, 491-496.

(11) Roh, J. G.; Hwang, H. R.; Yu, J. B.; Lim, J. O.; Huh, J. S. *J. Macromol. Sci., A* **2002**, *39*, 1095 - 1105.

(12) Tillman, E. S.; Koscho, M. E.; Grubbs, R. H.; Lewis, N. S. *Anal. Chem.* **2003**, *75*, 1748-1753.

(13) Krinichnyi, V. I.; Chemerisov, S. D.; Lebedev, Y. S. *Phys. Rev., B* **1997**, *55*, 16233-16244.

(14) Nazeer, K. P.; Jacob, S. A.; Thamilselvan, M.; Mangalaraj, D.; Narayandass, S. K.; Yi, J. *Polym. Int.* **2004**, *53*, 898-902.

(15) Fattoum, A.; Arous, M.; Gmati, F.; Dhaoui, W.; Mohamed, A. B. *J. Phys. D: Appl. Phys.* **2007**, *40*, 4347-4354.

(16) Baibarac, M.; Cochet, M.; Lapkowski, M.; Mihut, L.; Lefrant, S.; Baltog, I. *Synth. Met.* **1998**, *96*, 63-70.

(17) Afzal, A. B.; Akhtar, M. J.; Nadeem, M.; Ahmad, M.; Hassan, M. M.; Yasin, T.; Mehmood, M. *J. Phys. D: Appl. Phys.* **2009**, *42*, 15411.

(18) Afzal, A. B.; Akhtar, M. J.; Nadeem, M.; Hassan, M. M. *Journal of Physical Chemistry C* **2009**, *113*, 17560-17565.

(19) Berrada, K.; Quillard, S.; Louam, G.; Lefrant, S. *Synth. Met.* **1995**, *69*, 201-204.

(20) Hugot-Le Goff, A.; Bernard, M. C. *Synth. Met.* **1993**, *60*, 115-131.

(21) Aslam, M.; Fu, L.; Su, M.; Vijayamohanan, K.; Dravid, V. P. *J. Mater. Chem.* **2004**, *14*, 1795-1797.

(22) Qu, Y.; Appleton, T. G.; Hoeschele, J. D.; Farrell, N. *Inorg. Chem.* **1993**, *32*, 2591-2593.

(23) Murray, B. J.; Walter, E. C.; Penner, R. M. *Nano Lett.* **2004**, *4*, 665-670.

3. MODELING OF THE RESPONSE OF NANOSTRUCTURED POLYANILINE GAS SENSORS

Zhe-Fei Li[a], Frank D. Blum[a,b,c], Massimo F. Bertino[d], Chang-Soo Kim[e,f],

[a] Department of Materials Science and Engineering, Missouri University of Science and Technology, Rolla, MO 65409

[b]Department of Chemistry, Missouri University of Science and Technology, Rolla, MO 65409

[c] Department of Chemistry, Oklahoma State University, Stillwater, OK, 74078

[d] Department of Physics, Virginia Commonwealth University, Richmond, VA 23824

[e] Department of Electrical and Computer Engineering, Missouri University of Science and Technology, Rolla, MO 65409

[f] Department of Biological Sciences, Missouri University of Science and Technology, Rolla, MO 65409

1. ABSTRACT

Polyaniline/Ag nanocomposite gas sensors have been fabricated with a single-step technique. The current response of the sensors to triethylamine and toluene was monitored and analyzed. The time dependence of the sensors was found to be exponential and fit to chemisorption and diffusion models. The equilibrium absorption amounts from the chemisorption model were found to obey a Langmuir isotherm. The application of the diffusion model was consistent with a dual sorption process, i.e., diffusive and non-diffusive adsorption sites. The estimated diffusion coefficient was found to increase with the concentration of diluent, probably due to the swelling of the polymer by the organic

vapors. Our fitting results suggest that both models can be employed to mathematically fit the sensor response.

Keywords: Nanostructured, Polyaniline, Polyaniline/Ag nanocomposites, Nanofibers, Gas sensor, Adsorption, Diffusion, Langmuir Isotherm.

2. INTRODUCTION

Gas sensors, sometimes denoted as electronic noses, have been widely studied ever since the design of a gas sensor was reported by Seiyama et al. in 1962.[148] Chemical instrumental methods for determining unknown species, such as gas chromatography/mass spectrometry (GC/MS), are time-consuming, expensive, and require trained personnel. There is a need to develop miniature devices for rapid and inexpensive analysis of volatile compounds. Recently, significant research has been focused on conducting polymer–based gas sensors.[83] Polyaniline is a promising candidate polymer for gas sensing applications because of its relatively easy synthesis, low cost, high sensitivity, and fast response.[25,87] In particular, nanostructured polyaniline-based gas sensors have shown excellent performance because of their large surface areas and high porosity of nanostructured polyaniline.[62,64-65,133] However, a facile one-step environmental-friendly method is still in demand due to the poor processibility of polyaniline. Our group has reported a novel method to synthesize polyaniline nanofibers and nanocomposites based on either gamma or ultra-violet radiation.[24,75,77] This technique can be utilized to fabricate nanostructured polyaniline-based electrochemical gas sensors in a single step. This type of sensor has shown a fast response to various organic vapors.[136]

Although considerable research has been carried out in development of novel conducting-polymer sensors, some basic problems still remain, especially with respect to nanostructured conducting-polymer sensors. The modeling of time-dependent sensor response is particularly relevant. The gas sensor response is basically controlled by two factors. One is the transport process of gas molecules into the sensor film. The other is

the interaction of the sensing material and gas molecules, i.e., a physical interaction or chemical reaction. A few models have been proposed for conducting-polymer–based gas sensors, including those that are either based on a complicated mathematic model[149] or incapable of studying the time-dependence sensor response.[150-151] Hu et al. recently proposed an adsorption model for polyaniline thin film optical sensors.[152]

Our previous work has shown that the sensor response can be fit with an exponential decay as a function of time.[136] This paper reports the response of one-step polyaniline/Ag based sensors and interprets the response in terms two simple mathematical models (i.e., chemisorption and diffusion) to fit the current response of nanostructured polyaniline based gas sensors to organic vapors, such as triethylamine and toluene. Both fitting methods are consistent with an exponential decay function. The fitted constant I_∞, obtained from the chemisorption model, was found to obey a Langmuir isotherm, while the diffusion model was consistent with a dual sorption mechanism.

3. EXPERIMENTAL

1. Synthesis of polyaniline/Ag nanocomposites. To produce nanocomposites for the sensors, 0.1 M aniline (93 mg), 0.01 M $AgNO_3$ (17 mg) and 0.1 M nitric acid were first dissolved in 10 mL distilled water. The aniline began to polymerize after the addition of 0.05 M ammonium persulfate (114 mg). After vigorous shaking, the solution was immediately irradiated with a low-pressure Hg UV light source (Model: PASCO Scientific OS-9286A).

2. Fabrication of polyaniline/Ag nanocomposite sensors. Sensors were fabricated by placing a 10 μL drop of premixed precursor solution on the active area of an interdigitated microelectrode array. The precursor solution had the same composition as described above. The drop was then illuminated with a UV lamp. After the reaction (approximately 30 min), the polyaniline thin films were washed with distilled water and dried at room temperature before being used for measurements.

3. Characterization. The changes in current for polyaniline/Ag based thin film sensors were measured at room temperature as a function of time and exposure to organic vapors. The real-time current changes were monitored using a Keithley 4200 semiconductor analyzer operated at 0.1 V. To test the sensors, nitrogen gas was used as the carrier and diluting gas. The carrier gas was passed through the neat liquids in a bubbler. The resulting gas mixtures were then diluted with the additional diluting gas and then directed to the sensor, which was kept at room temperature. The concentration of gases was determined using Eq. 1:

$$C = (M/\rho)/(M/\rho + L_1 + L_2) \quad (1)$$

where M is the weight loss rate of the liquid sample (in g/min), ρ is the density of the vapor (in g/L), L_1 is the nitrogen carrier gas flow rate (in L/min), and L_2 is the nitrogen diluting gas flow rate (in L/min). The flow rate of the nitrogen diluting gas was 1.5 L/min, and the pressure of the total gas was about 15 psi.

4. THEORY

1. Chemisorption model. The derivation of this model is based on the monolayer chemisorption theory, which states that the rate of adsorption is affected by the evaporation and condensation processes.[101-103,153] The model is based on the following assumptions:

1) The conductivity of polyaniline is proportional to the number of conduction sites (dopant sites), N, uniformly distributed on the polymer surface. These sites can adsorb species that affect the conductivity.
2) All dopant sites are equivalent and the probability of a gas molecule adsorbing on any site is the same. Each site can only adsorb one molecule.

The adsorption process is described by the following equation:

$$\mathrm{A} + (\text{dopant site}) \underset{\mathrm{k}_{-1}}{\overset{\mathrm{k}_1}{\rightleftharpoons}} (\mathrm{A}) \qquad (2)$$

where A is the adsorbate, (A) is the adsorbate at an occupied site, k_1 is the adsorption rate constant and k_{-1} is the desorption rate constant. Thus, the net adsorption rate equals

$$R = \frac{d\theta}{dt} = k_1 c f(\theta) - k_{-1}\theta \qquad (3)$$

where c is the vapor concentration (in volume ppm), f(θ) is a surface coverage function, θ is the surface coverage, M_0 is the maximum adsorption coverage for a monolayer. By assuming that k_1 and k_{-1} are independent of θ, integrating Eq. 3 gives

$$\theta_{ads}(t) = \frac{M_0 k_1 c}{k_1 c + k_{-1}} (1 - e^{-(\mathrm{k}_1 \mathrm{c} + \mathrm{k}_{-1})\mathrm{t}}) \qquad (4)$$

The desorption equation can also be written in a similar expression as

$$\theta_{des}(t) = \mathrm{M}_0 (1 - e^{-\mathrm{k}_{-1}\mathrm{t}}) \qquad (5)$$

2. Langmuir adsorption isotherm. Langmuir suggested in 1918 that the adsorption process is controlled by the rates of evaporation and condensation. At equilibrium, the rates of evaporation and condensation are equal.[104] Thus

$$k_1 P_0 c f(\theta) = k_{-1} \tag{6}$$

Since normally 100% adsorption is improbable, a maximum adsorption coverage factor M_0 is incorporated, which gives $f(\theta) = M_0 - \theta$. Therefore, Eq. 5 can be written in the form

$$\theta = \frac{M_0 k_1 c}{k_1 c + k_{-1}} = \frac{M_0 bc}{bc+1} \tag{7}$$

with $k_1/k_{-1} = b$, which is the Langmuir adsorption constant.

3. Diffusion model. According to Fick's first law,[106] the rate of transfer of diffusing substance through the unit area of a section is proportional to the concentration gradient that is normal to that section, i.e.

$$J = -D\left(\frac{dc}{dx} + \frac{dc}{dy} + \frac{dc}{dz}\right) \tag{8}$$

where J is the flux of diffusant, D is the diffusion coefficient, C is the concentration of diffusant, and x, y, z are the spatial coordinates. Since the net flux into the element under consideration should be equal to the change in concentration (equation of continuity), Fick's second law can be obtained in the form of

$$\frac{dC}{dt} = \frac{d}{dx}\left(D\frac{dC}{dx}\right) + \frac{d}{dy}\left(D\frac{dC}{dy}\right) + \frac{d}{dz}\left(D\frac{dC}{dz}\right) \tag{9}$$

For diffusion in a long circular cylinder where diffusion is everywhere radial,[154] through substitution of $x = r\cos\theta$ and $y = r\sin\theta$, we can obtain the following equation,

$$\frac{dC}{dt} = \frac{1}{r}\frac{d}{dr}\left(rD\frac{dC}{dr}\right) \tag{10}$$

In the cylinder of radius, a, the boundary conditions are

$C = C_0$, r = a, t ≥ 0,

C= 0, 0 < r <a, t = 0,

By solving Eq. 10, one can obtain

$$C(r,t) = C_0\left(1 - \frac{2}{a}\sum_{n=1}^{\infty}\frac{\exp(-D\alpha_n^2 t)J_0(r\alpha_n)}{\alpha_n J_1(a\alpha_n)}\right) \quad (11)$$

where $J_0(x)$ is the Bessel function of the first kind of order zero, and $J_1(x)$ is the Bessel function of the first kind of order one. Integrating C(r, t) as a function of r from 0 to a gives[154]

$$M_t = \int_0^a C(r,t)dr = M_\infty\left(1 - \sum_{n=1}^{\infty}\frac{4}{a^2\alpha_n^2}\exp(-D\alpha_n^2 t)\right) \quad (12)$$

where M_t denotes the quantity of substance that diffuses into the cylinder in time t, M_∞ is the corresponding quantity after infinite time (i.e., equilibrium sorption amount), and α_ns are roots of Bessel function of the first kind of order zero.

4. Sorption. In 1958, Barrer et al. proposed a dual sorption model to describe the sorption isotherms of small gas molecules in polymers.[107] In glassy polymers, there exists a distribution of "holes" frozen in the structure. These holes can immobilize some of penetrant molecules by entrapment or by binding various sites. Therefore, this model consists of two concurrent mechanisms of sorption: ordinary dissolution and "hole-filling". The equilibrium sorption uptake can be expressed by the following equation:[108-109,155]

$$C = C_D + C_H = k_D P + \frac{C_H' bP}{1+bP} \quad (13)$$

where k_D is the Henry's law constant, P is the vapor pressure of the penetrant, C_H' is the maximum uptake in holes, b is the hole affinity constant. The first term C_D represents

sorption of normally diffusible species, while the second term C_H represents the sorption in holes.

5. RESULTS AND DISCUSSION

Figure 1 shows the scanning electron microscopy (SEM) and transmission electron microscopy (TEM) of polyaniline/Ag nanocomposite thin films grown on the interdigitated electrodes. These images clearly show a nanofiber structure with an average fiber diameter of about 51 nm, as analyzed by ImageJ.[156] The morphology is consistent with our previous results.[77]

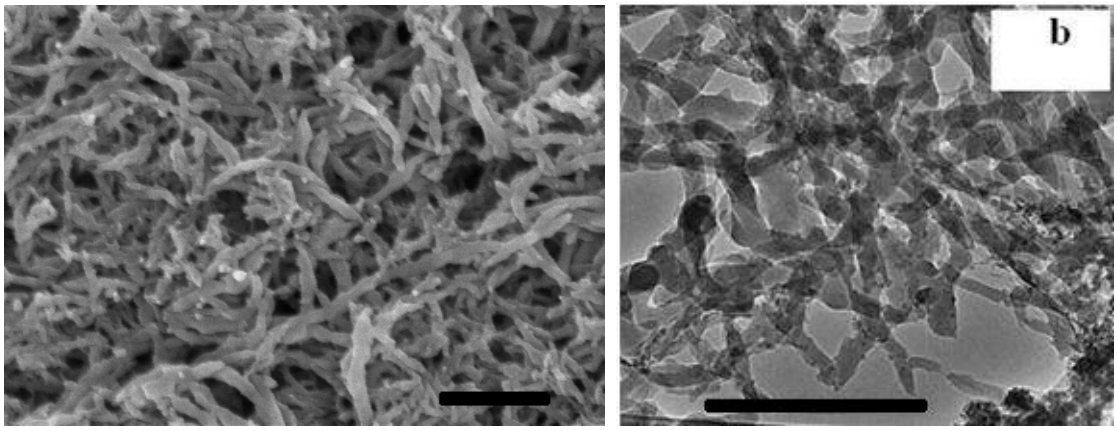

Figure 1. SEM (a) and TEM (b) images of polyaniline/Ag nanocomposites grown on the interdigitated electrodes. The scale bar in the TEM image is 500 nm.

The change in current in our sensors in response to vapors was monitored. Figure 2 displays the real-time change in the normalized current of the nanocomposite sensors upon exposure to triethylamine at various concentrations. We observed a fast current decrease within 120 s as a result of the dedoping of polyaniline and decrease in the charge transfer by triethylamine. The dedoping of polyaniline/Ag is generally a reversible process after replacing the triethylamine vapor with pure N_2. As shown in the figure, the

current decreases very fast in the early stage and then tends to level off. In our previous work, it was demonstrated that these decay curves can be fit by a single exponential function.[136]

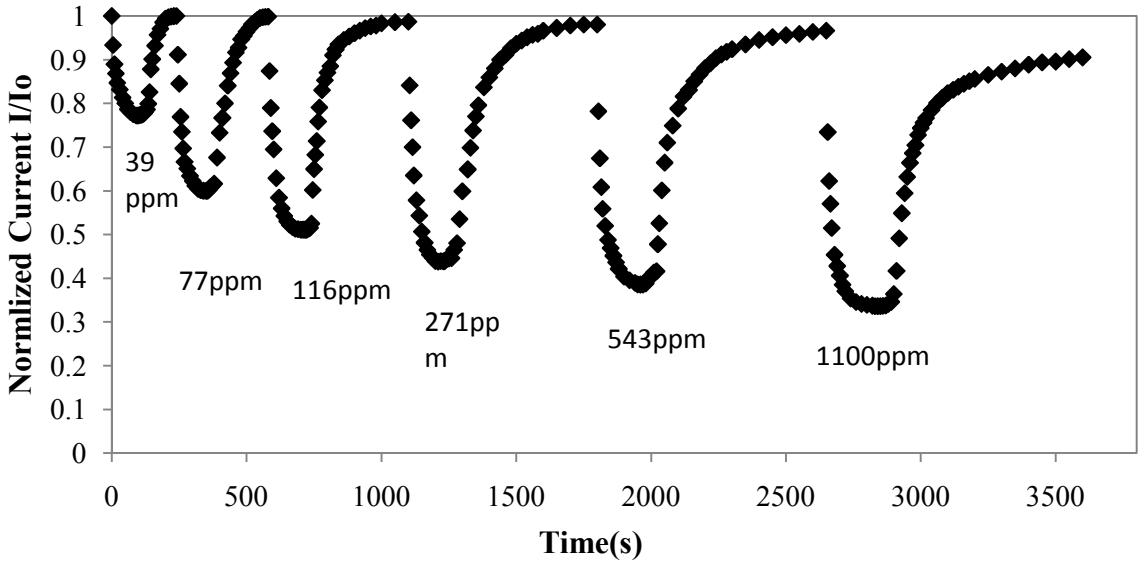

Figure 2. Sensor response and recovery curves of the polyaniline/Ag nanocomposite sensor upon the exposure of triethylamine. The sensor was exposed to the triethylamine vapor for 100 s and then exposed to pure nitrogen until the current became stable before it was exposed to the next concentration of triethylamine.

1. Analysis based on the chemisorption model. The adsorption of nitrogen gas on or in the polyaniline film does not significantly affect the conductivity of the polyaniline, especially compared to the response to triethylamine and toluene. If the conductivity is proportional to the number of conductive sites, the normalized current should be proportional to the fraction of unoccupied sites, or

$$I_{norm}(t) = 1 - \theta(t) = 1 - \frac{M_0' k_1 c}{k_1 c + k_{-1}}(1 - e^{-(k_1 c + k_{-1})t}) \qquad (14)$$

where M_o' is the fraction of occupied sites, and $b=k_1/k_{-1}$.

Figure 3 shows the individual polyaniline/Ag composite sensor responses as a function of time to triethylamine at various concentrations. The y-axis is the normalized current monitored by the electrometer, and the x-axis is the gas exposure time. The current changes follow exponential decays with the time constants increasing with increasing concentrations. These decay curves were fit by a least-squares fit to

$$I_{norm}(t) = 1 - I_{\infty} \times (1 - e^{-t/\tau_a}) \quad (15)$$

Comparing Eq. 14 and 15, the functional form becomes

$$I_{\infty} = \frac{M_0 bc}{bc+1} \quad (16)$$

and $$\tau_a = \frac{1}{k_1 c + k_{-1}} \quad (17)$$

Similarly, the recovery curves were fit to an exponential growth or:

$$I_{norm}(t) = 1 - I_{\infty} e^{-t/\tau_d} \quad (18)$$

In this case, I_{∞} is taken as the value from the fitted decay curve which means that the I_{∞} values vary from sample to sample. As shown by Figures 3 and 4, the fitting curves are consistent with the measured data. The time constants τ_a and τ_d are for adsorption and desorption, respectively. Table 1 shows the value of the fitting constants I_{∞}, τ_a and τ_d for these curves. As is evident from the curves, I_{∞} and τ_d increases with the triethylamine concentration, while τ_a decreases with it. This effect seems indicative of a strong interaction of the solvent with the polymer. For the highest amount of triethylamine there is a noticeable deviation from a single exponential for the recovery curve. The time constants, τ_a and τ_d, were unable to fit with Eq. 17. However, they can be fit to a power law in the form of $\tau_a = 0.683c^{-0.33}$ and $\tau_d = 2655c^{0.43}$. A power law relationship was also observed for NO_2 adsorbed on polyaniline.[152,157] The cause of this problem is still

unknown. A possible explanation is that during the derivation τ_a and τ_d were assumed to be independent of concentration, which may not be the case.

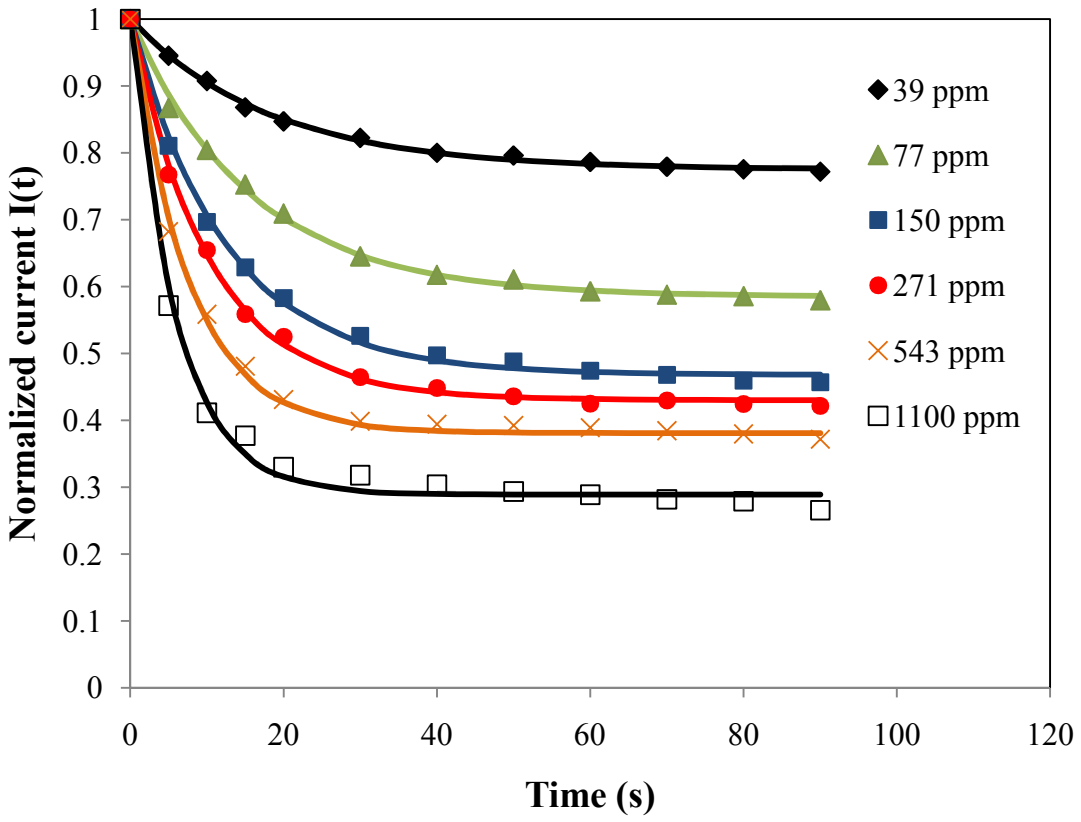

Figure 3. Polyaniline/Ag nanocomposite sensor response to triethylamine vapor of various concentrations fit to exponential decays. The curves are best fits from Eq. 15.

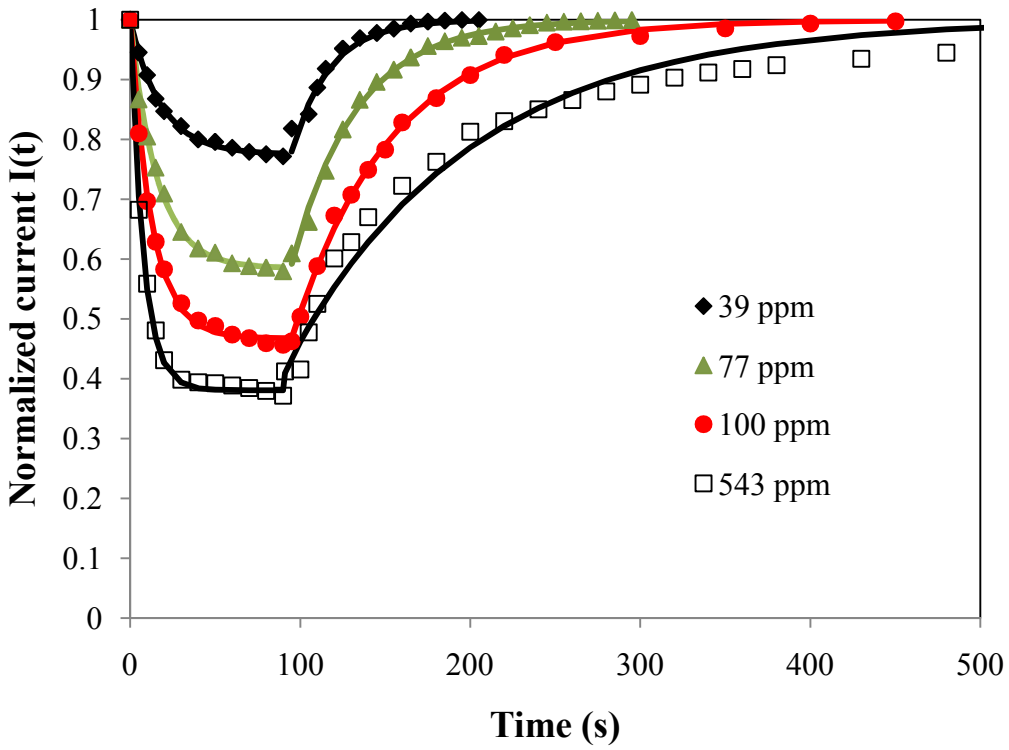

Figure 4. Polyaniline/Ag nanocomposite recovery curves to triethylamine vapor of various concentrations fit to an exponential increase after the organic vapor was removed. The curves are best fits from Eq. 15 until 100s then Eq. 18.

Table 1. Fitting constants of the polyaniline/Ag sensor exposed to triethylamine from Eqs. 15 and 18

Concentration (ppm)	I_∞	τ_a (s)	τ_d (s)
39	0.225	18.3	22.4
77	0.410	16.7	37.9
116	0.486	13.9	48.6
150	0.526	12.5	58.9
271	0.570	10.4	94.1
543	0.619	7.5	109
1100	0.719	5.9	131

Figure 5 shows the polyaniline/Ag composite sensor response as a function of time exposed to toluene at various concentrations. These curves were also fit using an exponential decay. Recovery curves were not measured for toluene. Values of fitting constants I_∞ and τ are shown in Table 2. Similarly, I_∞ also increases with the toluene vapor concentration and τ_a decreases. The time constants for toluene were larger (longer times) than for triethylamine. The time constant τ_a was fit to a power law in concentration as: $\tau_a = 2.89c^{0.25}$.

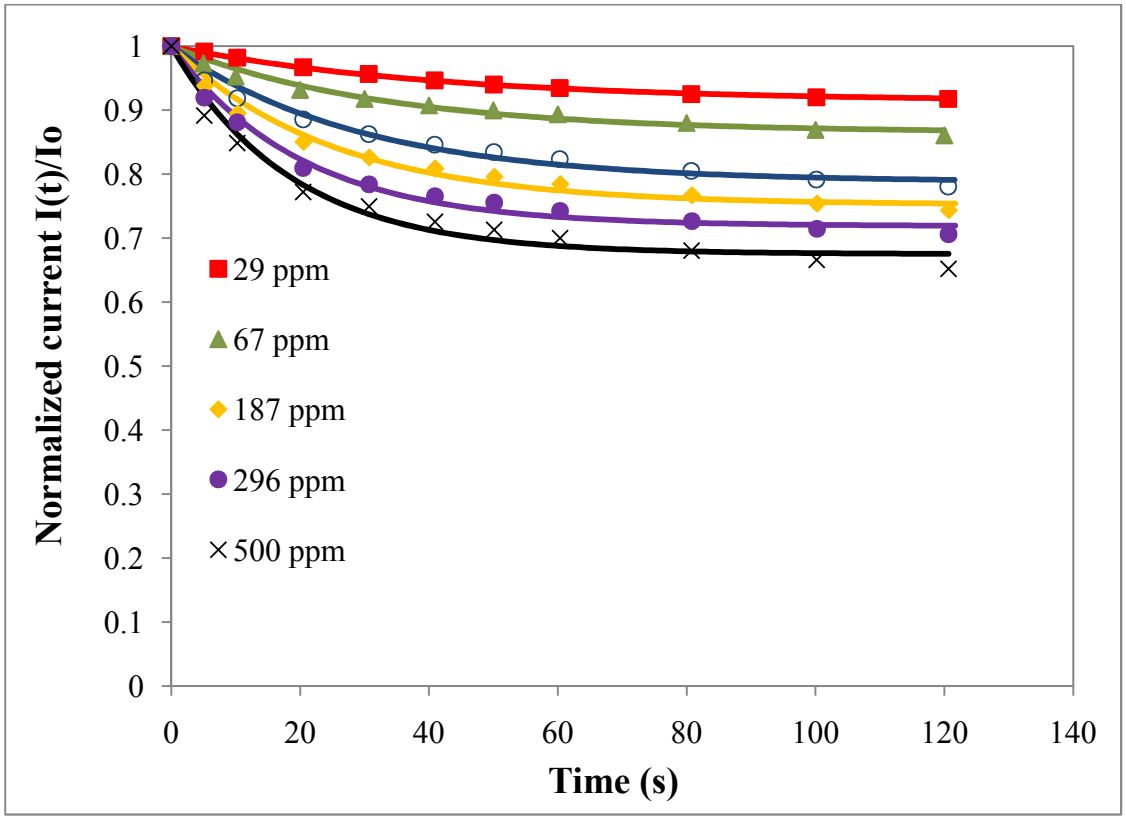

Figure 5. Polyaniline/Ag nanocomposite sensor response to toluene vapor of various concentrations fit to an exponential decay. The curves are best fits from Eq. 15.

Table 2. Fitting constants of the polyaniline/Ag sensor exposed to toluene from Eq. 15

Concentration (ppm)	I_∞	τ_a(sec)
23	0.086	41.2
67	0.135	32.9
146	0.212	29.2
187	0.248	25.0
296	0.281	20.2
500	0.325	18.6

In this chemisorption model, the fitting constant, I_∞, was related to the adsorbed amount, obtained from the fit at each triethylamine concentration. Figure 6 is a plot of the fitting constant, I_∞, as a function of triethylamine and toluene concentrations. It is shown that these curves can be fit to the Langmuir isotherm equation. Based on equation 7, the normalized maximum adsorption amount, M_0, is equal to 0.733 and 0.407 for toluene and triethylamine, respectively. The Langmuir constant, b, for triethylamine and toluene are 1.48×10^4 atm^{-1} and 7.86×10^3 atm^{-1}, respectively. The values of Langmuir constant are higher with those values reported for triethylamine adsorbed on CdSe (380 atm^{-1}) and toluene adsorbed on active carbon (2845 atm^{-1}).[158-159] This may be due to the strong interaction of triethylamine and toluene with polyaniline/Ag composites.

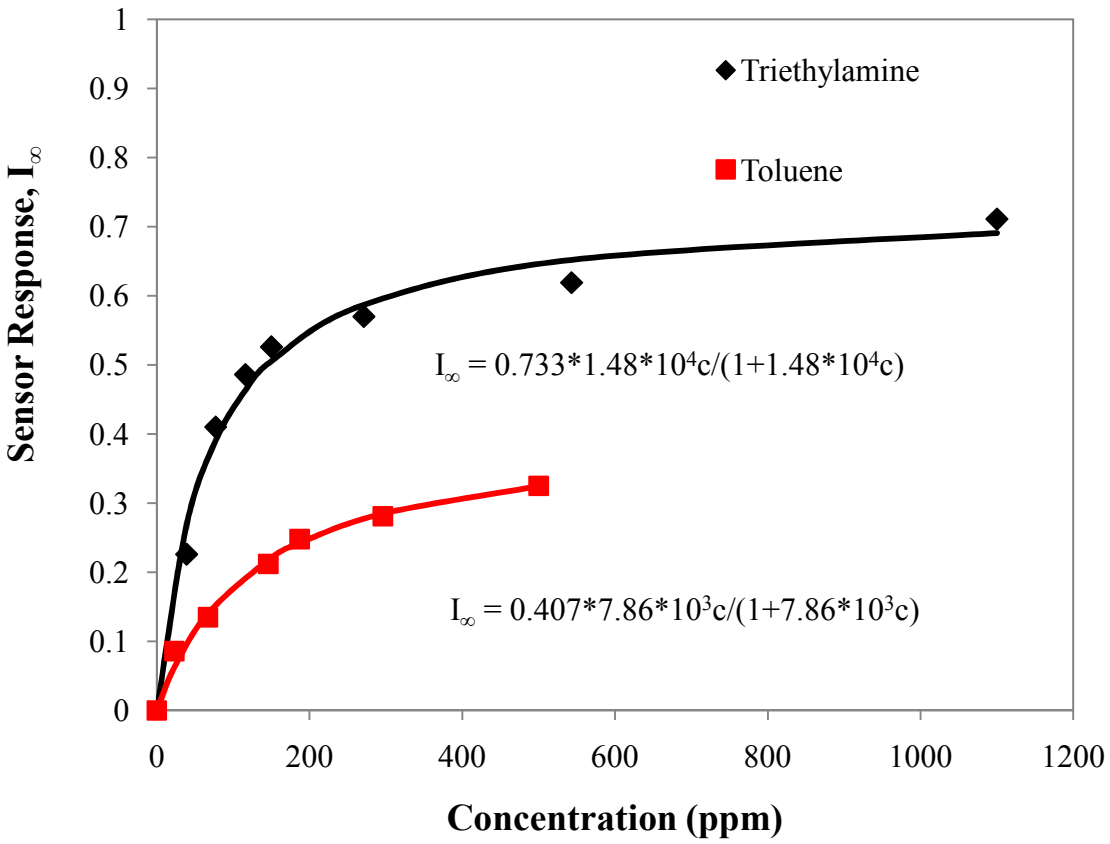

Figure 6. Plot of the sensor response, I_∞, as a function of toluene and triethylamine vapor concentrations fit to a Langmuir isotherm.

2. Analysis based on the diffusion model. Adsorption normally only occurs at the surface of the adsorbate. In our work, the polyaniline consists of mainly interconnected network of nanofibers. Diffusion in a cylinder may also be appropriate to describe the transport process. Therefore, the sensor response curves were also fit using a diffusion model for comparison. It has been reported previously that there is a charge transfer effect between polyaniline and Ag nanoparticles. The response of polyaniline/Ag composite sensor to triethylamine was caused by both the dedoping of polyaniline and a reduction in the charge transfer. For simplicity, we assume that the effect of charge transfer can be modeled in the same way as dedoping process. The conductivity through

the polyaniline film is linearly proportional to the concentration of the dopant, [DP], which is equal to the initial dopant concentration, $[DP]_0$, minus the reacted dopant.[4] As discussed in the previous section, the sensing mechanism of triethylamine is based on the reaction between the triethylamine and the acid dopant. The enthalpy of reaction of the protonation of triethylamine was determined to be about -43.4 kJ/mol, indicating that this reaction is exothermic. Therefore, we assume that each triethylamine molecule that diffuses into the polyaniline film will react with a dopant molecule. The conductivity of polyaniline can be given as

$$\sigma \propto [DP] = [DP]_0 - [Triethylamine] \quad (19)$$

Then, the normalized current can be expressed in the form of

$$I_{norm}(t) = 1 - \frac{M_\infty}{[DP]_0}\left(1 - \sum_{n=1}^{\infty} \frac{4}{a^2 \alpha_n{}^2} \exp(-D\,\alpha_n t)\right) \quad (20)$$

The result of fitting the data from the polyaniline/Ag sensor exposed to gaseous toluene at concentrations of 39 to 1100 ppm is shown in Figure 7. Two fitting constants, $M_\infty/[DP]_0$ and D, were obtained from a least-square fit based on Eq. 20. The values of the fitting constants for these curves are shown in Table 3. It was apparent that $M_\infty/[DP]_0$ and D increase with the toluene concentration. Since $[H^+]_0$ should be a constant for all of our sensors, the fitting constant, $M_\infty/[H^+]_0$, then should be proportional to the final absorbed amount, M_∞.

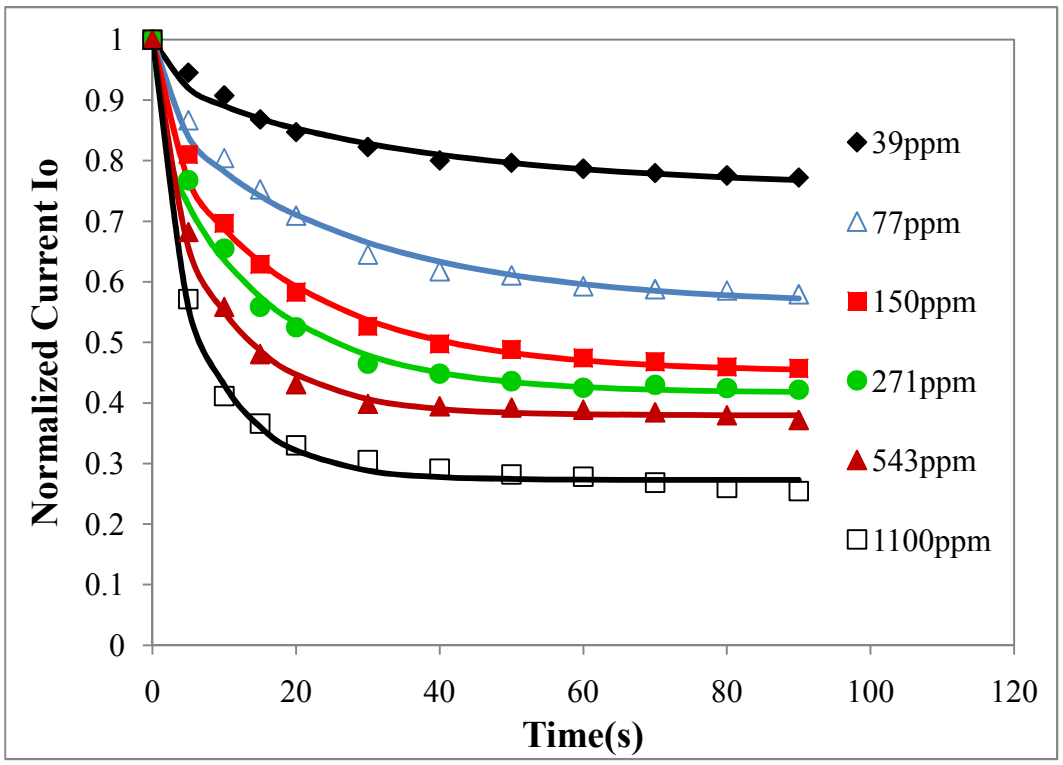

Figure 7. Polyaniline/Ag nanocomposite sensor response to triethylamine vapor of various concentrations fit with the diffusion model. The curves are best fits from Eq. 20.

Table 3. Fitting constants of the polyaniline/Ag sensor exposed to triethylamine

Concentration (ppm)	$M_\infty/[DP]_0$	$D*10^{18}(m^2/s)$
39	0.244	3.12
77	0.440	4.01
116	0.511	4.71
150	0.549	5.57
271	0.583	7.02
543	0.620	10.4
1100	0.727	13.1

Toluene is a solvent that can swell the polymer and increase the polymer interchain distance; consequently causing a conductivity decrease. The conductivity of a conducting polymer is dependent on the hopping distance, i.e., the interchain distance. It can be expressed in an exponential term:[46,48-49]

$$\sigma = \sigma_0 \exp(-\beta\delta) \quad (21)$$

where σ_0 is the preexponential constant, β is the electron-tunneling coefficient, δ is the hopping distance. The swelling phenomenon of polymers generally consists of the diffusion of solvent molecules and the chain relaxation process. The relaxation process is considerably slower than the diffusion and may take hours to occur.[160] If this is the case, the interchain distance is only proportional to the uptake of a diffusing substance.

$$\frac{\delta(t)-\delta_1}{\delta_\infty-\delta_1} \propto M(t) \quad (22)$$

where δ_1 stands for the initial interchain distance, δ_∞ denotes the interchain distance when swelling is at equilibrium. Thus, the normalized current of polyaniline during the swelling can be expressed as

$$I_{norm}(\mathrm{t}) = \exp\left(-\Delta\delta_\infty\beta M_\infty\left(1-\sum_{\mathrm{n}=1}^{\infty}\frac{4}{\mathrm{a}^2\alpha_\mathrm{n}{}^2}\exp(-\mathrm{D}\,\alpha_\mathrm{n}\mathrm{t})\right)\right) \quad (23)$$

where $\Delta\delta$ is the maximum interchain distance change.

Figure 8 shows the sensor response upon exposure to toluene at various concentrations fit with the diffusion model. The values of fitting constants, $\Delta\delta_\infty\beta M_\infty$ and D, are listed in Table 4. Similar to the fitting constants for triethylamine, the quantity $\Delta\delta_\infty\beta M_\infty$ is considered as the product for study of sorption uptake, because $\Delta\delta_\infty$, and β are constants.

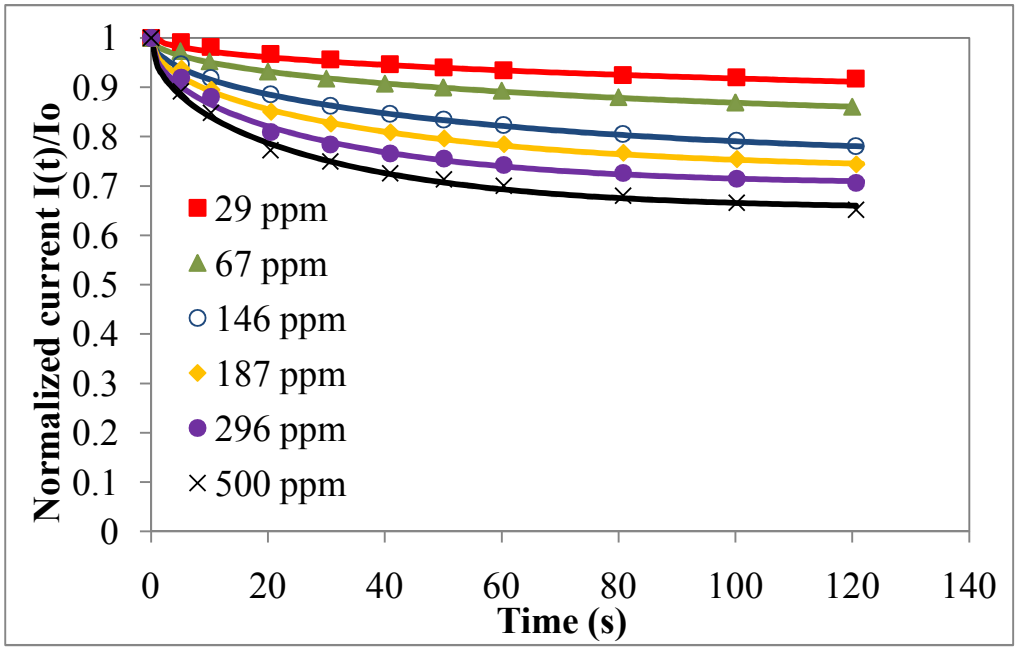

Figure 8. Polyaniline/Ag nanocomposite sensor response to toluene vapor of various concentrations and the fits with the diffusion model. The curves are best fits from Eq. 23.

Table 4. Fitting constants of the polyaniline/Ag sensor exposed to toluene using Eq. 23

Concentration (ppm)	$\Delta\delta_\infty\beta M_\infty$	$D*10^{18}$ (m^2/s)
29	0.150	0.2757
67	0.209	0.852
146	0.307	1.23
187	0.326	1.90
296	0.362	2.59
500	0..441	2.96

Plots of the normalized uptake of toluene and triethylamine as a function of concentration are shown in Figure 9 and 10. These curves were fit with the dual sorption model and Langmuir isotherm. It was found that both models fit the sorption uptake of

triethylamine very well (i.e., the fitting error (sum of the squares of the residuals) from the dual sorption model was only 5% smaller than that of that by Langmuir isotherm). However, the fitting error from the dual sorption model was 76% smaller than that from Langmuir isotherm. Thus, the sorption model fits the toluene data better. Comparing fitting equations with Eq. 22, we can determine that the normalized uptake in holes is equal to 0.701 and 0.336 for toluene and triethylamine, respectively. The Langmuir constant of triethylamine is about 1.86×10^4 atm^{-1}, which is close to that from the chemisorption model. However, the Langmuir constant of toluene is found to be 2.33×10^4 atm^{-1}, much larger than that predicted by the chemisorption model. The Henry's Law dissolution constant of triethylamine and toluene is determined to be 39.3 and 259.4 atm^{-1}, respectively. This may result from the higher solubility of toluene in polyaniline. The diffusion coefficients of toluene and triethylamine are plotted as a function of concentration and shown in Figure 11. The diffusion coefficients show an increase with the vapor concentration and can be fit into an empirical power law or an exponential function. The fitting equations for triethylamine was determined as $D = 273.5c^{0.44}$ or $D = 12.7x(1 - e^{-3684.8c})$. For toluene, the fits yielded, $D = 417c^{0.64}$ or $D = 3.62x(1 - e^{-3660.3c})$. Again, the increase in diffusion coefficient was probably due to the swelling effect of these organic vapors, which greatly increases the solubility.[161-162]

Although direct measurements of the toluene and triethylamine gas diffusion coefficients are not available in polyaniline, one can estimate the diffusion coefficient of a gas in polymers from kinetic diameters using an empirical equation proposed by Michaels and Bixler.[163-164] From these, the estimated values of vapor diffusion coefficients of toluene and triethylamine in polyaniline are on the order of 10^{-16} m^2/s,

which are larger than those determined in our model. In their empirical model, the interaction of the gas molecules and the polymer was ignored. However, our diffusion substances showed a strong interaction with the polyaniline which would be expected to lower the diffusion coefficient. Given this, the values obtained in this work seem reasonable.

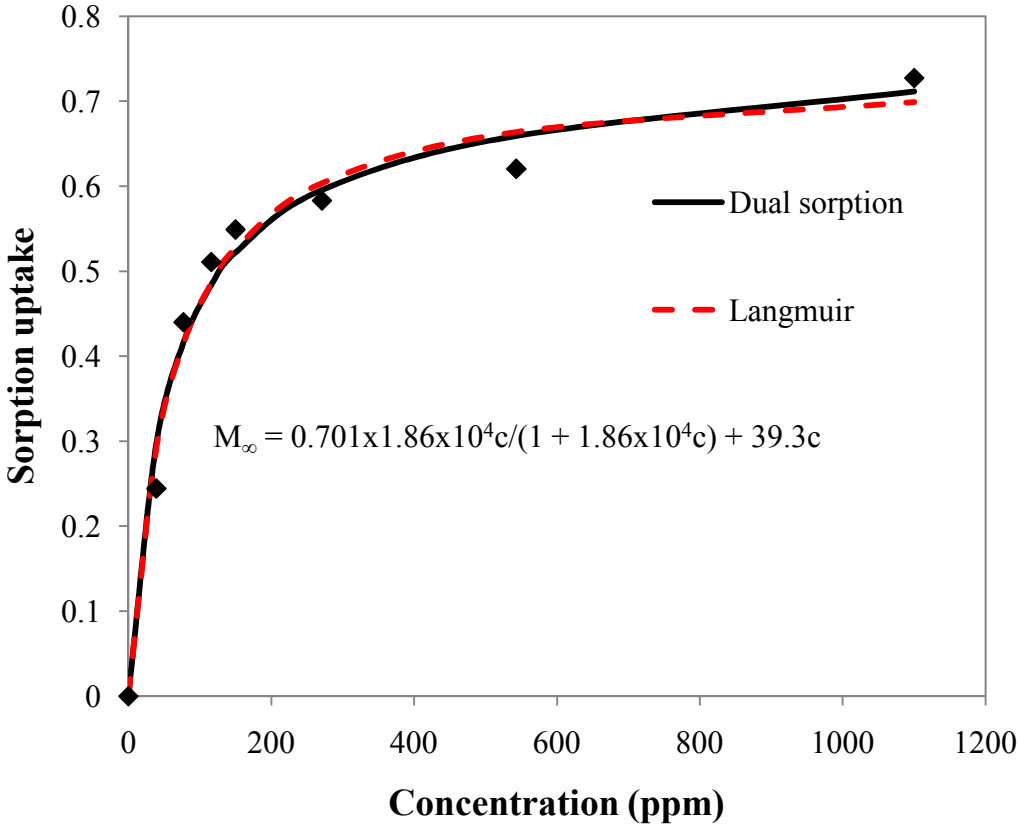

Figure 9. Plot of sorption uptake of triethylamine as a function of concentration. The curves were fit by the dual sorption and Langmuir isotherm models.

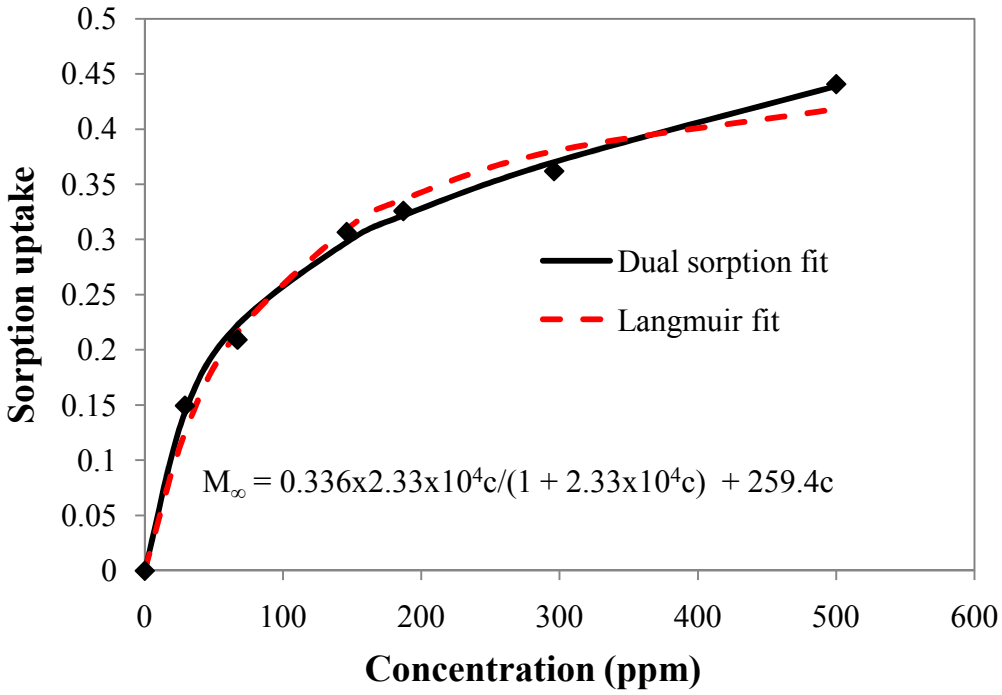

Figure 10. Plot of sorption uptake of toluene as a function of concentration with the fit for the dual sorption model and Langmuir isotherm models.

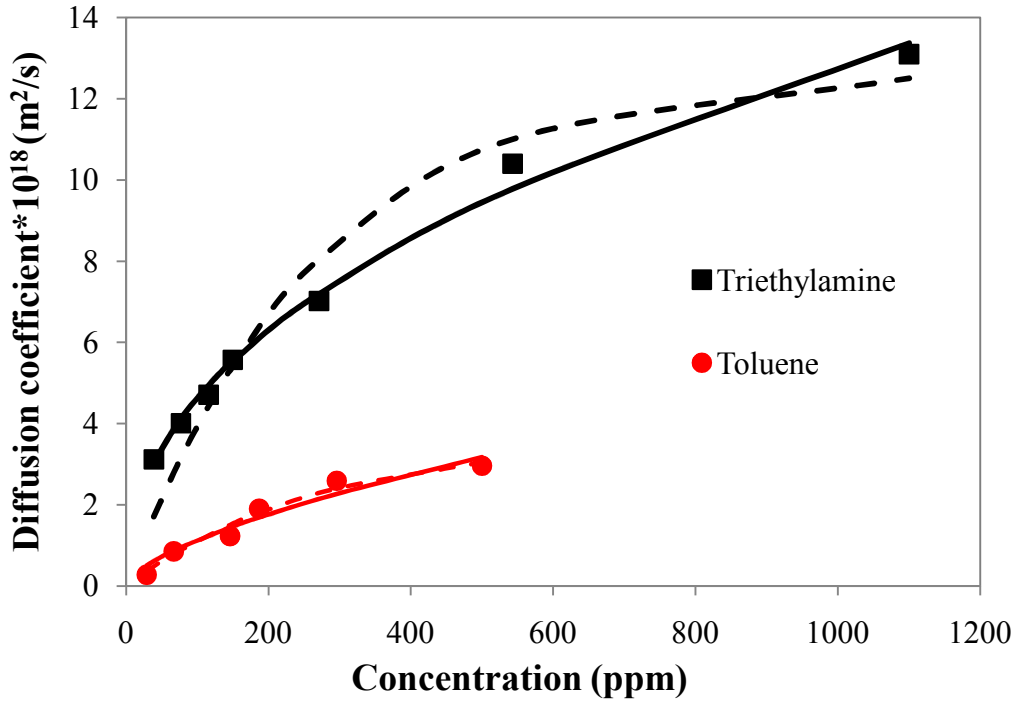

Figure 11. Diffusion coefficients of toluene and triethylamine as a function of concentration fit with a power law (curve) and an exponential function (dashed curve).

3. Reproducibility and fitting error. The reproducibility of independent measurements is illustrated in Figure 12 for the sensor response to 39 ppm triethylamine. The individual data points were averaged from four independent experiments. From each of the 4 runs, the values of the uptakes and diffusion coefficients were calculated. The resuting means and standard deviations were also calcualted and are shown in Table 5.A small standard deviation (about 1.4%) was found for the sorption uptake, and a larger error (about 6.7%) was attained for the diffusion coefficient.

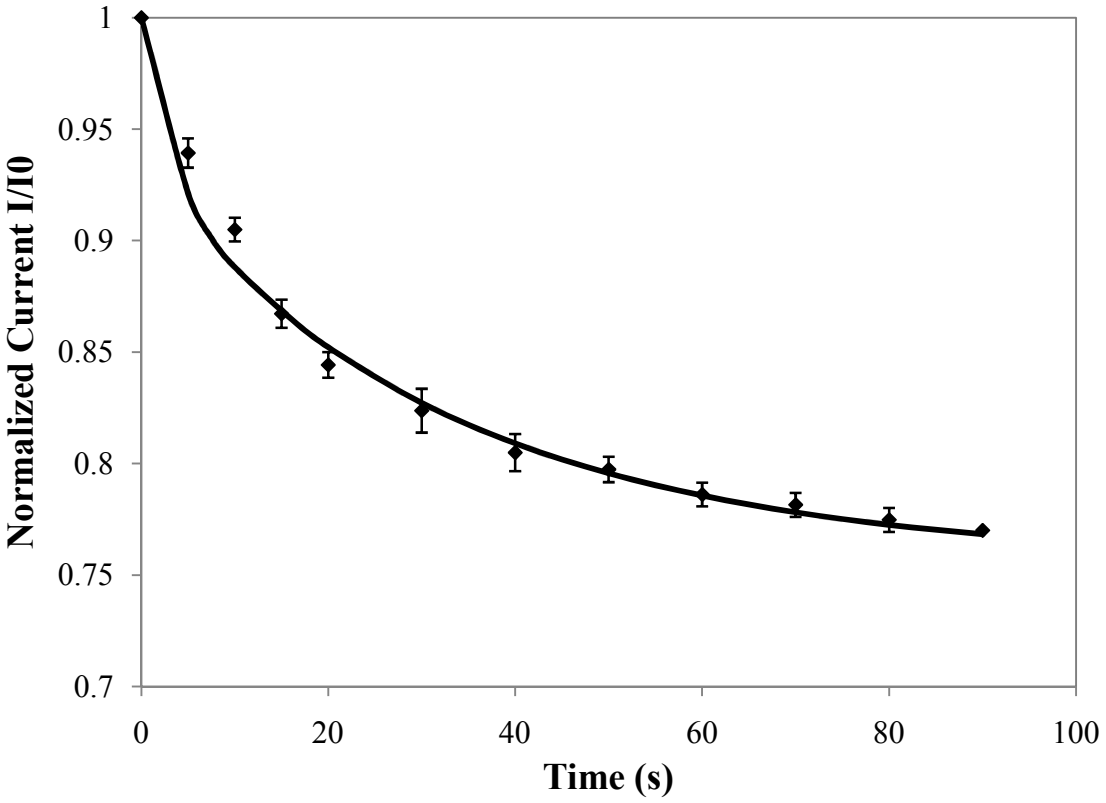

Figure 12. Sensor responses to 39 ppm triethylamine plotted with the error bar representing the averages of 4 runs from independent experiments. The curve is the best fit of the averaged data, using the diffusion model.

Table 5. Fitting constants of the polyaniline/Ag sensor exposed to 39 ppm triethylamine

Run	No. 1	No. 2	No. 3	No. 4	Average	Standard Deviation
$M_\infty/[DP]_0$	0.248	0.246	0.244	0.239	0.244	1.43%
$D*10^{18}$ (m^2/s)	3.26	3.14	3.55	3.05	3.24	6.7%

Since the experimental data was fit using the least-square method, the least squares from the fitting were considered as the fitting error. Table 6 and 7 shows the values of averaged least squares (the square root of the least square divided by the number of data points).

Table 6. Averaged least squares of two models for sensor response to triethylamine

Concentration (ppm)	39	77	116	150	271	543	1100
Chemisorption model	0.0083	0.0133	0.0076	0.0134	0.0074	0.0096	0.0171
Diffusion Model	0.0067	0.0074	0.0096	0.0085	0.0117	0.0104	0.0120

Table 7. Averaged least squares of two models for sensor response to toluene

Concentration (ppm)	29	67	143	150	271	543
Chemisorption model	0.00512	0.00557	0.00868	0.0093	0.00906	0.0132
Diffusion Model	0.00341	0.00311	0.00292	0.0134	0.0147	0.0104

6. CONCLUSIONS

A chemisorption and diffusion model has been used to fit the responses of polyaniline/Ag nanocomposite sensors exposed to triethylamine and toluene at several different concentrations. Both models can mathematically fit the sensor response as a

function of time. As determined from the fitting constants, a Langmuir adsorption isotherm was used in the chemisorption fit, while a dual sorption mechanism was required for the diffusion fit. In addition, the diffusion coefficient obtained in the diffusion fit was found to increase with the vapor concentration, probably due to the swelling effect by organic vapors. Fitting errors from the two models were small, both allowing reasonable mathematical forms for the time-dependent and concentration behavior. These fitting results are consistent with the behavior predicted by these models. Our results also show the potential for studying the adsorption or diffusion process of conducting polymers based on conductivity measurements.

7. ACKNOWLEDGEMENTS

The authors acknowledge Terry Colberg and Balika Khatiwada for assistance in obtaining the TEM pictures. FDB acknowledges the financial support of the National Science Foundation under grant DMR-1005606 and of Materials Research Center, Missouri S and T.

8. REFERENCES

(1) Seiyama, T.; Kato, A.; Fujiishi, K.; Nagatani, M. *Anal. Chem.* **1962**, *34*, 1502.

(2) *Solid State Chemical Sensors*; Janata, J.; Huber, R. J., Eds.; Academic Press: Orlando, 1985.

(3) Dhawan, S. K.; Kumar, D.; Ram, M. K.; Chandra, S.; Trivedi, D. C. *Sens Actuators B* **1997**, *40*, 99.

(4) Nicolas-Debarnot, D.; Poncin-Epaillard, F. *Anal. Chim. Acta* **2003**, *475*, 1.

(5) Kanungo, M.; Kumar, A.; Contractor, A. Q. *Anal. Chem.* **2003**, *75*, 5673.

(6) Liu, H.; Kameoka, J.; Czaplewski, D. A.; Craighead, H. G. *Nano Lett.* **2004**, *4*, 671.

(7) Virji, S.; Huang, J. X.; Kaner, R. B.; Weiller, B. H. *Nano Lett.* **2004**, *4*, 491.

(8) Virji, S.; Kaner, R. B.; Weiller, B. H. *Chem. Mater.* **2005**, *17*, 1256.

(9) Pillalamarri, S. K.; Blum, F. D.; Tokuhiro, A. T.; Story, J. G.; Bertino, M. F. *Chem. Mater.* **2004**, *17*, 227.

(10) Werake, L. K.; Story, J. G.; Bertino, M. F.; Pillalamarri, S. K.; Blum, F. D. *Nanotechnology* **2005**, *16*, 2833.

(11) Pillalamarri, S. K.; Blum, F. D.; Tokuhiro, A. T.; Bertino, M. F. *Chem. Mater.* **2005**, *17*, 5941.

(12) Li, Z. F.; Blum, F. D.; Bertino, M. F.; Kim, C. S.; Pillalamarri, S. K. *Sens Actuators B* **2008**, *134*, 31.

(13) Gardner, J. W.; Bartlett, P. N.; Pratt, K. F. E. *IEE P-Circ. Dev. Syst.* **1995**, *142*, 321.

(14) Hwang, B. J.; Yang, J.-Y.; Lin, C.-W. *J. Electrochem. Soc.* **1999**, *146*, 1231.

(15) Lin, C. W.; Liu, S. S.; Hwang, B. J. *J. Appl. Polym. Sci.* **2001**, *82*, 954.

(16) Hu, H.; Trejo, M.; Nicho, M. E.; Saniger, J. M.; García-Valenzuela, A. *Sens Actuators B* **2002**, *82*, 14.

(17) *Introduction to Surface Chemistry and Catalysis*; Somorjai, G. A., Ed.; Wiley-Interscience: New York, 1994.

(18) *Physical Chemistry of Surfaces*; Adamson, A. W.; Gast, A. P., Eds.; John Wiley & Sons, Inc: New York, 1997.

(19) *Adsorption By Powders & Porous Solids*; Rouquerol, F.; Rouquerol, J.; Sing, K., Eds.; Academic Press: London, 1999.

(20) Panczyk, T.; Rudzinski, W. *Langmuir* **2003**, *19*, 1173.

(21) Langmuir, I. *J. Am. Chem. Soc.* **1918**, *40*, 1361.

(22) Fick, A. E. *Ann. Phys. Chem.* **1855**, *170*, 59.

(23) *The Mathematics of Diffusion, 2nd Edition*; Crank, J., Ed.; Oxford University Press: New York, 1975.

(24) Barrer, R. M.; Barrie, J. A.; Slater, J. *J. Polym. Sci.* **1958**, *27*, 177.

(25) *Diffusion In and Through Polymers*; Vieth, W. R., Ed.; Hanser: New York, 1979.

(26) *Diffusion In Polymers*; Neogi, P., Ed.; Marcel Dekker: New York, 1996.

(27) Vieth, W. R.; Tam, P. M.; Michaels, A. S. *J. Colloid Interface Sci.* **1966**, *22*, 360.

(28) Rasband, W. S.; US National Institutes of Health: Bethesda, MD, 1997-2010.

(29) Elizalde-Torres, J.; Hu, H.; García-Valenzuela, A. *Sens Actuators B* **2004**, *98*, 218.

(30) Qinghong, Y.; Stephanie, L. B. *Nanotechnology* **2010**, *21*, 115502.

(31) Benkhedda, J.; Jaubert, J.-N.; Barth, D.; Perrin, L. *J. Chem. Eng. Data* **2000**, *45*, 650.

(32) Chiang, J.-C.; MacDiarmid, A. G. *Synth. Met.* **1986**, *13*, 193.

(33) Conwell, E. M.; Perlstein, J.; Shaik, S. *Phys. Rev. B* **1996**, *54*, 2308.

(34) Wuelfing, W. P.; Murray, R. W. *J. Phys. Chem. B* **2002**, *106*, 3139.

(35) Zamborini, F. P.; Smart, L. E.; Leopold, M. C.; Murray, R. W. *Anal. Chim. Acta* **2003**, *496*, 3.

(36) Wind, J. D.; Sirard, S. M.; Paul, D. R.; Green, P. F.; Johnston, K. P.; Koros, W. J. *Macromolecules* **2003**, *36*, 6442.

(37) Wang, B.-G.; Yamaguchi, T.; Nakao, S.-i. *Polymer* **2001**, *42*, 5225.

(38) Krüger, K.-M.; Sadowski, G. *Macromolecules* **2005**, *38*, 8408.

(39) Chang, M.-J.; Liao, Y.-H.; Myerson, A. S.; Kwei, T. K. *J. Appl. Polym. Sci.* **1996**, *62*, 1427.

(40) Michaels, A. S.; Bixler, H. J. *J. Polym. Sci.* **1961**, *50*, 413.

4. A TEMPLATELESS ROUTE TO POLYTHIOPHENE NANOFIBERS: EFFECT OF SYNTHETIC CONDITIONS AND MECHANISM OF FORMATION

Zhe-Fei Li[a], Frank D. Blum[a,b,c], Massimo F. Bertino[d], Chang-Soo Kim[e,f],

[a] Department of Materials Science and Engineering, Missouri University of Science and Technology, Rolla, MO 65409

[b]Department of Chemistry, Missouri University of Science and Technology, Rolla, MO 65409

[c] Department of Chemistry, Oklahoma State University, Stillwater, OK, 74078

[d] Department of Physics, Virginia Commonwealth University, Richmond, VA 23824

[e] Department of Electrical and Computer Engineering, Missouri University of Science and Technology, Rolla, MO 65409

[f] Department of Biological Sciences, Missouri University of Science and Technology, Rolla, MO 65409

1. ABSTRACT

An oligomer-assisted polymerization method has been employed to synthesize polythiophene nanofibers. A small amount (about 3-5 wt%) of oligothiophene (i.e., bithiophene and terthiophene) was incorporated into the polymerization system, producing polythiophene nanofibers with diameters typically around 30-60 nm. Polythiophene nanofibers were found to exhibit higher crystallinity and better thermal stability than bulk polythiophene. The effect of synthetic conditions, such as concentration, temperature, and solvent, on the morphology was studied. It was

determined that nanofiber formation was generally favored for reactions performed at higher oxidant concentrations and lower monomer concentrations in relatively polar solvents. An intermolecular oligomer nucleation theory was proposed to explain the probable formation mechanism.

Keywords: Conducting polymers, polythiophene, nanofibers, oligomer, nucleation.

2. INTRODUCTION

Low-dimensional nanoscale materials, especially 1-dimensional nanostructures, have attracted considerable attention in recent years.[165] Nanostructured conducting polymers have advantages in various applications over conventional bulk polymers due to their high surface areas and fast charge transport.[63,136] A variety of methods have been used to synthesize conducting polymer nanofibers. Physical routes, such as electrospinning, have been developed and widely used for fabrication of nanofiber devices.[67-68] The template-synthesis procedure also has been employed using different templates, such as porous alumina and polycarbonate membranes, to control the morphology of the polymer.[69,166] In order to simplify template removal, hard templates have sometimes been replaced by soft templates, such as surfactants and micelles.[13,70] Recently, research has been focused on templateless synthesis methods, such as gamma-rays or UV-irradiation techniques,[24,75] interfacial polymerization,[9] rapid-mixing,[71] dilution polymerization,[72] oligomer-assisted polymerization,[23,167] and nanofiber seeding.[73-74] However, the nature of the nanofiber formation mechanism is still uncertain. For instance, Li and Kaner pointed out that that the formation of polyaniline nanofibers was a result of homogeneous nucleation and suppression of the secondary nucleation.[168] In contrast, Surwade et al. proposed that polyaniline nanofiber formation is controlled by a double heterogeneous nucleation process.[169]

Polythiophene is a widely studied conducting polymer with good stability and a low band gap (i.e., 2.1 eV for unsubstituted polythiophene).[170] The electrical and optical properties of polythiophene have been investigated extensively due of its potential for applications in electronic and optoelectronic devices, such as sensors,[171] field-effect

transistors,[172] light-emitting diodes,[173] and solar cells.[174] The solubility of polythiophene, however, is very poor in most common solvents, limiting its processibility. One way to overcome this problem is to synthesize soluble 3-alkyl substituted polythiophene with the sacrifice of some conductivity.[16,59] The other method is to synthesize dispersible polythiophene nanostructures.[175-176]

In the present work, we report a simple inexpensive approach to synthesize polythiophene nanofibers with the aid of polythiophene oligomers, such as bithiophene and terthiophene. The effect of monomer concentration, oxidant concentration, solvent, and temperature on the polymer morphology was studied. A possible formation mechanism is proposed based on intermolecular oligomer nucleation.[113]

3. EXPERIMENTAL

1. Materials. Thiophene, bithiophene, and ferric chloride were obtained from Alfa Aesar. Terthiophene and acetonitrile were purchased from Acros Organics. Acetone, chloroform, dichloromethane, and 1,2-dichlorobenzene were purchased from Sigma Aldrich. Thiophene was distilled before use, and other chemicals were used as received.

2. Synthesis. Bulk polythiophene was synthesized by chemical oxidative polymerization. Typically, 0.1 M of thiophene (84 mg) and 0.2 M of anhydrous $FeCl_3$ (324 mg) was dissolved in 10 mL acetonitrile and the solution was allowed to react for 24 h. To synthesize polythiophene nanofibers, 5 mL of an acetonitrile solution, containing 0.1 M thiophene and about 4 mg oligothiophene was first prepared, and then mixed with 5 mL of an acetonitrile solution of 0.1 M anhydrous $FeCl_3$. The mixture was intensely

shaken by hand for 5 s and left undisturbed for 12 h. After the reaction, the product was centrifuged and washed with acetonitrile. For reactions carried out in other solvents, a small amount (0.5 mL) of acetonitrile was added to increase the solubility of the oligomer.

3. Characterization. The morphology of the products was characterized using a Hitachi S-4700 scanning electron microscope (SEM) operated at an accelerating voltage of 5 kV. Fourier-transform infrared (FT-IR) spectra were taken with a Thermo Nicolet Nexus spectrometer. The UV-vis spectra of samples dispersed in acetonitrile were obtained using a Varian Cary 50 Bio spectrophotometer. X-Ray Diffraction (XRD) was acquired by a PANalytical X'Pert multipurpose diffractometer utilizing a Cu source (1.5418 Å). Thermogravimetric analysis was carried out on a TA Instruments 2950 Thermogravimetric Analyzer at a heating rate of 20 °C/min.

4. RESULTS

In oligomer-assited experiments, we observed an immediate color change from brown to dark blue after the mixing of thiophene, bithiophene/terthiophene, and $FeCl_3$ in acetonitrile. In the absence of the oligomer, however, this color change occurred after one to two hours following the mixing for the reaction. The faster color change was due to the lower oxidation potential of the oligomers, as compared to the thiophene monomer, that resulted in a faster polymerization rate.[22] Figure 1 shows SEM images of polythiophene synthesized with and without the addition of bithiophene and terthiophene. As shown in the figure, polythiophene obtained in the presence and absence of the oligomer exhibited

different morphologies. The polythiophene synthesized without the terthiophene consisted of mostly aggregated clusters. However, when a small amount of bithiophene or terthiophene (typically 3-5 wt% of monomer amount) was added into the reaction mixture, the polythiophene showed an interconnected network of nanofibrilar morphology, with an average diameter of about 54 and 56 nm, respectively, as determined by ImageJ.[156] The polythiophene nanofibers could be well dispersed in acetonitrile and the polymer dispersions remained stable for months.

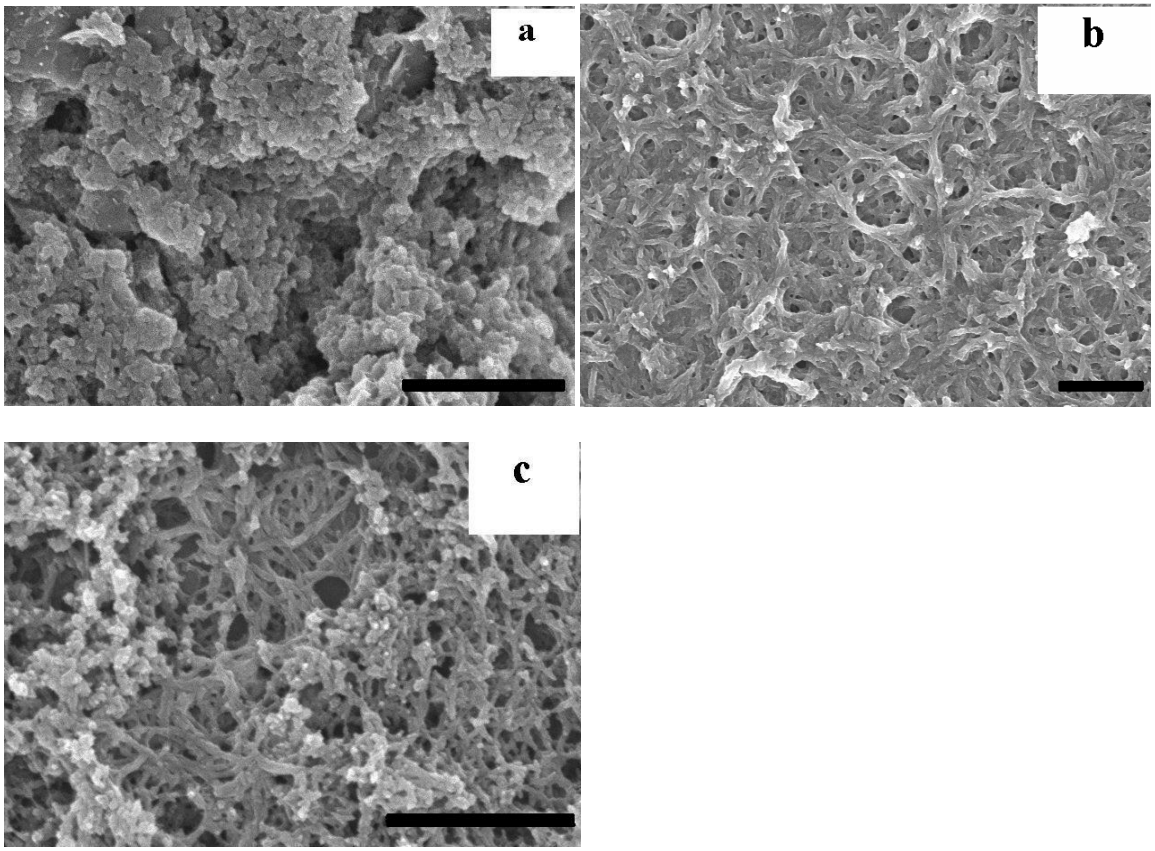

Figure 1. SEM images of polythiophene synthesized at room temperature in acetonitrile a) using conventional method, b) with the addition of terthiophene, and c) with the addition of bithiophene. The scale bar is 1 μm.

The UV–visible spectra of bulk polythiophene and polythiophene nanofibers dispersed in acetonitrile are shown in Figure 2. Both spectra show an absorption band at

around 500 nm, which is attributed to the π–π* interband transition. The absorption peak intensity greater than 600 nm indicates that the polymer is in the partially doped/oxidized state. These results are comparable to previously reported spectra for bulk polythiophene.[56,177]

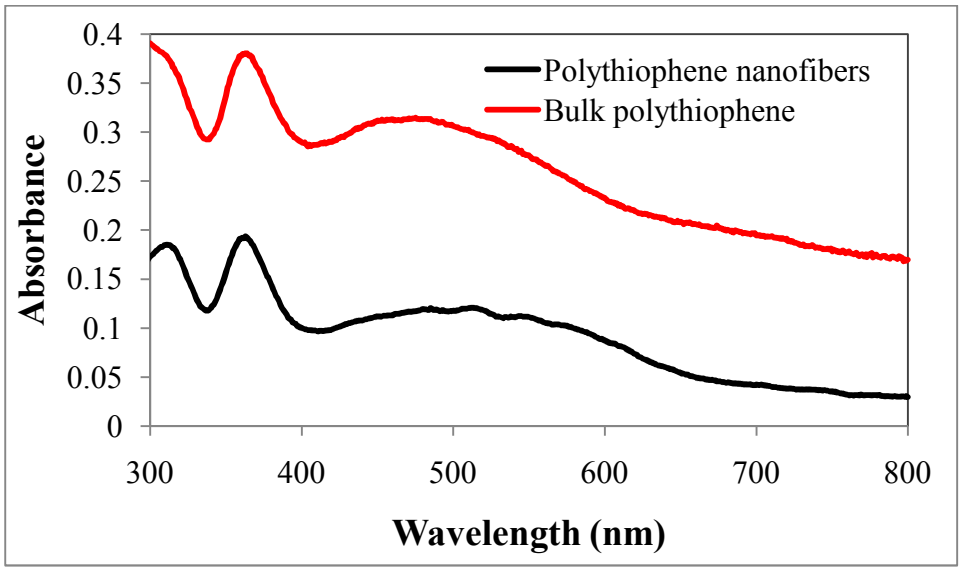

Figure 2. UV-vis spectra of bulk polythiophene and polythiophene nanofibers.

The FT-IR spectra of bulk polythiophene and polythiophene nanofibers are shown in Figure 3. The absorption band at 1491 cm^{-1} is attributed to the C=C stretching. The peaks at 788 and 1039 cm^{-1} can be attributed to the out-of-plane C–H deformation and in-plane C–H deformation, respectively. A weak peak at about 3100 cm^{-1} is caused by the C-H stretching. Three dopant-induced bands were also observed at 1350, 1208 and 1130 cm^{-1}, illustrating that both bulk polythiophene and polythiophene nanofibers were in their doped state. These resonances are consistent with those previously reported results, indicating that the addition of terthiophene did not substantially change the composition of the polythiophene. [178-179]

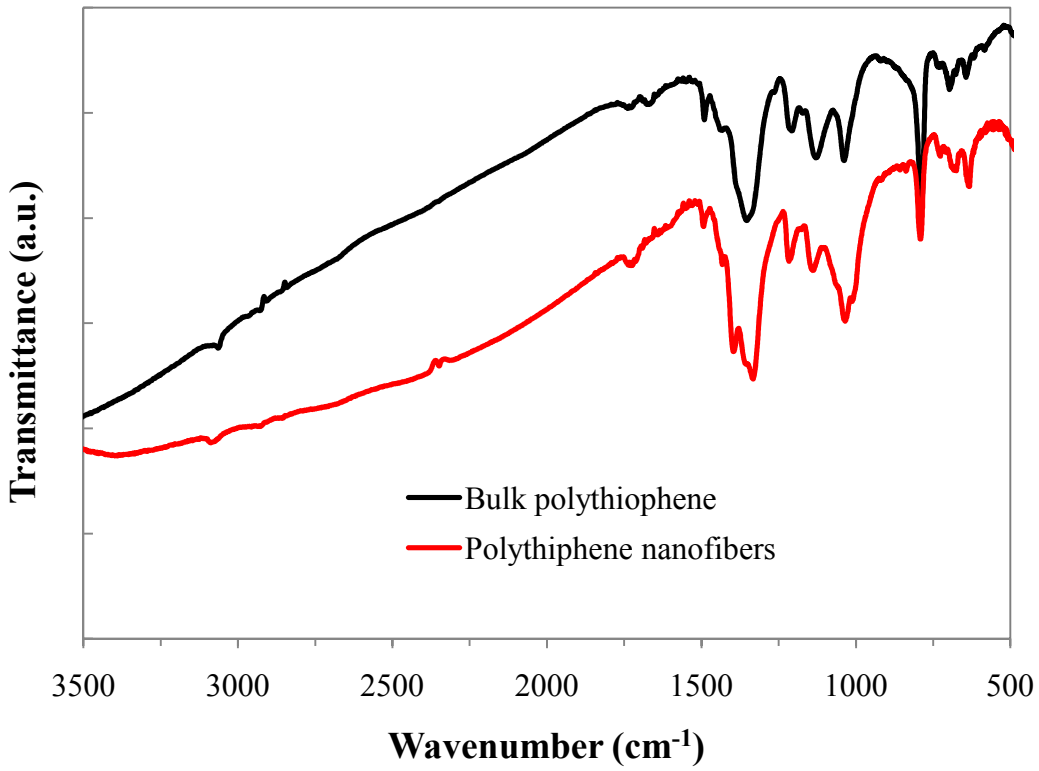

Figure 3. FT-IR absorption spectra of bulk polythiophene and polythiophene nanofibers.

Additional structural studies on the crystalline nature of polythiophene (Figure 4) were done using XRD. As shown in the figure, bulk polythiophene exhibited only a weak and broad peak centered at about 2θ = 22°. This peak is ascribed to the amorphously stacked polythiophene main chain.[180-181] In the XRD pattern of polythiophene nanofibers, the broad peak showed components at around 2θ = 19° and 24°, indicating that the polythiophene nanofibers had higher crystallinity than the bulk polythiophene.

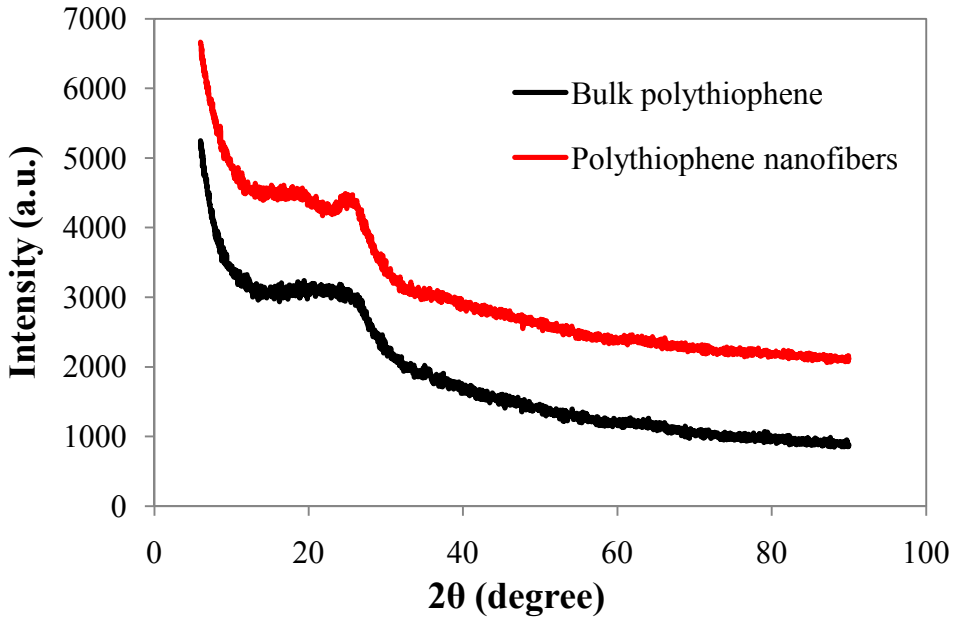

Figure 4. XRD patterns of bulk polythiophene and polythiophene nanofibers.

Thermal stability of bulk polythiophene and polythiophene nanofibers was examined with thermogravimetric analysis, as shown in Figure 5. The polythiophene was found to be stable up to 350 °C. Above 350 °C, bulk polythiophene exhibited a very fast weight loss, while the polythiophene nanofibers started to decompose at a higher temperature and at a slower rate. A possible explanation is that the higher crystallinity of polythiophene nanofibers leads to an increase in the chain-chain lateral stacking.[182] In addition, the nanofibers may crosslink when heated to certain temperatures, leading to a stronger interaction between polymer chains.[183] The thermal behavior under N_2 showed additional thermal stability compared to that in air.

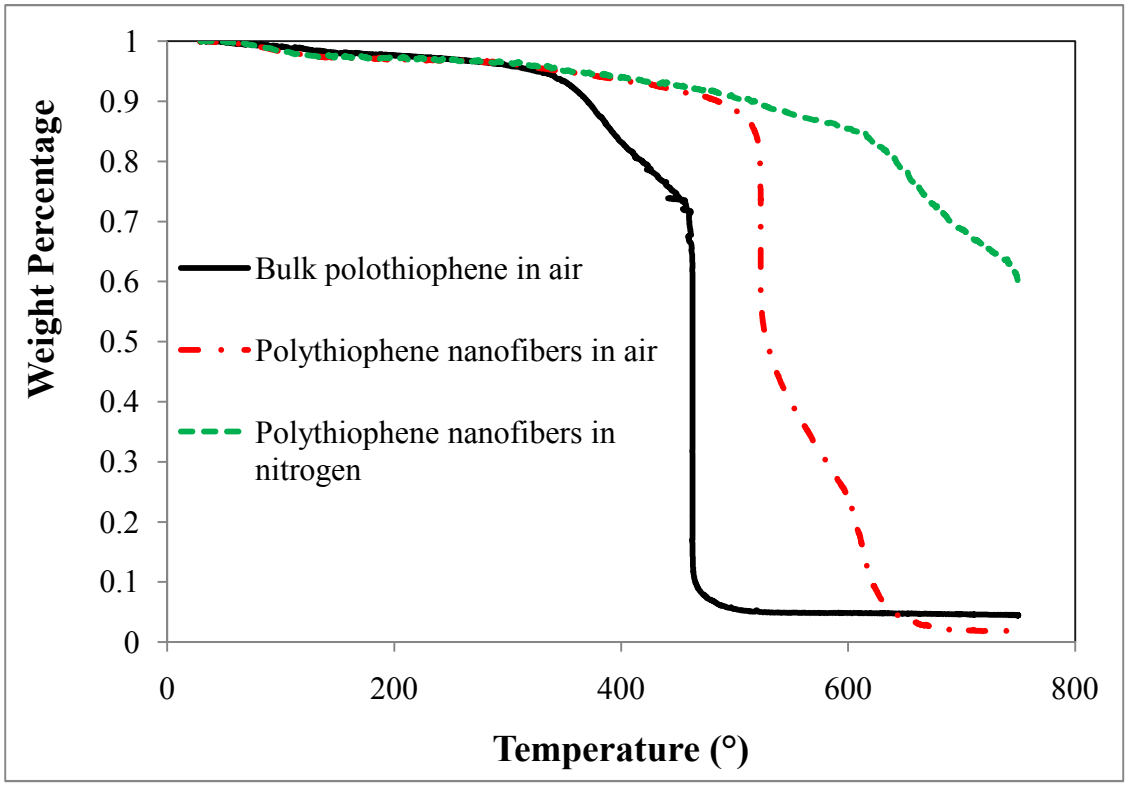

Figure 5. Thermogravimetric curves of bulk polythiophene and polythiophene nanofibers at a heating rate of 20°C/min in air and nitrogen.

To understand the formation mechanism of polythiophene nanofibers, a series of polymers were made under various synthetic conditions, with changes in concentration, temperature, and solvent. SEM images for the polythiophene prepared with different monomer and oxidant ratios are shown in Figure 6. It was observed that, at room temperature, the morphology of polythiophene significantly changed from a low oxidant concentration to a high concentration. When the ratio of the monomer to the oxidant was 2:1 (Figure 6a), the morphology of polythiophene was more bulk-like. As the ratio was changed to 1:1 (Figure 1b), polythiophene with a branched nanofiber structure resulted. For polythiophene synthesized with a monomer to an oxidant ratio of over 1:2 (Figure 6b and 6c), the polythiophene nanofibers exhibited less aggregation, less branching, smaller

diameters, and narrower fiber diameter distribution. At a higher reactant concentration, nanofibers were produced with some aggregated structure attached to them (Figure 6d). The average diameter and diameter distributions of those polythiophene nanofibers prepared at different concentrations are displayed in Figure 7. In brief, the morphology of polythiophene can be affected by the monomer and oxidant concentration.

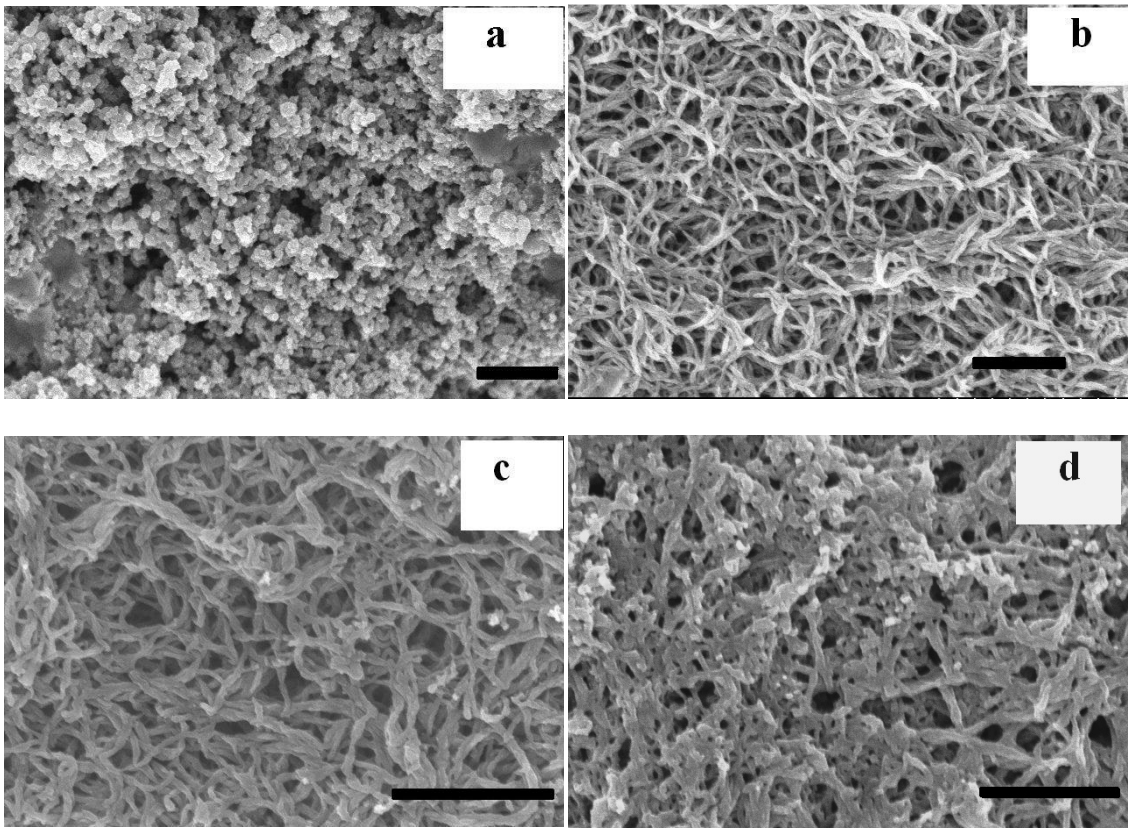

Figure 6. SEM images of polythiophene synthesized with 4 mg terthiophene a-c) at a thiophene concentration of 0.1 M and different concentrations of $FeCl_3$: a) 0.05 M, b) 0.2 M, and c) 0.3 M. and d) polythiophene prepared at a higher concentration of 0.3 M thiophene and 0.4 M $FeCl_3$. The scale bar is 1 μm.

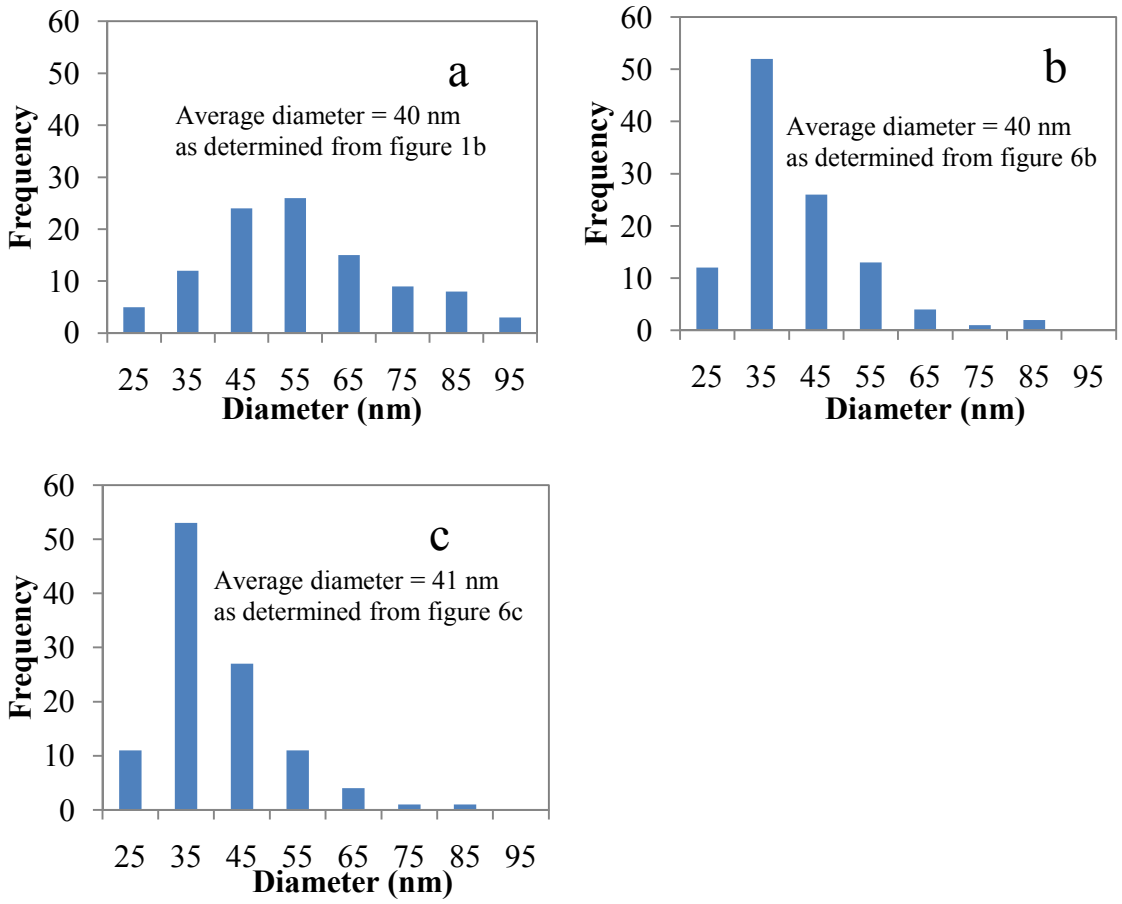

Figure 7. Distributions of diameters of polythiophene nanofibers synthesized with terthiophene a) 0.1 M, b) 0.2 M, and c) 0.3 M.

The effect of temperature on the polythiophene morphology is illustrated in Figure 8. Typically, a lower reaction temperature favors nanofiber formation for reactions carried out at the oxidant to monomer ratio of 1:1. As shown in the figure, the polythiophene nanofibers synthesized at -8 °C (Figure 8a) showed a similar morphology to Figure 6c and 6d. For nanofibers prepared at room temperature (Figure 1b) and 65°C (Figure 8b) had more branched structures and more aggregation. However, at high oxidant concentrations (i.e., oxidant to monomer ratio of 2:1), a significant temperature dependence was not observed and all polythiophene basically showed relatively long nanofibrilar morphology.

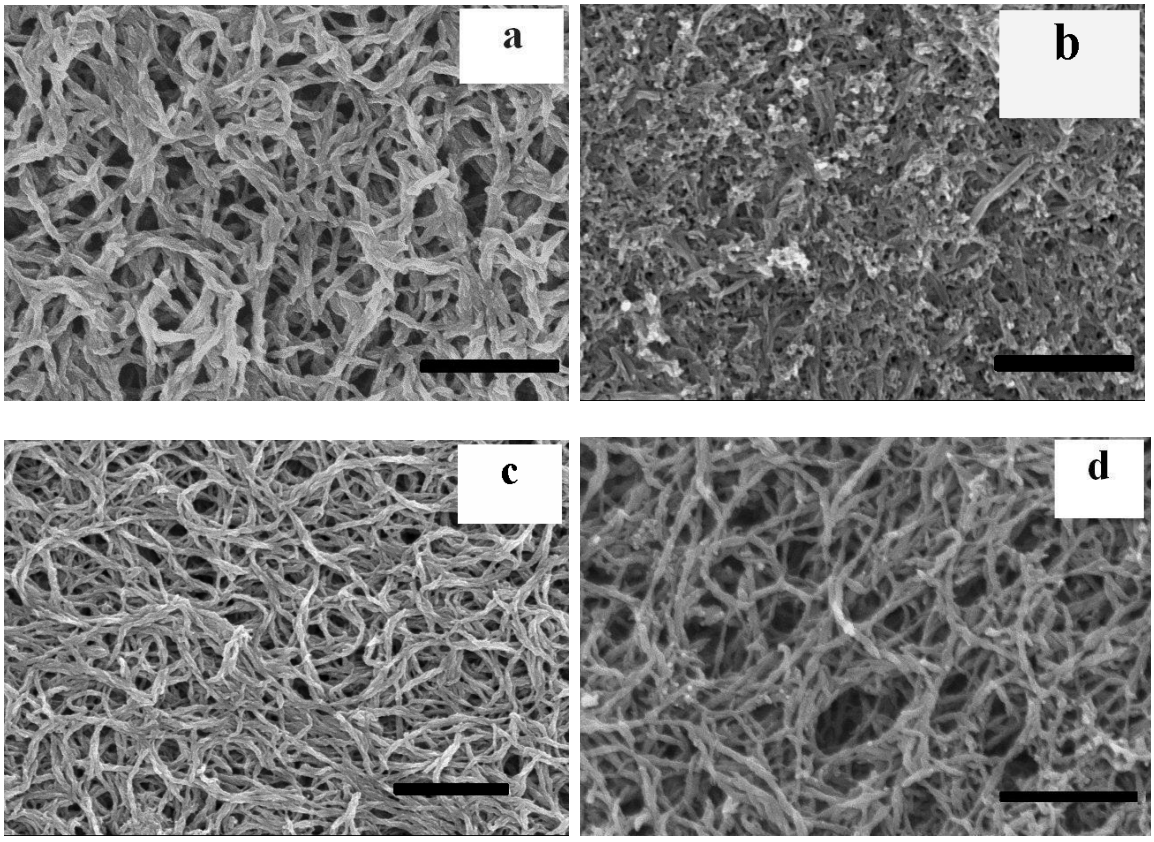

Figure 8. SEM images of polythiophene nanofibers synthesized in the presence of terthiophene (4 mg), thiophene (0.1 M) with an oxidant to monomer ratio of 1:1 at a) -8°C and b) 65°C; and with an oxidant to monomer ratio of 2:1 at c) -8°C and d) 65°C. The scale bar is 1 μm.

The choice of solvent has been reported to affect the nucleation and growth of polythiophene.[184] In this work, a variety of solvents, such as acetonitrile, chloroform, dichloromethane, and 1,2-dichlorobenzene, were selected to study the effect of these solvents on the morphology (Figures 6 and 9). Only polythiophene prepared in acetonitrile exhibited pure nanofiber morphology (Figure 6b). Polythiophene synthesized in chloroform showed a mixture of nanofibers and some aggregated particles attached to them (Figure 9a). Reactions in other solvents, such as dichloromethane and 1,2-dichlorobezene, resulted in mostly aggregates and bulk-like morphology (Figure 9b and 9c).

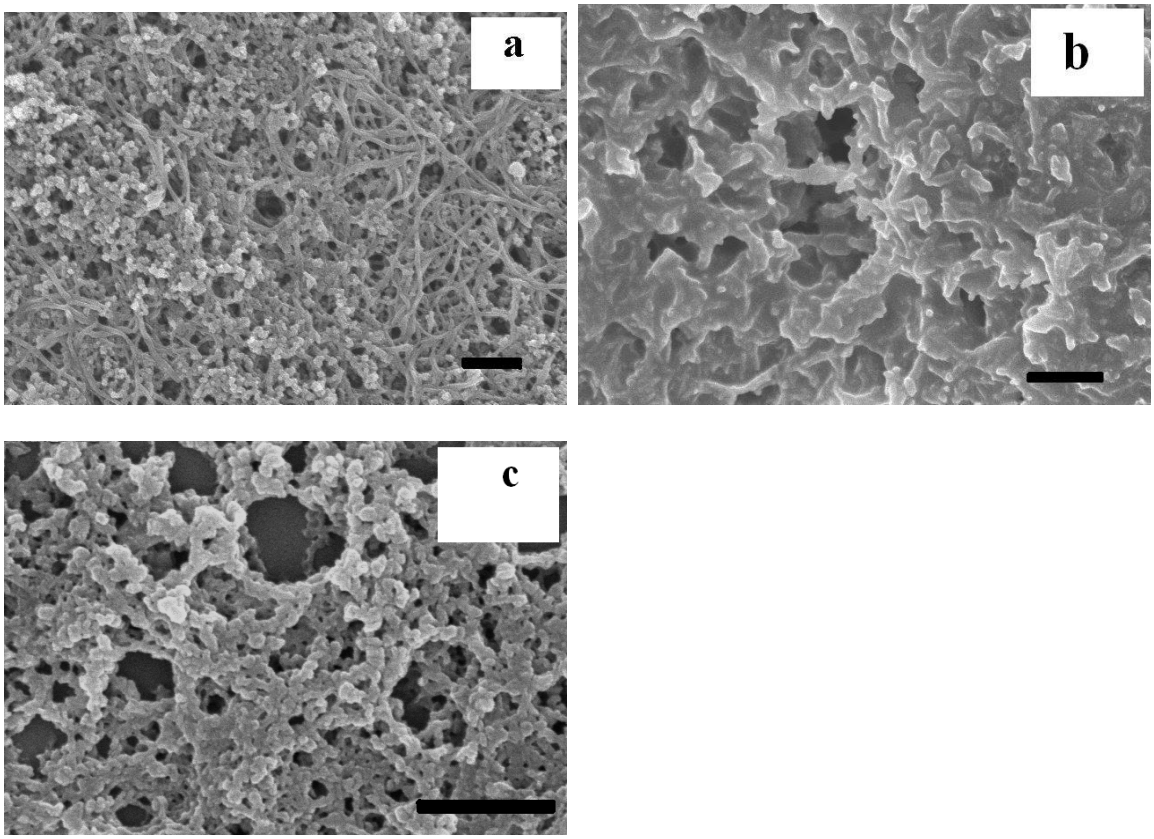

Figure 9. Typical SEM images showing the morphology of polythiophene obtained with the addition of 4 mg terthiophene at a concentration of 0.1 M monomer and 0.2 M oxidant in different solvents: a) chloroform, b) 1,2-dichlorobenzene, and c) dichloromethane. The scale bar is 500 nm. Note: The corresponding SEM for acetonitrile is in Figure 6b).

5. DISCUSSION

The mechanism for the formation of conducting polymer nanofibers is still unclear. In our experiments with the addition of oligomer, we observed a rapid precipitation of polythiophene, which showed nanofiber structures. The traditional bulk polymerization, without the addition of oligomer, showed a long incubation time before precipitation, which only yielded the aggregated morphology. We believe that the formation of polythiophene nanofibers may be explained by a difference in the nucleation process.

According to classic nucleation theory, homogeneous nucleation occurs when a supersaturation of nuclei at critical size is achieved. Different from the nucleation of small molecules, polymer nucleation usually involves only part of a polymer, portions of several polymers, or even the oligomers. The monomer size is much smaller than the dimensions of the critical nucleus. Thus, a certain concentration of at least oligomers must be formed before intermolecular oligomer nucleation can occur. Intermolecular oligomer nucleation has been proposed to explain the nucleation process during polymerization of polyphosphates.[113,185] The oligomer nucleus, especially if it were rigid, would be expected to have a cylinder-like shape and active growth sites at the chain ends. One-dimensional growth is favored when further nucleation of additional molecules on the nucleated crystal is inhibited.

In these experiments, the presence of oligomers and their aggregration likely resulted in the the formation of bundles of oligothiophene. The terthiophene produced more fiber-like structures than bithiophene. It has been demonstrated that thiophene oligiomers have a lower oxidation potential than the thiophene monomer.[22] Therefore, polymerization is likely to be initiated and likely propagated in those bundles. Since oligothiophene is rigid, the initial nuclei should be cylinder-like. The nucleating cylinder-like nuclei would be expected to grow more rapidly along the direction of the polymer chain.[186] The large nuclei generally diffuse more slowly than the monomer, so it is easier for a monomer to add to the existing nucleus than growing the nuclei Therefore, it is not surprising that anisotropic growth of the polythiophene was observed. In the conventional bulk synthesis without the addition of oligomers, the formation of oligomers may be much slower. However, after a while, a large number of oligomer nuclei may form and

precipitate spontaneously, followed by further aggregation and secondary nucleation on the existing oligomer nuclei. This is probably because the concentration of oligomer nuclei formed in conventional polymerization was much higher, and, consequently, resulted in aggregated morphology.[187]

Based on this assumption, one would expect that polymerization of pure oligomers might yield aggregates. The morphology of polythiophene synthesized from bithiophene and terthiophene is shown in Figure 10. Polythiophene prepared from bithiophene possessed mostly aggregated granular structure similar to bulk polythiophene. Similar effects of the oligomer concentration were reported in the synthesis of polyaniline derivatives. With the addition of a high concentration of aniline dimer, only aggregates were produced.[188] An interesting lamellar morphology was found for polythiophene synthesized from terthiophene. In both samples, a small amount of nanofibers can be observed, indicating that the formation of cylinder-like nuclei maybe intrinsic during the polymerization in the presence of oligomers. A schematic illustration of possible formation mechanism is shown in Figure 11.

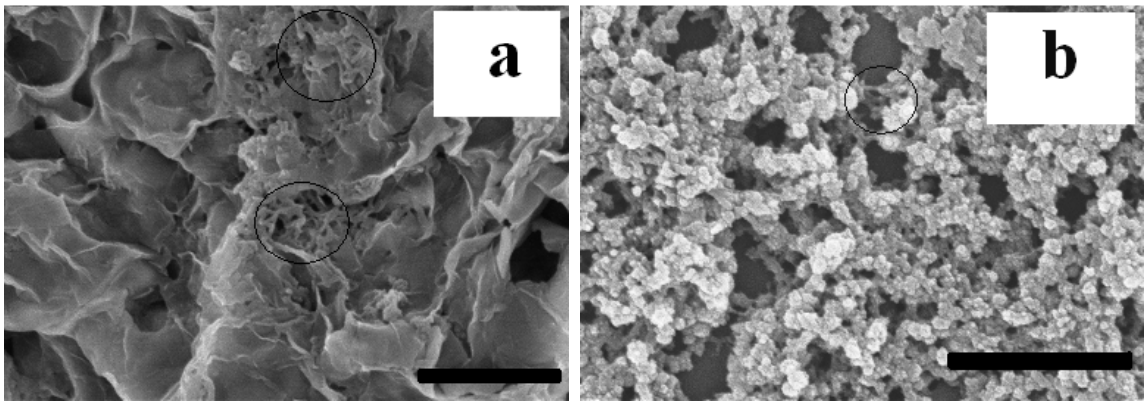

Figure 10. SEM images of polythiophene prepared by oxidative polymerization from a) terthiophene and b) bithiophene. Some nanofiber structures are shown in the circles. The scale bar is 1 μm.

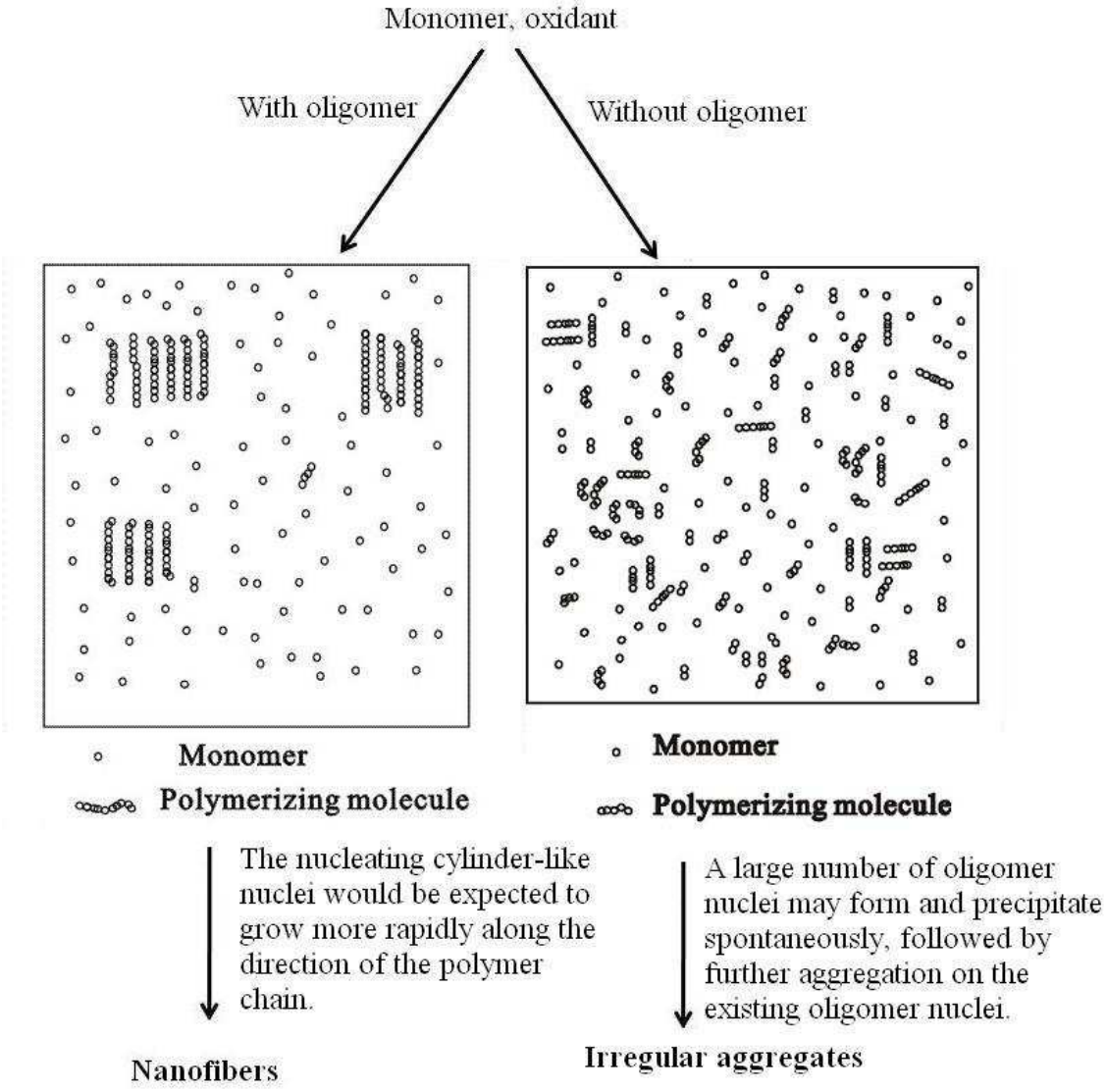

Figure 11. A schematic illustration of the formation of polythiophene nanofibers and aggregates.

The effect of synthetic conditions on morphology can also be explained based upon this nucleation scheme. At a high monomer concentration, the polymerization was faster, which increased the concentration of oligomers (Figure 6d). The possibility of additional nucleation on existing nuclei would be increased, yielding more aggregated

clusters.[189] The higher oxidant concentrations can increase the rate of polymerization of the existing nuclei, thus, promoting the fibrillar growth (Figure 6b and 6c).[190] The effect of the solvent on morphology can be attributed to the solvent polarity on the nucleation step. When the solvency of the medium decreased (i.e., the polarity increased), the oligomers were inclined to aggregate, lead to a fibrillar growth. Another possibility is that the increase in the solvency retarded critical nuclei formation and, therefore, the chance of aggregation and secondary nucleation was greatly increased, producing large aggregates.[71] This is illustrated by the morphology of polythiophene prepared in dichloromethane and 1,2-dichlorobenzene (Figure 9b and 9c), which have lower polarity than acetonitrile and chloroform.

6. CONCLUSIONS

Polythiophene nanofibers have been successfully synthesized via the addition of thiophene oligomers into the conventional chemical oxidative polymerization. Compared with bulk polythiophene, polythiophene nanofibers have similar optical absorption properties, but higher crystallinity and better thermal stability. The synthetic conditions were found to affect the formation of nanofibers. It was determined that nanofiber formation as favored by reactions performed at higher oxidant to monomer concentrations and lower reactant concentrations in relatively polar solvents. We believe that the difference in polythiophene morphology is intrinsically controlled by the intermolecular nuclei nucleation during polymerization. Our results showed that the morphology of polythiophene, prepared by chemical oxidative polymerization, can be easily altered by the incorporation of a small amount of the thiophene oligomers.

7. ACKNOWLEDGEMENTS

The authors acknowledge Terry Colberg and Balika Khatiwada for assistance in obtaining the TEM pictures. FDB acknowledges the financial support of the National Science Foundation under grant DMR-1005606 and of Materials Research Center, Missouri S and T.

8. REFERENCES

(1) Kuchibhatla, S. V. N. T.; Karakoti, A. S.; Bera, D.; Seal, S. *Prog. Mater Sci.* **2007**, *52*, 699.

(2) Aleshin, A. N. *Adv. Mater.* **2006**, *18*, 17.

(3) Li, Z. F.; Blum, F. D.; Bertino, M. F.; Kim, C. S.; Pillalamarri, S. K. *Sens. Actuators, B* **2008**, *134*, 31.

(4) Darrell, H. R.; Iksoo, C. *Nanotechnology* **1996**, *7*, 216.

(5) Pinto, N. J.; Johnson, A. T.; MacDiarmid, A. G.; Mueller, C. H.; Theofylaktos, N.; Robinson, D. C.; Miranda, F. A. *Appl. Phys. Lett.* **2003**, *83*.

(6) Parthasarathy, R. V.; Martin, C. R. *Chem. Mater.* **1994**, *6*, 1627.

(7) Martin, C. R. *Chem. Mater.* **1996**, *8*, 1739.

(8) Li, G.; Zhang, Z. *Macromolecules* **2004**, *37*, 2683.

(9) Han, M. G.; Foulger, Stephen H. *Small* **2006**, *2*, 1164.

(10) Pillalamarri, S. K.; Blum, F. D.; Tokuhiro, A. T.; Story, J. G.; Bertino, M. F. *Chem. Mater.* **2004**, *17*, 227.

(11) Werake, L. K.; Story, J. G.; Bertino, M. F.; Pillalamarri, S. K.; Blum, F. D. *Nanotechnology* **2005**, *16*, 2833.

(12) Huang, J.; Kaner, R. B. *J. Am. Chem. Soc.* **2004**, *126*, 851.

(13) Huang, J.; Kaner, R. B. *Angew. Chem. Int. Ed.* **2004**, *43*, 5817.

(14) Chiou, N.-R.; Epstein, A. J. *Adv. Mater.* **2005**, *17*, 1679.

(15) Li, W.; Wang, H.-L. *J. Am. Chem. Soc.* **2004**, *126,* 2278.

(16) Tran, H. D.; Shin, K.; Hong, W. G.; D'Arcy, J. M.; Kojima, R. W.; Weiller, B. H.; Kaner, R. B. *Macromol. Rapid Commun.* **2007**, *28*, 2289.

(17) Zhang, X.; Manohar, S. K. *J. Am. Chem. Soc.* **2004**, *126*, 12714.

(18) Zhang, X.; Lee, J.-S.; Lee, G. S.; Cha, D.-K.; Kim, M. J.; Yang, D. J.; Manohar, S. K. *Macromolecules* **2005**, *39*, 470.

(19) Li, D.; Kaner, R. B. *J. Am. Chem. Soc.* **2006**, *128*, 968.

(20) Surwade, S. P.; Manohar, N.; Manohar, S. K. *Macromolecules* **2009**, *42*, 1792.

(21) *Handbook of conducting polymers*; 2nd ed.; Terje A. Skotheim, R. L. E., John R. Reynolds, Ed.; Marcel Dekker: New York, 1998.

(22) Chang, J. B.; Liu, V.; Subramanian, V.; Sivula, K.; Luscombe, C.; Murphy, A.; Liu, J.; Frechet, J. M. J. *J. Appl. Phys.* **2006**, *100*, 014506.

(23) Tsumura, A.; Koezuka, H.; Ando, T. *Synth. Met.* **1988**, *25*, 11.

(24) Perepichka, I. F.; Perepichka, D. F.; Meng, H.; Wudl, F. *Adv. Mater.* **2005**, *17*, 2281.

(25) Fan, B.; Wang, P.; Wang, L.; Shi, G. *Sol. Energy Mater. Sol. Cells* **2006**, *90*, 3547.

(26) Yutaka, O.; Masao, U.; Keiro, M.; Katsumi, Y. *Solid State Commun.* **1991**, *80*, 605.

(27) Yamamoto, T.; Morita, A.; Miyazaki, Y.; Maruyama, T.; Wakayama, H.; Zhou, Z. H.; Nakamura, Y.; Kanbara, T.; Sasaki, S.; Kubota, K. *Macromolecules* **1992**, *25*, 1214.

(28) Lee, S. J.; Lee, J. M.; Cheong, I. W.; Lee, H.; Kim, J. H. *J. Polym. Sci., Part A: Polym. Chem.* **2008**, *46*, 2097.

(29) Zhang, X.; Surwade, S. P.; Dua, V.; Bouldin, R.; Manohar, N.; Manohar, S. K. *Chem. Lett.* **2008**, *37*, 526.

(30) *Macromolecular Physics*; Wunderlich, B., Ed.; Academic Press: New York, 1976; Vol. 2.

(31) Wei, Y.; Tian, J. *Macromolecules* **1993**, *26*, 457.

(32) Rasband, W. S.; US National Institutes of Health: Bethesda, MD, 1997-2010.

(33) Patil, A. O.; Heeger, A. J.; Wudl, F. *Chem. Rev.* **1988**, *88*, 183.

(34) Hosseini, S. H.; Entezami, A. A. *Polym. Adv. Technol.* **2001**, *12*, 524.

(35) Mohammad, F. *J. Phys. D: Appl. Phys.* **1998**, *31*, 951.

(36) Ma, X.; Li, G.; Xu, H.; Wang, M.; Chen, H. *Thin Solid Films* **2006**, *515*, 2700.

(37) Karim, M. R.; Lee, C. J.; Lee, M. S. *J. Polym. Sci., Part A: Polym. Chem.* **2006**, *44*, 5283.

(38) Ong, B. S.; Wu, Y.; Liu, P.; Gardner, S. *Adv. Mater.* **2005**, *17*, 1141.

(39) Mo, Z.; Lee, K. B.; Moon, Y. B.; Kobayashi, M.; Heeger, A. J.; Wudl, F. *Macromolecules* **1985**, *18*, 1972.

(40) Huang, J.; Kaner, R. B. *Nat. Mater.* **2004**, *3*, 783.

(41) del Valle, M. A.; Cury, P.; Schrebler, R. *Electrochim. Acta* **2002**, *48*, 397.

(42) Wunderlich, B. *Angewandte Chemie International Edition in English* **1968**, *7*, 912.

(43) Flyvbjerg, H.; Jobs, E.; Leibler, S. *Proc. Nat. Acad. Sci. U.S.A.* **1996**, *93*, 5975.

(44) Chiou, N.-R.; Epstein, A. J. *Synth. Met.* **2005**, *153*, 69.

(45) Tran, H. D.; Norris, I.; D'Arcy, J. M.; Tsang, H.; Wang, Y.; Mattes, B. R.; Kaner, R. B. *Macromolecules* **2008**, *41*, 7405.

(46) *Handbook of engineering polymeric materials*; Cheremisinoff, N. P., Ed.; CRC Press, 1997.

(47) Ito, T.; Shirakawa, H.; Ikeda, S. *J. Polym. Sci., Part A: Polym. Chem.* **1974**, *12*, 11.

SECTION

3. CONCLUSIONS

Sensors based on polyaniline nanofiber thin films have been fabricated by UV-irradiating a precursor solution of 0.1 M aniline, 0.1 M acid dopant, and 0.05 M APS in an environmental-friendly single-step process. The polyaniline fibers had typical diameters around 50 nm and lengths of 1-3 μm. Solutions that were not irradiated yielded bulk-like polyaniline films. The sensors were ready for use immediately after polymerization. The response of those sensors was examined by exposing the sensors to organic vapors. Different sensing mechanisms were proposed. Toluene can act as a solvent and decrease the current by swelling the polymer chains, while the triethylamine can affect the doping level, consequently leading to a rapid current decrease. Polyaniline nanofiber-based sensors were found to be much more sensitive than bulk polyaniline sensors, due to their higher surface area and porous structure. Sensors fabricated using our technique have characteristics comparable to other polyaniline bulk and nanofiber sensors.

Polyaniline/metal nanocomposite sensors can also be fabricated using this technique by irradiating an aqueous solution of 0.1 M aniline, 0.1 M acid dopant, 0.05 M APS, and 0.01 M metal salts, such as $AgNO_3$ and $KPtCl_4$. The polyaniline/metal nanocomposites showed a nanofiber structure similar to polyaniline nanofibers. Thermogravimetric analysis results indicated that nanostructure polyaniline has relatively good thermal stability. At 750 °C, pure polyaniline completely decomposed, while polyaniline/metal nanocomposites still exhibited some metal residues of approximately 15%. These sensors showed good response to organic vapors, such as toluene and

triethylamine. The sensor response of nanocomposites exposed to toluene was only 15-20 % faster compared to pure polyaniline nanofibers. Surprisingly, the response time of Ag-containing composites to triethylamine was about 3 times faster than that of the nanofibers alone and about 1.5 times faster than that of Pt-nanofiber composites. The change in resistivity was about 6 times larger for Ag nanocomposites and more than 4 times larger than for the Pt nanocomposites. Raman spectroscopy suggested that there was a charge transfer between polyaniline and metal nanoparticles, which increased the conductivity of polyaniline. Exposure to triethylamine reduces the charge transfer and therefore the doping, thereby amplifying the response to the analyte. Our finding could be used as a basis to prepare multiplexed sensors with a high degree of sensitivity and specificity.

A chemical chemisorption model and a diffusion model were proposed to fit the sensor response against the exponential decay function. Both models fit the experimental data very well with the normalized least-squares of about 3%. The equilibrium absorption amount, obtained by the chemisorption model, was found to obey a Langmuir Isotherm, while the diffusion model was consistent with the notion that the adsorbing molecules undergoe a dual sorption process, i.e., Langmuir Isotherm and gas dissolution. A decrease in the adsorption time constant with the concentration and an increase in the desorption time constant was observed. The diffusion coefficient was determined to increase with the concentration, probably due to the swelling of the polymer by organic vapors. Our results also show the potential for studying the adsorption or diffusion process of conducting polymers based on conductivity measurements.

Polythiophene nanofibers have been successfully synthesized using an oligomer-assisted polymerization. Compared with conventional chemical oxidative polymerization, a small amount of oligomer, such as bithiophene or terthiophene, was incorporated into the polymerization system. Polythiophene nanofibers have similar optical absorption properties, but higher crystallinity and better thermal stability. The synthetic conditions were found to affect the formation of nanofibers. It was determined that nanofiber formation was favored by reactions performed at higher oxidant to monomer concentrations and lower reactant concentrations in relatively polar solvents. We believe that the difference in polythiophene morphology is intrinsically controlled by the intermolecular nuclei nucleation during polymerization. Our results showed that the morphology of polythiophene, prepared by chemical oxidative polymerization, can be altered by the incorporation of a small amount of the thiophene oligomers. This method may lead to a facile way to fabricate polythiophene and its derivatives-based electronic devices.

APPENDIX A

MATHEMATICA CODE FOR LEAST-SQUARE CURVE FITTING

The following is the typical Mathematica code of lease-square fit for the diffusion model.

```
fp=Import["file name","Table"]
MatrixForm[%]
$HistoryLength=2
besselfunction[n_]=n*Pi-0.750
fft=FindFit[fp,1- k*(1-Sum[(4/( besselfunction[n])^2)*Exp[-
x*d*(bjzfun2[n])^2],{n,1,3000}]), {{k,1/2},{d,1/300}},x]
fit = 1-k*(1-Sum[(4/(BesselJZero[0,n])^2)*Exp[-
x*d*(BesselJZero[0,n])^2],{n,1,1000}])/. fft ;
yCalc  = Table[ crvt /. x---> fp[[j,1]],{j,1,Length[fp]}]
MatrixForm[yCalc]
residuals=yCalc - N[fp[[All,2]]]
ListLinePlot[{fp,Transpose[{fp[[All,1]],yCalc}],Transpose[{fp[[All,1]],residuals}]}]
```

`

APPENDIX B

VIBRATIONAL STUDY OF POLYANILINE

1. INTRODUCTIONS

A molecular vibration occurs when atoms in a molecule are in periodic motion. Infrared (IR) and Raman spectroscopy are widely used to study the vibrational, sometimes rotational, and other information in polymeric materials. IR spectroscopy depends on a change in the permanent dipole moment with the vibrational normal mode in order to produce absorption. For Raman spectroscopy, a change in the polarizability with the vibration is required for Raman activity. This difference enables these two techniques to sometimes be sensitive to different vibrational motions. A new technique called SERS (Surface Enhanced Raman Spectroscopy) was discovered by Van Duyne based on the electromagnetic amplification of the Raman scattering.[191]

2. EXPERIMENTAL

Polyaniline was synthesized via the chemical oxidative polymerization. Typically, 0.1 M aniline, 0.1 M HCl, and 0.05 APS was dissolved in 10 mL aqueous solution. Then it was allowed to react for 12 h. After the reaction, the product was centrifuged and washed with water and acetone. Camphorsulfonic acid was used as the alternative dopant. To synthesize polyaniline/Au composites, 0.01 M HAuCl4 was added into the solution. FT-IR spectroscopy was operated on a with a Thermo Nicolet Nexus spectrometer. A few drops of polyaniline dispersion solutions were deposited on a AgCl substrate and dried under ambient conditions. Raman spectra were taken with a Horiba Jobin Yvon LabRAm ARAMIS spectrometer. For Raman spectroscopy, glass slides or glass slides coated with a roughly 200 nm gold layer were used as the substrates.

3. RESULTS AND DICSUSSION

3.1. Raman study of polyaniline. The Raman spectra of polyaniline doped with HCl and CSA taken with a HeNe laser source (632.8 nm) is shown in Figure 1. Polyaniline doped with these two acids typically showed similar resonances. The intensity of peaks below 1000 cm^{-1} are relatively low except for peaks around 600 and 800 cm^{-1}, which can be ascribed to the benzene ring deformation.[192] The peaks at about 1180, 1580, and 1600 cm^{-1} can be attributed to the C-H bending of benzene ring, C-C stretching of quinoid and benzene ring, respectively. Resonances at around 1320-1380 and 1480 cm^{-1} are characteristic of protonated C-N stretching and C=N stretching.[193] It was observed, that in doped samples, the intensity of the protonated peak is greater than that of C=N peak. The opposite effect was found for the dedoped sample. The assignments of Raman bands for polyaniline are shown in Table 1.

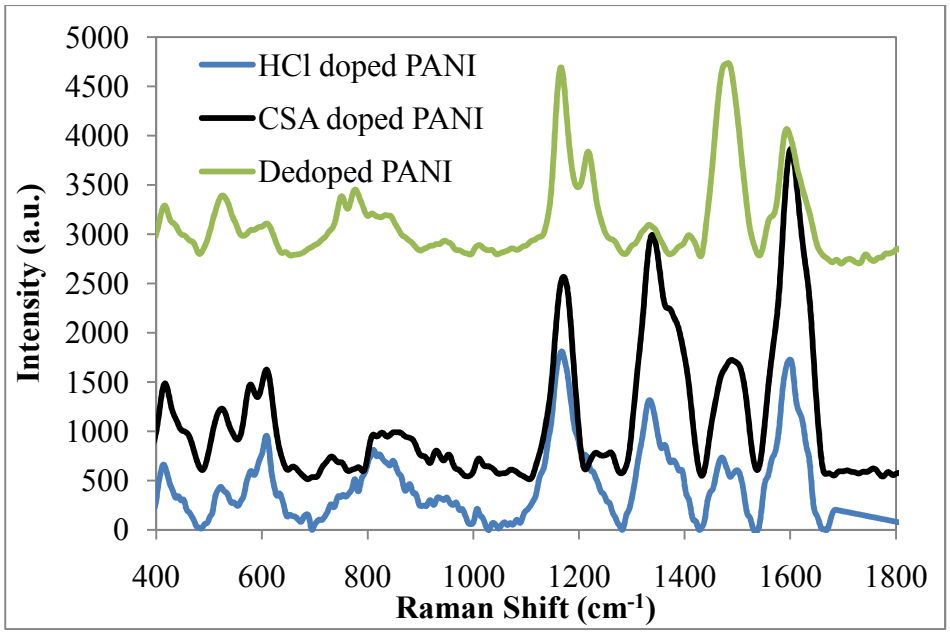

Figure 1. Raman spectra of dedoped polyaniline and polyaniline doped with HCl and CSA.

Table 1. Assignments for Raman Bands for polyaniline.

Band (cm^{-1})	Assignment
600, 800	ring deformation of benzene and quinoid rings
1180	C-H bending of benzene ring
1320-1380	protonated C-N stretching.
1480	C=N stretching.
1580	C-C stretching of and benzene ring,
1600	C-C stretching of benzene ring,

The SERS spectra of polyaniline was obtained and shown in Figure 2 along with that on a glass slide. As shown in the figure, the intensity of Raman spectrum of polyaniline deposited on SERS substrate was about 4-5 times higher than that deposited on the glass substrate, indicating that the Raman scattering is enhanced by the gold layer. It is noted that the peak positions did not change.

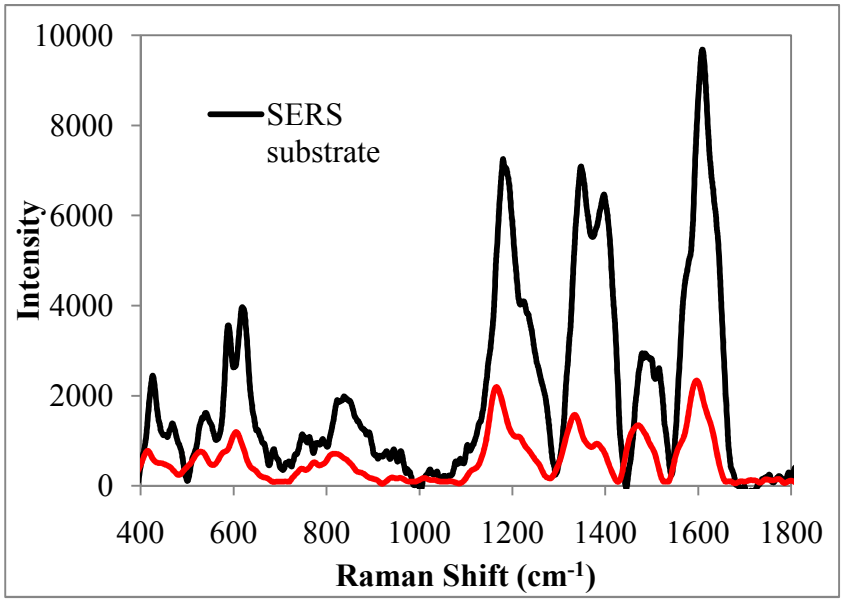

Figure 2. Raman spectra of polyaniline on a glass substrate and on a SERS substrate.

The Raman spectra of polyaniline exposed to 3 mL of 14.5 mM ammonia solution is shown in Figure 3. After the exposure, the intensity of the protonated C-N^+ greatly decreased, while the intensity of C=N stretching increased. This indicated that polyaniline was dedoped by the ammonia solution. Figure 4 shows the Raman spectra of polyaniline on a SERS substrate exposed to pure water. It was shown that the intensity of C=N stretching increased with the sacrifice of the protonated structure, indicating that the water itself could behave as a dedopant similar to ammonia. This might be caused by an interface reaction catalyzed on the gold surface.[194]

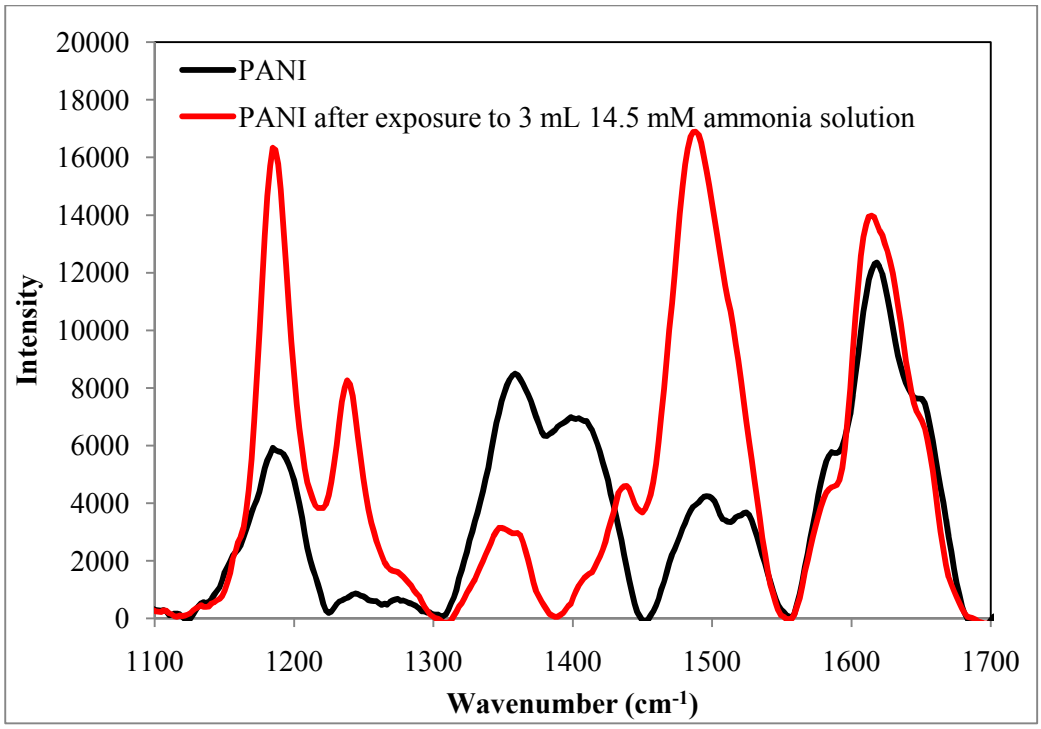

Figure 3. Raman spectra of polyaniline on a SERS substrate exposed to 14.5 mM ammonia solution.

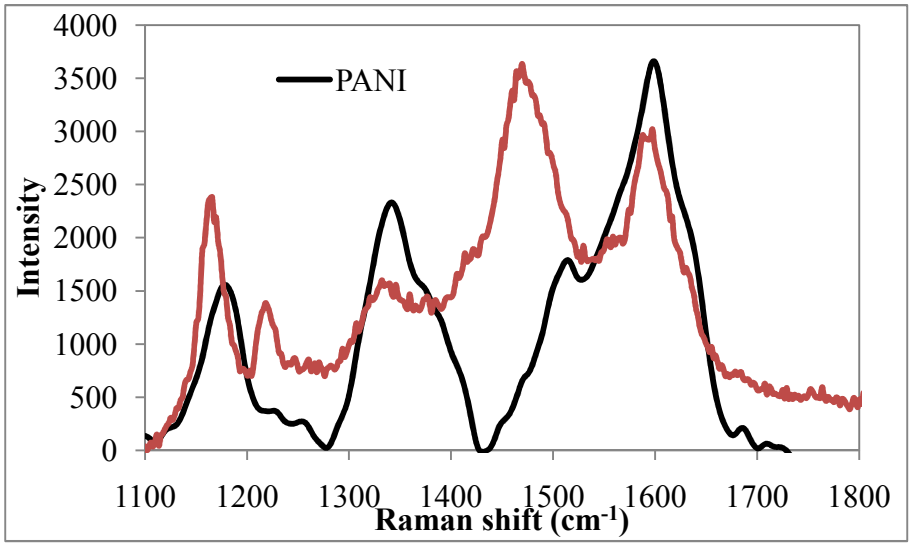

Figure 4. Raman spectra of polyaniline on a SERS substrate exposed to pure water.

The Raman spectra were fit by the Grams software using the Gaussian function. Figure 5 shows the fitting curves for the Raman spectrum of HCl doped polyaniline. Fitting all those peaks may allow us to quantitatively analyze the ratio of some target peaks.

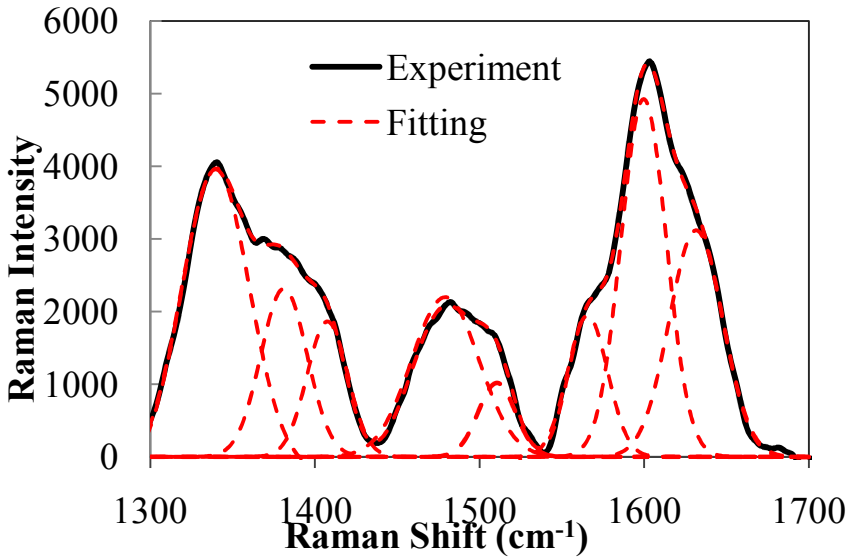

Figure 5. Raman spectra of polyaniline fit by Grams in the range of 1300 to 1700 cm^{-1}.

3.2. FT-IR study of polyaniline

Figure 6 shows the typical spectra of dedoped polyaniline and HCl doped polyaniline. For the doped polyaniline, the peaks in the frequency range of 3000-3400 cm^{-1} are due to the stretching vibrations of N-H bond. The bands at around 1580 and 1500 cm^{-1} correspond to the C=C stretching vibration of benzeniod and quinoid rings, respectively. The peak at 1300 cm^{-1} relates to the C-N stretching vibration of a secondary aromatic amine, and the 1140 cm^{-1} can be ascribed to the quinoid unit. We also noticed that the peaks at 1140 cm^{-1} for dedoped polyaniline shifted to higher wavenumbers and its intensity decreased.[195] We believe that this resonance is associated with the protonation and deprotonation of polyaniline. Assignments of FT-IR Bands for polyaniline are listed in Table 2. Figure 7 shows the fitting results of dedoped polyaniline fit by Grams in the range of 1100 to 1700 cm^{-1}.

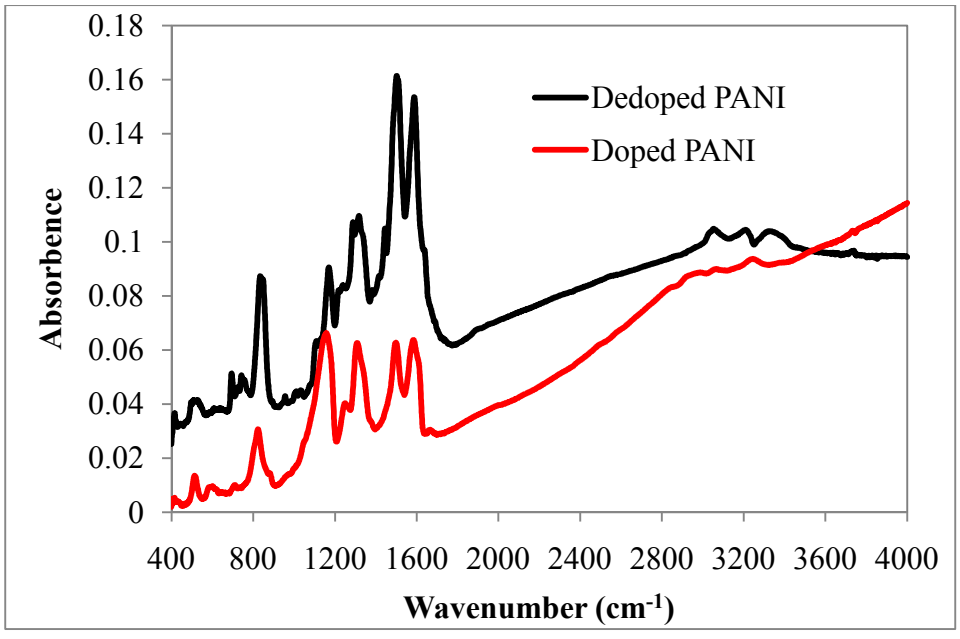

Figure 6. FT-IR spectra of doped and dedoped polyaniline. Note: The spectra are plot in absorbance rather than transmittance.

Table 2. Assignments of FT-IR Bands for polyaniline.

Band (cm^{-1})	Assignment
3000-3400	stretching vibrations of N-H bond
1580	C=C stretching vibration of benzeniod
1500	C=C stretching vibration of quinoid rings
1300	C-N stretching vibration of a secondary aromatic amine
1140	quinoid unit
815	Amine deformation

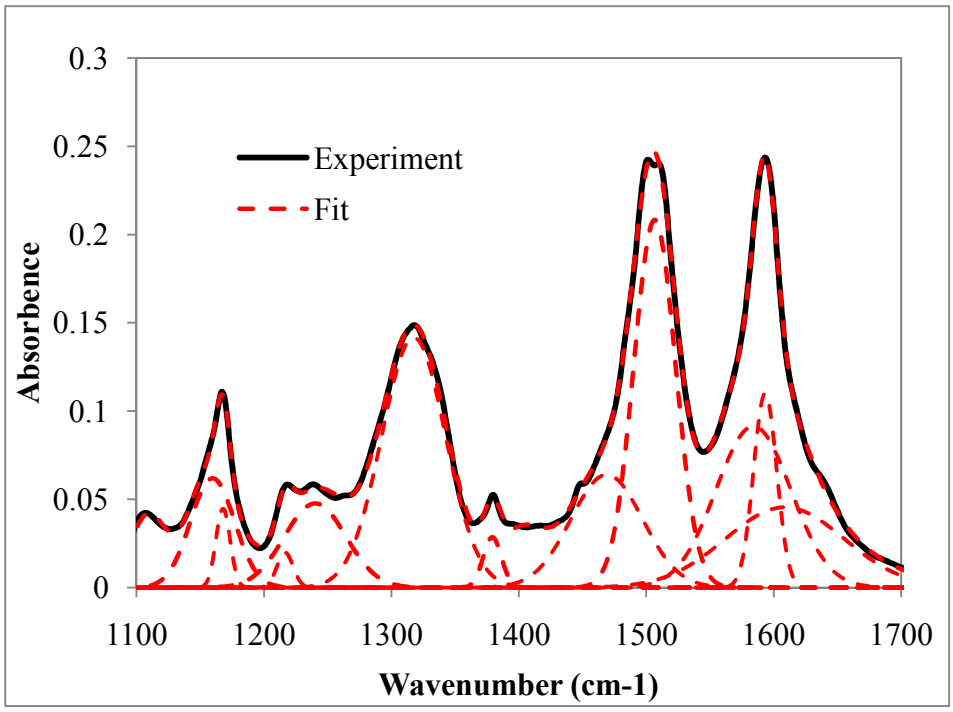

Figure 7. FT-IR spectra of dedoped polyaniline fit by Grams in the range of 1300 to 1700 cm^{-1}.

The FT-IR spectra of HCl doped, dedoped, and HCl redoped polyaniline are shown in Figure 8. The resonance intensity at about 1140 cm^{-1} increases with the doping level.

The resonance intensity area was obtained by fitting these spectra by Grams. The doping level, defined as the molar ratio of Cl to N, was estimated by Elemental Analysis. The peak area ratio of 1140 cm^{-1} to 1150 cm^{-1} at different doping levels is listed in Table 3.

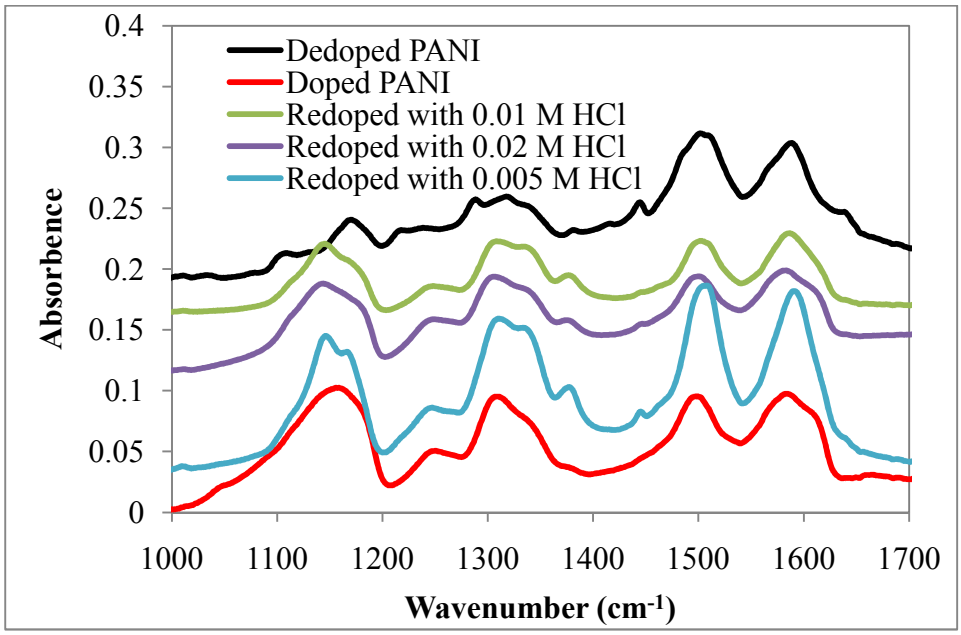

Figure 8. FT-IR spectra of doped, dedoped and redoped polyaniline.

Table 3. The peak area ratio of 1140 cm^{-1} to 1150 cm^{-1} at different doping levels

Sample	Fully Dedoped	0.005 M HCl Redoped	0.01 M HCl Redoped	0.02 M HCl Redoped	Fully Doped
Doping level	0	27.2	36.5	46.1	50
Peak area ratio	0.38	0.89	1.16	1.58	1.67

4. CONCLUSIONS

Raman and FT-IR spectra have been taken and fit with the Gaussian function to study the structural information of different polyaniline samples. It was shown that the intensity of protonated structure changed when polyaniline was exposed to a base. This was due to the dedoping of polyaniline. Quantitative analysis may allow us to monitor the structural change of polyaniline upon exposure to some analytes.

REFERENCES

(1) Sangodkar, H.; Sukeerthi, S.; Srinivasa, R. S.; Lal, R.; Contractor, A. Q. *Anal. Chem.* **1996**, *68*, 779-783.

(2) Virji, S.; Kaner, R. B.; Weiller, B. H. *Chem. Mater.* **2005**, *17*, 1256-1260.

(3) Yan, X. B.; Han, Z. J.; Yang, Y.; Tay, B. K. *Sens. Actuators, B* **2007**, *123*, 107-113.

(4) Virji, S.; Kaner, R. B.; Weiller, B. H. *J. Phys. Chem. B* **2006**, *110*, 22266-22270.

(5) Li, Z. F.; Blum, F. D.; Bertino, M. F.; Kim, C. S.; Pillalamarri, S. K. *Sens. Actuators, B* **2008**, *134*, 31-35.

(6) Tseng, R. J.; Huang, J. X.; Ouyang, J.; Kaner, R. B.; Yang, Y. *Nano Lett.* **2005**, *5*, 1077-1080.

(7) Tseng, R. J.; Baker, C. O.; Shedd, B.; Huang, J. X.; Kaner, R. B.; Ouyang, J. Y.; Yang, Y. *Appl. Phys. Lett.* **2007**, *90*, 053101

(8) Werake, L. K.; Story, J. G.; Bertino, M. F.; Pillalamarri, S. K.; Blum, F. D. *Nanotechnology* **2005**, *16*, 2833-2837.

(9) Pillalamarri, S. K.; Blum, F. D.; Tokuhiro, A. T.; Bertino, M. F. *Chem. Mater.* **2005**, *17*, 5941-5944.

(10) Virji, S.; Huang, J. X.; Kaner, R. B.; Weiller, B. H. *Nano Lett.* **2004**, *4*, 491-496.

(11) Roh, J. G.; Hwang, H. R.; Yu, J. B.; Lim, J. O.; Huh, J. S. *J. Macromol. Sci., A* **2002**, *39*, 1095 - 1105.

(12) Tillman, E. S.; Koscho, M. E.; Grubbs, R. H.; Lewis, N. S. *Anal. Chem.* **2003**, *75*, 1748-1753.

(13) Krinichnyi, V. I.; Chemerisov, S. D.; Lebedev, Y. S. *Phys. Rev., B* **1997**, *55*, 16233-16244.

(14) Nazeer, K. P.; Jacob, S. A.; Thamilselvan, M.; Mangalaraj, D.; Narayandass, S. K.; Yi, J. *Polym. Int.* **2004**, *53*, 898-902.

(15) Fattoum, A.; Arous, M.; Gmati, F.; Dhaoui, W.; Mohamed, A. B. *J. Phys. D: Appl. Phys.* **2007**, *40*, 4347-4354.

(16) Baibarac, M.; Cochet, M.; Lapkowski, M.; Mihut, L.; Lefrant, S.; Baltog, I. *Synth. Met.* **1998**, *96*, 63-70.

(17) Afzal, A. B.; Akhtar, M. J.; Nadeem, M.; Ahmad, M.; Hassan, M. M.; Yasin, T.; Mehmood, M. *J. Phys. D: Appl. Phys.* **2009**, *42*, 15411.

(18) Afzal, A. B.; Akhtar, M. J.; Nadeem, M.; Hassan, M. M. *Journal of Physical Chemistry C* **2009**, *113*, 17560-17565.

(19) Berrada, K.; Quillard, S.; Louam, G.; Lefrant, S. *Synth. Met.* **1995**, *69*, 201-204.

(20) Hugot-Le Goff, A.; Bernard, M. C. *Synth. Met.* **1993**, *60*, 115-131.

(21) Aslam, M.; Fu, L.; Su, M.; Vijayamohanan, K.; Dravid, V. P. *J. Mater. Chem.* **2004**, *14*, 1795-1797.

(22) Qu, Y.; Appleton, T. G.; Hoeschele, J. D.; Farrell, N. *Inorg. Chem.* **1993**, *32*, 2591-2593.

(23) Murray, B. J.; Walter, E. C.; Penner, R. M. *Nano Lett.* **2004**, *4*, 665-670.

APPENDIX C

SUPPORTING DOCUMENTATION: AMPLIFIED RESPONSE AND ENHANCED SELECTIVITY OF METAL-PANI FIBER COMPOSITE SENSORS

SUPPORTING DOCUMENTATION: AMPLIFIED RESPONSE AND ENHANCED SELECTIVITY OF METAL-PANI FIBER COMPOSITE SENSORS

Zhe-Fei Li[a], Frank D. Blum[a,b,c,], Massimo F. Bertino[d], Chang-Soo Kim[e,f],

[a] Department of Materials Science and Engineering, Missouri University of Science and Technology, Rolla, MO 65409

[b] Department of Chemistry, Missouri University of Science and Technology, Rolla, MO 65409

[c] Department of Chemistry, Oklahoma State University, Stillwater OK, 74078

[d] Department of Physics, Virginia Commonwealth University, Richmond, VA 23824

[e] Department of Electrical and Computer Engineering, Missouri University of Science and Technology, Rolla, MO 65409

[f] Department of Biological Sciences, Missouri University of Science and Technology, Rolla, MO 65409

The thermal stability of the different PANI species is illustrated in Figure S1 by through the use of thermogravimetric analysis. PANI normally exhibits three stages of decomposition. Below 100 °C, the weight loss can be ascribed to the release of water. The decomposition between 100 and 290 °C is likely due to the loss of dopant. PANI main chains start to decompose above 290 °C and after 600 °C the mass of conventional bulk PANI and PANI nanofibers effectively goes to 0%. PANI/metal nanocomposites show different thermal behavior with Pt composites showing initial thermal stability, but later, the Pt appears to enhance degradation. At 600 °C, the residual mass is due to metal residues of approximately 18 and 20% for Ag and Pt, respectively.

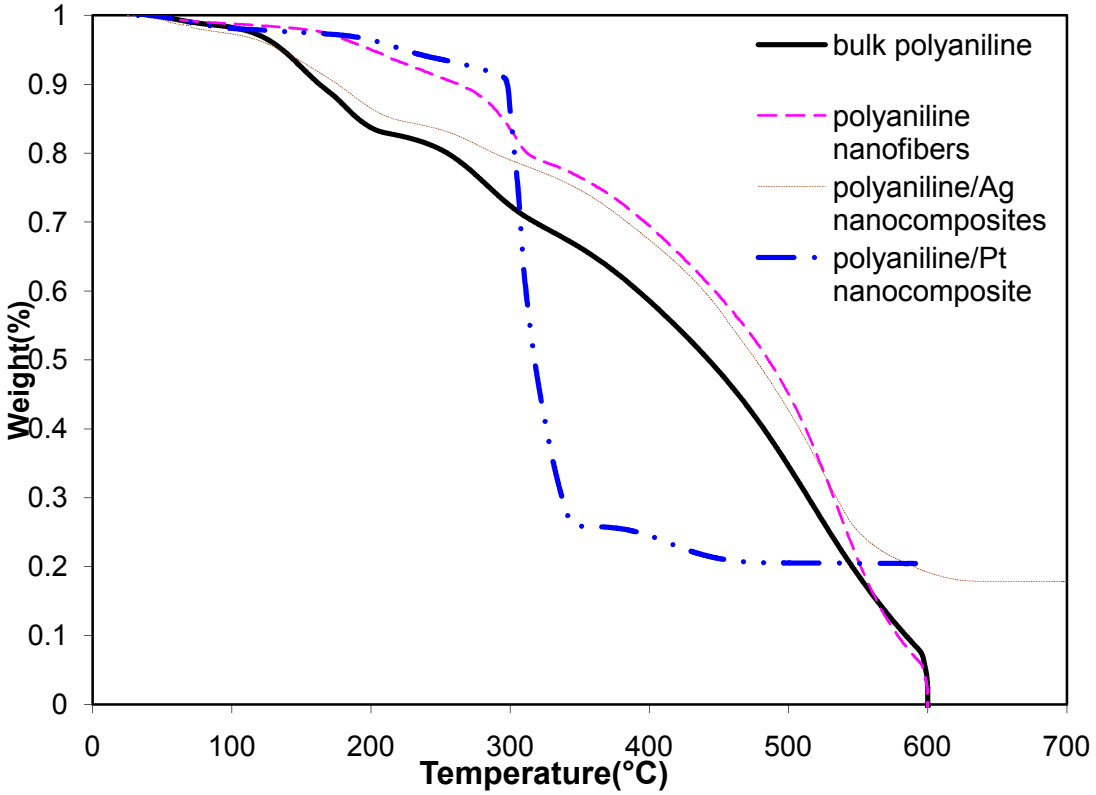

Figure S1. Thermogravimetric curves of bulk PANI, PANI nanofibers, PANI/Pt nanocomposites, and PANI/Ag nanocomposites at a heating rate of 20°C/min under an air atmosphere.

Shown in Figure S2 are the Raman spectra of Pt nanocomposites before and after exposure to triethylamine. The shape of the 1370 and 1330 cm^{-1} bands are similar in both spectra. The 1370 cm^{-1} band was decreased in intensity by about 20% upon exposure to triethylamine suggesting a small charge transfer induced by the analyte.

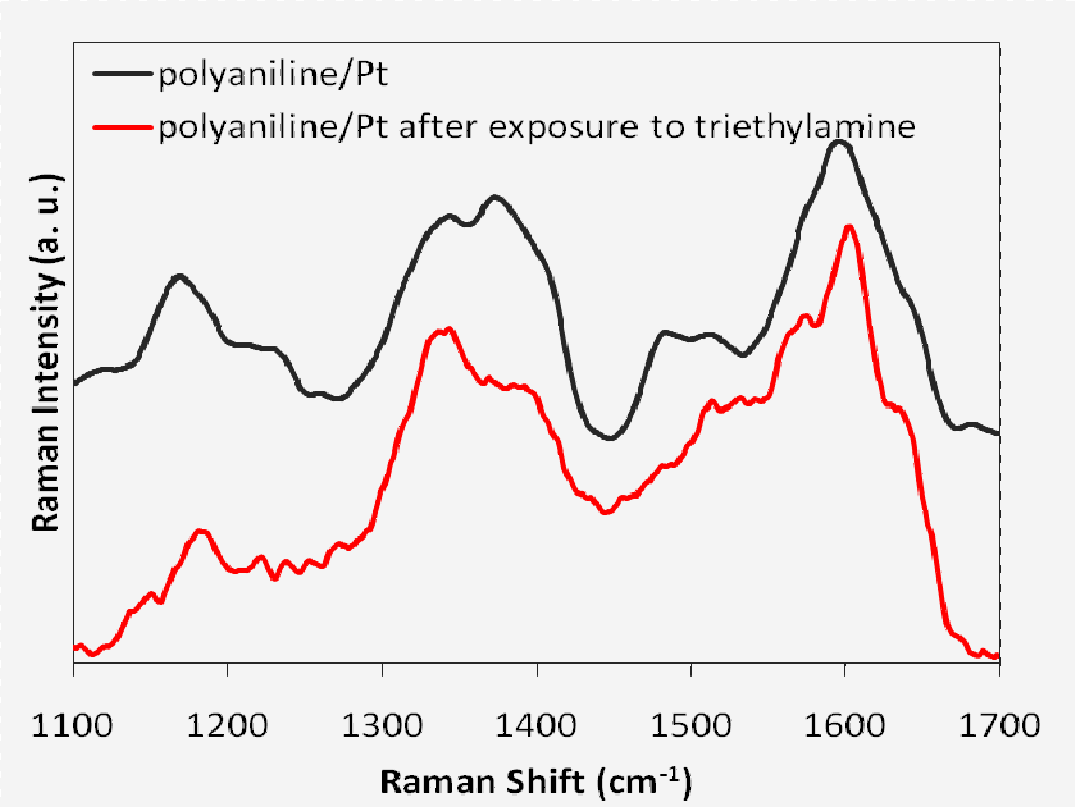

Figure S2. Raman Spectra of PANI/Pt, and PANI/Pt after exposure to triethylamine.

Shown in Figure S3 are the Raman spectra of Ag nanocomposites before and after exposure to toluene. The shape of the 1370 and 1330 cm^{-1} bands are very similar in both spectra. This suggests that the PANI structures are chemically unaffected by the presence of toluene.

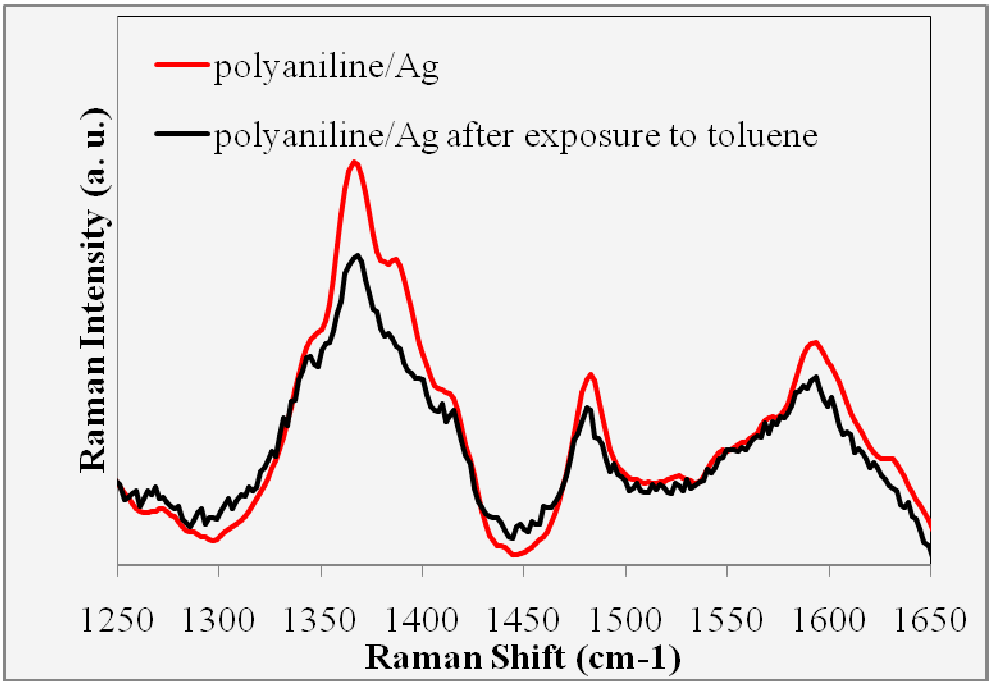

Figure S3. Raman Spectra of PANI/Ag before and after exposure to toluene.

BIBLIOGRAPHY

(1) Shirakawa, H.; Louis, E. J.; MacDiarmid, A. G.; Chiang, C. K.; Heeger, A. J. *Chem. Commun.* **1977**, 578.

(2) Chiang, C. K.; Druy, M. A.; Gau, S. C.; Heeger, A. J.; Louis, E. J.; MacDiarmid, A. G.; Park, Y. W.; Shirakawa, H. *J. Am. Chem. Soc.* **1978**, *100*, 1013.

(3) *Conducting Polymers, Fundamentals and Applications*; Chandrasekhar, P., Ed.; Kluwer Acedemic Publishers, 1999.

(4) Chiang, J.-C.; MacDiarmid, A. G. *Synt. Met.* **1986**, *13*, 193.

(5) Macdiarmid, A. G.; Chiang, J. C.; Richter, A. F. *Synt. Met.* **1987**, *18*, 285.

(6) Epstein, A. J.; Ginder, J. M.; Zuo, F.; Woo, H.-S.; Tanner, D. B.; Richter, A. F.; Angelopoulos, M.; Huang, W.-S.; MacDiarmid, A. G. *Synt. Met.* **1987**, *21*, 63.

(7) Huang, W.-S.; Humphrey, B. D.; MacDiarmid, A. G. *J. Chem. Soc., Faraday Trans. 1* **1986**, *82*, 2385.

(8) Chun, D. H. R. a. I. *Nanotechnology* **1997**, *7*, 216.

(9) Huang, J.; Kaner, R. B. *J. Am. Chem. Soc.* **2004**, *126*, 851.

(10) Huang, J.; Kaner, R. B. *Angew. Chem., Int. Ed.* **2004**, *43*, 5817.

(11) Zhang, X.; Goux, W. J.; Manohar, S. K. *J. Am. Chem. Soc.* **2004**, *126*, 4502.

(12) Martin, C. R. *Chem. Mater* **1996**, *8*, 1739.

(13) Li, G.; Zhang, Z. *Macromolecules* **2004**, *37*, 2683.

(14) Li, W.; Wang, H.-L. *J. Am. Chem. Soc.* **2004**, *126*, 2278.

(15) Patil, A. O.; Heeger, A. J.; Wudl, F. *Chem. Rev.* **1988**, *88*, 183.

(16) Yutaka, O.; Masao, U.; Keiro, M.; Katsumi, Y. *Solid State Commun.* **1991**, *80*, 605.

(17) Ohmori, Y.; Uchida, M.; Muro, K.; Yoshino, K. *Jpn. J. Appl. Phys.* **1991**, *30*, 1938.

(18) McCullough, R. D.; Ewbank, P. C.; Loewe, R. S. *J. Am. Chem. Soc.* **1997**, *119*, 633.

(19) McCullough, R. D.; Lowe, R. D. *J. Chem. Soc., Chem. Commun.* **1992**, 70.

(20) Samitsu, S.; Shimomura, T.; Ito, K. *Thin Solid Films* **2008**, *516*, 2478.

(21) Ihn, K. J.; Moulton, J.; Smith, P. *J. Polym. Sci., Part B: Polym. Phys.* **1993**, *31*, 735.

(22) Wei, Y.; Tian, J. *Macromolecules* **1993**, *26*, 457.

(23) Tran, H. D.; Shin, K.; Hong, W. G.; D'Arcy, J. M.; Kojima, R. W.; Weiller, B. H.; Kaner, R. B. *Macromol. Rapid Commun.* **2007**, *28*, 2289.

(24) Werake, L. K.; Story, J. G.; Bertino, M. F.; Pillalamarri, S. K.; Blum, F. D. *Nanotechnology* **2005**, *16*, 2833.

(25) Dhawan, S. K.; Kumar, D.; Ram, M. K.; Chandra, S.; Trivedi, D. C. *Sens. Actuators, B* **1997**, *40*, 99.

(26) Sakai, G.; Matsunaga, N.; Shimanoe, K.; Yamazoe, N. *Sens. Actuators, B* **2001**, *80*, 125.

(27) Österholm, J. E.; Passiniemi, P.; Isotalo, H.; Stubb, H. *Synt. Met.* **1987**, *18*, 213.

(28) Letheby, H. *J. Chem. Soc.* **1862**, *15*, 161.

(29) Chiang, C. K.; Fincher, C. R.; Park, Y. W.; Heeger, A. J.; Shirakawa, H.; Louis, E. J.; Gau, S. C.; MacDiarmid, A. G. *Phys. Rev. Lett.* **1977**, *39*, 1098.

(30) *Introduction to Solid State Physics, 4th ed.*; Kittel, C., Ed.; Wiley: New York 1971.

(31) *Solid State Electronic Devices*; Streetman, B. G., Ed.; Prentice Hall, 1990.

(32) *Modern physics, 2nd ed.*; Krane, K. S., Ed.; Wiley: New York 1996.

(33) Joo, J.; Long, S. M.; Pouget, J. P.; Oh, E. J.; MacDiarmid, A. G.; Epstein, A. J. *Phys. Rev. B: Condens. Matter* **1998**, *57*, 9567.

(34) Heeger, A. J.; Kivelson, S.; Schrieffer, J. R.; Su, W. P. *Rev. Mod. Phys.* **1988**, *60*, 781.

(35) Su, W. P.; Schrieffer, J. R.; Heeger, A. J. *Phys. Rev. Lett.* **1979**, *42*, 1698.

(36) Clarke, T. C.; Geiss, R. H.; Kwak, J. F.; Street, G. B. *J. Chem. Soc., Chem. Commun.* **1978**.

(37) Fincher, C. R.; Ozaki, M.; Heeger, A. J.; MacDiarmid, A. G. *Phys. Rev. B: Condens. Matter* **1979**, *19*, 4140.

(38) Nigrey, P. J.; MacDiarmid, A. G.; Heeger, A. J. *J. Chem. Soc., Chem. Commun.* **1979**.

(39) De Leeuw, D. M.; Simenon, M. M. J.; Brown, A. R.; Einerhand, R. E. F. *Synt. Met.* **1997**, *87*, 53.

(40) Przyluski, J.; Roth, S. *Mater. Sci. Forum* **1989**, *42*, 17.

(41) *Electronic Porcesses in Non-Crystalline Materials, 2nd ed*; Mott, N. F.; Davis, E. A., Eds.; Oxford: Claredon, 1979.

(42) Epstein, A. J.; Rommelmann, H.; Bigelow, R.; Gibson, H. W.; Hoffmann, D. M.; Tanner, D. B. *Phys. Rev. Lett.* **1983**, *50*, 1866.

(43) Zuo, F.; Angelopoulos, M.; MacDiarmid, A. G.; Epstein, A. J. *Phys. Rev. B: Condens. Matter* **1987**, *36*, 3475.

(44) Wuelfing, W. P.; Green, S. J.; Pietron, J. J.; Cliffel, D. E.; Murray, R. W. *J. Am. Chem. Soc.* **2000**, *122*, 11465.

(45) Wuelfing, W. P.; Murray, R. W. *J. Phys. Chem. B* **2002**, *106*, 3139.

(46) *Scanning tunneling microscopy* Stroscio, J. A.; Kaiser, W. J., Eds.; Academic Press: Boston, 1993.

(47) Zamborini, F. P.; Smart, L. E.; Leopold, M. C.; Murray, R. W. *Anal. Chim. Acta* **2003**, *496*, 3.

(48) Conwell, E. M.; Perlstein, J.; Shaik, S. *Phys. Rev. B: Condens. Matter* **1996**, *54*, R2308.

(49) Bodalia, R. R.; Duran, R. S. *J. Am. Chem. Soc.* **1993**, *115*, 11467.

(50) Wei, Y.; Tang, X.; Sun, Y.; Focke, W. *J. Polym. Sci., Polym. Chem. Ed.* **1989**, *27*, 2385.

(51) Ding, Y.; Padias, A. B.; Jr., H. K. H. *J. Polym. Sci., Part A: Polym. Chem.* **1999**, *37*, 2569.

(52) Sabouraud, G.; Sadki, S.; Brodie, N. *Chemical Society Reviews* **2000**, *29*, 283.

(53) Macdiarmid, A. G.; Chiang, J.-C.; Halpern, M.; Huang, W.-S.; Mu, S.-L.; Nanaxakkara, L. D.; Wu, S. W.; Yaniger, S. I. *Mol. Cryst. Liq. Cryst.* **1985**, *121*, 173.

(54) DeBerry, D. W. *J. Electrochem. Soc.* **1985**, *132*, 1022.

(55) Inoue, M. B.; Velazquez, E. F.; Inoue, M. *Synt. Met.* **1988**, *24*, 223.

(56) Lin, J. W.-P.; Dudek, L. P. *J. Polym. Sci., Part A: Polym. Chem.* **1980**, *18*, 2869.

(57) Yamamoto, T.; Morita, A.; Miyazaki, Y.; Maruyama, T.; Wakayama, H.; Zhou, Z. H.; Nakamura, Y.; Kanbara, T.; Sasaki, S.; Kubota, K. *Macromolecules* **1992**, *25*, 1214.

(58) Jen, K.-Y.; Eckhardt, H.; Jow, T. R.; Shacklette, L. W.; Elsenbaumer, R. L. *J. Chem. Soc., Chem. Commun.* **1988**, 215.

(59) Xia, Y.; Yang, P.; Sun, Y.; Wu, Y.; Mayers, B.; Gates, B.; Yin, Y.; Kim, F.; Yan, H. *Adv. Mater.* **2003**, *15*, 353.

(60) Kanungo, M.; Kumar, A.; Contractor, A. Q. *Anal. Chem.* **2003**, *75*, 5673.

(61) Aleshin, A. N. *Adv. Mater.* **2006**, *18*, 17.

(62) Virji, S.; Huang, J. X.; Kaner, R. B.; Weiller, B. H. *Nano Lett.* **2004**, *4*, 491.

(63) Liu, H.; Kameoka, J.; Czaplewski, D. A.; Craighead, H. G. *Nano Lett.* **2004**, *4*, 671.

(64) Kline, R. J.; McGehee, M. D.; Kadnikova, E. N.; Liu, J.; Frechet, J. M. J.; Toney, M. F. *Macromolecules* **2005**, *38*, 3312.

(65) Darrell, H. R.; Iksoo, C. *Nanotechnology* **1996**, *7*, 216.

(66) Pinto, N. J.; Johnson, A. T.; MacDiarmid, A. G.; Mueller, C. H.; Theofylaktos, N.; Robinson, D. C.; Miranda, F. A. *Appl. Phys. Lett.* **2003**, *83*, 4244.

(67) Parthasarathy, R. V.; Martin, C. R. *Chem. Mater.* **1994**, *6*, 1627.

(68) Han, M. G.; Foulger, Stephen H. *Small* **2006**, *2*, 1164.

(69) Chiou, N.-R.; Epstein, A. J. *Adv. Mater.* **2005**, *17*, 1679.

(70) Zhang, X.; Manohar, S. K. *J. Am. Chem. Soc.* **2004**, *126*, 12714.

(71) Zhang, X.; Lee, J.-S.; Lee, G. S.; Cha, D.-K.; Kim, M. J.; Yang, D. J.; Manohar, S. K. *Macromolecules* **2005**, *39*, 470.

(72) Pillalamarri, S. K.; Blum, F. D.; Tokuhiro, A. T.; Story, J. G.; Bertino, M. F. *Chem. Mater.* **2004**, *17*, 227.

(73) Wang, X.; Feng, X.; Zhao, Y.; Zhang, R.; Sun, D. *Eur. Polym. J.* **2007**, *43*, 3679.

(74) Pillalamarri, S. K.; Blum, F. D.; Tokuhiro, A. T.; Bertino, M. F. *Chem. Mater.* **2005**, *17*, 5941.

(75) Qiu, G.; Wang, Q.; Nie, M. *J. Appl. Polym. Sci.* **2006**, *102*, 2107.

(76) Gao, J.; Li, S.; Wu, Y.; Zhao, G.; Bo, L.; Li, S. *Rare Met.* **2007**, *26*, 1.

(77) Guo, M.; Chen, J.; Li, J.; Tao, B.; Yao, S. *Anal. Chim. Acta* **2005**, *532*, 71.

(78) Tran, H. D.; Li, D.; Kaner, R. B. *Adv. Mater.* **2009**, *21*, 1487.

(79) *Encyclopedia of Sensors*; Grimes, C. A.; Dickey, E. C.; Pishko, M. V., Eds.; American Scientific Publishers: Stevenson Ranch, 2006.

(80) *Solid State Chemical Sensors*; Janata, J.; Huber, R. J., Eds.; Academic Press: Orlando, 1985.

(81) Francioso, L.; Presicce, D. S.; Epifani, M.; Siciliano, P.; Ficarella, A. *Sens. Actuators, B* **2005**, *107*, 563.

(82) Li, J.; Lu, Y.; Ye, Q.; Cinke, M.; Han, J.; Meyyappan, M. *Nano Lett.* **2003**, *3*, 929.

(83) Guernion, N.; Ewen, R. J.; Pihlainen, K.; Ratcliffe, N. M.; Teare, G. C. *Synt. Met.* **2002**, *126*, 301.

(84) Nicolas-Debarnot, D.; Poncin-Epaillard, F. *Anal. Chim. Acta* **2003**, *475*, 1.

(85) Huang, J.; Virji, S.; Weiller, B. H.; Kaner, R. B. *J. Am. Chem. Soc.,* **2003**, *125*, 314.

(86) Prasad, G. K.; Radhakrishnan, T. P.; Kumar, D. S.; Krishna, M. G. *Sens. Actuators, B* **2005**, *106*, 626.

(87) Chabukswar, V. V.; Pethkar, S.; Athawale, A. A. *Sens. Actuators, B* **2001**, *77*, 657.

(88) Xie, D.; Jiang, Y.; Pan, W.; Li, D.; Wu, Z.; Li, Y. *Sens. Actuators, B* **2002**, *81*, 158.

(89) Roh, J. G.; Hwang, H. R.; Yu, J. B.; Lim, J. O.; Huh, J. S. *J. Macromol. Sci., Phys. A* **2002**, *39*, 1095

(90) Li, B.; Santhanam, S.; Schultz, L.; Jeffries-El, M.; Iovu, M. C.; Sauvé, G.; Cooper, J.; Zhang, R.; Revelli, J. C.; Kusne, A. G.; Snyder, J. L.; Kowalewski, T.; Weiss, L. E.; McCullough, R. D.; Fedder, G. K.; Lambeth, D. N. *Sens. Actuators, B* **2007**, *123*, 651.

(91) Ramanathan, K.; Bangar, M. A.; Yun, M.; Chen, W.; Mulchandani, A.; Myung, N. V. *Nano Lett.* **2004**, *4*, 1237.

(92) Sawall, D. D.; Villahermosa, R. M.; Lipeles, R. A.; Hopkins, A. R. *Chem. Mater.* **2004**, *16*, 1606.

(93) Loffredo, F.; Burrasca, G.; Quercia, L.; Sala, D. D. *Macromol. Symp.* **2007**, *247*, 357.

(94) Maynor, B. W.; Filocamo, S. F.; Grinstaff, M. W.; Liu, J. *J. Am. Chem. Soc.* **2001**, *124*, 522.

(95) Jin, Z.; Su, Y.; Duan, Y. *Sens. Actuators, B* **2001**, *72*, 75.

(96) Grummt, U.-W.; Pron, A.; Zagorska, M.; Lefrant, S. *Anal. Chim. Acta* **1997**, *357*, 253.

(97) Christie, S.; Scorsone, E.; Persaud, K.; Kvasnik, F. *Sens. Actuators, B* **2003**, *90*, 163.

(98) *Physical Chemistry of Surfaces*; Adamson, A. W.; Gast, A. P., Eds.; Wiley-Interscience: New York, 1997.

(99) *Adsorption By Powders & Porous Solids*; Rouquerol, F.; Rouquerol, J.; Sing, K., Eds.; Academic Press: London, 1999.

(100) *Introduction to Surface Chemistry and Catalysis*; Somorjai, G. A., Ed.; Wiley-Interscience: New York, 1994.

(101) Langmuir, I. *J. Am. Chem. Soc.* **1918**, *40*, 1361.

(102) *Diffusion In Polymers*; Crank, J.; Park, G. S., Eds.; Academic Press: New York, 1968.

(103) Fick, A. E. *Ann. Phys. Chem.* **1855**, *170*, 59.

(104) Barrer, R. M.; Barrie, J. A.; Slater, J. *J. Polym. Sci.* **1958**, *27*, 177.

(105) *Diffusion In and Through Polymers*; Vieth, W. R., Ed.; Hanser: New York, 1979.

(106) *Diffusion In Polymers*; Neogi, P., Ed.; Marcel Dekker: New York, 1996.

(107) *Nucleation* Zettlemoyer, A. C., Ed.; Dekker: New York, 1969.

(108) *Kinetics of materials* Balluffi, R. W.; Allen, S. M.; Carter, W. C.; Kemper, R. A., Eds.; Wiley-Interscience: Hoboken, N.J., 2005.

(109) Turnbull, D.; Fisher, J. C. *J. Chem. Phys.* **1949**, *17*, 71.

(110) *Macromolecular Physics*; Wunderlich, B., Ed.; Academic Press: New York, 1976; Vol. 2.

(111) *Crystallization during polymerization* Wunderlich, B., Ed.; Springer: Berlin, 1968; Vol. 5.

VITA

Zhefei Li was born in Lixin, China on November 17th 1985. He received his BS in Polymer Science and Engineering from Anhui University in Hefei, China. Zhefei joined Missouri University of Science and Technology in August 2006 and received his MS degree in Materials Science and Engineering in August 2008. He finished his PhD in Materials Science and Engineering in 2010 on the synthesis and characterization of nanostructured conducting polymers and their applications in sensors.